

**INTEGRATED PETROPHYSICAL AND RESERVOIR
CHARACTERIZATION WORKFLOW TO ENHANCE
PERMEABILITY AND WATER SATURATION
PREDICTION**

BY
MESHAL ALI ALAMRI

A Thesis Presented to the
DEANSHIP OF GRADUATE STUDIES

KING FAHD UNIVERSITY OF PETROLEUM & MINERALS

DHAHRAN, SAUDI ARABIA

In Partial Fulfillment of the
Requirements for the Degree of

MASTER OF SCIENCE

In
PETROLEUM ENGINEERING

MAY 2015

KING FAHD UNIVERSITY OF PETROLEUM & MINERALS

DHAHRAN- 31261, SAUDI ARABIA

DEANSHIP OF GRADUATE STUDIES

This thesis, written by **MESHAL ALI ALAMRI** under the direction of his thesis advisor and approved by his thesis committee, has been presented and accepted by the Dean of Graduate Studies, in partial fulfillment of the requirements for the degree of **MASTER OF SCIENCE IN PETROLEUM ENGINEERING**.





Dr. Mohamed Naser
(Advisor)



Dr. Abdullah Sultan
Department Chairman



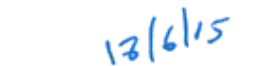
Dr. Hasan Al-Yousif
(Member)



Dr. Salam A. Zummo
Dean of Graduate Studies



Dr. Tariq A. Al-Ghamdi
(Member)



Date

© Meshal Ali Al-Amri

2015

This work is dedicated to the memory of my grandmother, Sa'diyah Al-Ghamdi (1947-2013)

ACKNOWLEDGMENTS

To God be the glory who allows me health and prosperity to finish this study. I would like to especially thank my thesis committee advisor and members: Dr. Mohamed Naser, Dr. Hasan Al-Yousef and Dr. Tariq Al-Ghamdi for their patience, guidance, mentorship and excellent feedback before, during and even after completing my thesis. Their insights and encouragement made the master thesis a truly rewarding and exciting experience. I also would like to extend sincere thanks to the management of Saudi Aramco for their support in completing the master thesis requirements which would not have been possible without their permission of using the company data. I don't want to forget to thank the Department of Petroleum Engineering at King Fahd University of Petroleum & Minerals, professors, technical staff, administrators and students, for their valuable knowledge, information and cooperation.

I would like to express my gratitude and thank my parents, wife, brothers (Ahmad, Anwar and Faisal) and sisters (Manar, Wa'ad and Raneem) for their continuing encouragement during the time of my studies. I also want to thank my friends and colleagues, especially Hamad Al-Kharraa and Abdulrahman Al-Nutaifi for the fulfilling experience throughout my graduate studies that started in 2011. Special thanks goes to my Saudi Aramco superiors, especially Dr. Faisal Al-Khelaiwi, Bandar Al-Khamies, Yousif Al-Tahan, Thamer Al-Shamekh and Nami Al-Amri for their continuous encouragement and support.

TABLE OF CONTENTS

ACKNOWLEDGMENTS	V
TABLE OF CONTENTS	VI
LIST OF TABLES	VIII
LIST OF FIGURES	IX
LIST OF ABBREVIATIONS.....	IX
ENGLISH ABSTRACT	XVI
ARABIC ABSTRACT	XVI1
1 CHAPTER 1 INTRODUCTION	1
1.1 BACKGROUND	1
1.2 FACIES DETERMINATION	3
1.3 PERMEABILITY DETERMINATION	3
1.4 SATURATION DETERMINATION.....	6
1.5 STATEMENT OF THE PROBLEM.....	8
1.6 RESEARCH OBJECTIVES	9
1.7 RESEARCH METHODOLOGY	9
2 CHAPTER 2 STATE OF THE ART LITERATURE REVIEW	11
3 CHAPTER 3 DATA DESCRIPTION AND VALIDATION	19
4 CHAPTER 4 PERMEABILITY MODELING	52
4.1 MODEL INPUTS.....	52

4.2 DATA TRAINING	55
4.3 PREDICTION SENSITIVITY	58
4.4 PERMEABILITY PREDICTION	67
4.5 VALIDATING PERMEABILITY MODEL	70
4.6 DYNAMIC PERMEABILITY INTEGRATION	74
4.7 RESERVOIR BAFFLES-COMMUNICATION IDENTIFICATION	79
5 CHAPTER 5 WATER SATURATION MODELING	89
5.1 SATURATION MODEL INPUTS	89
5.2 METHODOLOGY	90
5.3 MICP RESULT	92
5.4 WATER SATURATION PREDICTION	99
6 CHAPTER 6 CONCLUSIONS AND RECOMMENDATIONS	115
REFERENCES	118
APPENDIX A	121
APPENDIX B	122
VITAE	124

LIST OF TABLES

Table 3.1 Statistical data description of the core corrected porosity and permeability for filtered data	24
Table 3.2 Statistical data description of the absolute difference between core porosity and wireline logs porosity	28
Table 3.3 Statistical data description of the difference between corrected core porosity and wireline logs porosity	28
Table 3.4 Statistical data description of permeability values for each Lithofacie	33
Table 3.5 Statistical data description of logarithmic of permeability for each Lithofacie.....	34
Table 3.6 Depositional environment of the reservoir lithofacies	44
Table 4.1 Statistical Assessment for predicted permeability and predicted logarithmic value of permeability at KNN=2	62
Table 5.1 J-Function parameters for different Lithofacies 97Table 5.2: Summary of water saturation mean per Lithofacies	106

LIST OF FIGURES

Figure 1.1: Typical Oil-Water system relative permeability curves	2
Figure 1.2: Typical porosity-permeability cross-plots	5
Figure 1.3: Effect of pore system on porosity-permeability relationship	6
Figure 1.4: Leverett's J-function at different reservoir zones	7
Figure 3.1: well 142 depth shift technique for data preparation	21
Figure 3.2: well 101 depth shift technique for data preparation	22
Figure 3.3: Filtered corrected core porosity histogram	23
Figure 3.4: Filtered corrected core permeability histogram	23
Figure 3.5: Filtered logarithmic corrected core permeability histogram	24
Figure 3.6: Well-115 showing process of data removal using grain density measurement. (6th and 5th tracks show porosity before and after data filtration, respectively)	26
Figure 3.7: Histogram of absolute difference between corrected core porosity and neutron- density values	27
Figure 3.8: Histogram of difference between corrected core porosity and neutron-density values	27
Figure 3.9: well 143 removed permeability values in red which falls outside the recommended range for porosity standard deviation	29
Figure 3.10: well 182 removed permeability values in red which falls outside the recommended range for permeability standard deviation	30
Figure 3.11: Lithofacie-1 permeability and logarithmic of permeability histogram	35
Figure 3.12: Lithofacie-2 permeability and logarithmic of permeability histogram	35
Figure 3.13: Lithofacie-4 permeability and logarithmic of permeability histogram	36
Figure 3.14: Lithofacie-7 permeability and logarithmic of permeability histogram	36
Figure 3.15: Lithofacie-8 permeability and logarithmic of permeability histogram	37
Figure 3.16: Lithofacie-9 permeability and logarithmic of permeability histogram	37
Figure 3.17: Lithofacie-10 permeability and logarithmic of permeability histogram	38
Figure 3.18: Lithofacie-11 permeability and logarithmic of permeability histogram	38
Figure 3.19: Lithofacie-15 permeability and logarithmic of permeability histogram	39
Figure 3.20: Lithofacie-16 permeability and logarithmic of permeability histogram	39
Figure 3.21: Lithofacie-17 permeability and logarithmic of permeability histogram	40
Figure 3.22: Lithofacie-18 permeability and logarithmic of permeability histogram	40
Figure 3.23: Lithofacie-19 permeability and logarithmic of permeability histogram	41
Figure 3.24: Lithofacie-20 permeability and logarithmic of permeability histogram	41
Figure 3.25: Lithofacie-21 permeability and logarithmic of permeability histogram	42
Figure 3.26: Lithofacie-22 permeability and logarithmic of permeability histogram	42
Figure 3.27: Lithofacie-23 permeability and logarithmic of permeability histogram	43
Figure 3.28: well 182 lithofacies versus core permeability	46

Figure 3.29: well 142 lithofacies versus core permeability	47
Figure 3.30: Lithofacies-1 and 4 porosity-permeability relationship	49
Figure 3.31: well-64 microporosity interpretation using cores, sonic and neutron/density data	50
Figure 3.32: well-143 microporosity interpretation using cores, sonic and neutron/density data	51
Figure 4.1: A systematic workflow used in in this study to predict permeability with the training data set	54
Figure 4.2: Cross –correlations show trend between density log and core permeability and logarithmic value of permeability	55
Figure 4.3: Cross –correlations show trend between neutron log and core permeability and logarithmic value of permeability.....	56
Figure 4.4: Cross –correlations show trend between sonic log and core permeability and logarithmic value of permeability	56
Figure 4.5: Cross –correlations show trend between the differences between sonic and density-neutron, and core permeability and logarithmic value of permeability to include diagenesis effect in the model training.....	57
Figure 4.6: Cross –correlations show core permeability and logarithmic value of permeability ranges for each lithofacies.....	57
Figure 4.7: Cross-plot of predicted model permeability versus corrected core permeability for KNN=2	59
Figure 4.8: Cross-plot of predicted model permeability versus corrected core permeability for KNN=3	60
Figure 4.9: Cross-plot of predicted model permeability versus corrected core permeability for KNN=4	60
Figure 4.9: Cross-plot for predicted logarithmic value of permeability versus logarithmic value of corrected core permeability for KNN=2	61
Figure 4.10: Lithofacies-1 permeability distribution from core data which exhibit a permeability mean of 428.94 mD	63
Figure 4.11: Lithofacies-1 permeability and logarithmic value of permeability distribution from the prediction model which exhibit a permeability mean of 333.47 mD	63
Figure 4.12: Lithofacies-4 permeability distribution from core data which exhibit a permeability mean of 6.28 mD	64
Figure 4.13: Lithofacies-4 permeability distribution from core data which exhibit a permeability mean of 6.37 mD	64
Figure 4.14: Lithofacies-18 permeability distribution from core data which exhibit a permeability mean of 5.14 mD	65
Figure 4.15: Lithofacies-18 permeability distribution from core data which exhibit a permeability mean of 5.97 mD	65

Figure 4.16: Well 101 predicted permeability (black curve) over the corrected core permeability (red dots) for KNN = 2, 3 and 4	66
Figure 4.17: comparison between with and without lithofacies inputs predicted permeability for well-43. Lithofacies inputs clearly enhanced prediction of permeability	68
Figure 4.18: Permeability prediction in well-121, oil producer, from the model	68
Figure 4.19: Permeability prediction in well-219, water injector, from the model	69
Figure 4.20: Permeability prediction in well-221, water injector, from proposed model...	69
Figure 4.21: Validating modeling permeability using kh value from modeling (black curve), buildup test (blue curve) and core measurements (red curve) in cored well-19 (observation key well) which demonstrate a good match among three different validation mechanisms	70
Figure 4.22: Validating modeling permeability using kh value from modeling (black curve) and buildup test (blue curve) in well-115 (oil producer) which demonstrate a good observed match	71
Figure 4.23: Validating modeling permeability using kh value from modeling (black curve) and buildup test (blue curve) in well-64 (oil producer) which demonstrate a good observed match	72
Figure 4.24: Validating modeling permeability using kh value from modeling (black curve) and falloff test (blue curve) in well-215 (water injector) which demonstrate a good observed match.....	73
Figure 4.25: Converting static permeability (modeling) to dynamic permeability in well-19 (observation key well) with almost no required multiplier (5th track black curve)	75
Figure 4.26: Converting static permeability (modeling) to dynamic permeability in well-79 (observation well) with almost minimal required multiplier (5th track black curve)	76
Figure 4.27: Converting static permeability (modeling) to dynamic permeability in well-92 (observation well) with almost matching model and PLT Kh however well test Kh value require further investigation	77
Figure 4.28: Converting static permeability (modeling) to dynamic permeability for the understudy reservoir with $R^2 = 0.73$	78
Figure 4.29: Lorenz Plot for lithofacies-1 which shows an excellent zone in the reservoir for both production and injection with storage and high capacity (define and label axes, identify curves)	80
Figure 4.30: Lorenz Plot for lithofacies-2 which shows a good zone in the reservoir with high storage and low capacity due to diagenesis	80
Figure 4.31: Lorenz Plot for lithofacies-4 which shows a good zone in the reservoir with high storage and low capacity due to diagenesis	81
Figure 4.32: Lorenz Plot for lithofacies-7 which shows a good zone in the reservoir	

with medium storage and good capacity	81
Figure 4.33: Lorenz Plot for lithofacaies-8 which shows a good zone in the reservoir with medium storage and low capacity	82
Figure 4.34: Lorenz Plot for lithofacaies-9 which shows a baffle zone in the reservoir with low storage and very low capacity	82
Figure 4.35: Lorenz Plot for lithofacaies-10 which shows a baffle zone in the reservoir with low storage and very low capacity	83
Figure 4.36: Lorenz Plot for lithofacaies-11 which shows a zone in the reservoir with low storage and medium capacity	83
Figure 4.37: Lorenz Plot for lithofacaies-15 which shows an excellent zone in the reservoir for both production and injection with storage and high capacity...	84
Figure 4.38: Lorenz Plot for lithofacaies-16 which shows a good zone in the reservoir with medium storage and good capacity	84
Figure 4.39: Lorenz Plot for lithofacaies-17 which shows a good zone in the reservoir with high storage and good capacity	85
Figure 4.40: Lorenz Plot for lithofacaies-18 which shows a zone in the reservoir with low storage and medium capacity	85
Figure 4.41: Lorenz Plot for lithofacaies-19 which shows a good zone in the reservoir with medium storage and high capacity	86
Figure 4.42: Lorenz Plot for lithofacaies-20 which shows a zone in the reservoir with medium storage and medium capacity	86
Figure 4.43: Lorenz Plot for lithofacaies-21 which shows a zone in the reservoir with high storage and medium capacity	87
Figure 4.44: Lorenz Plot for lithofacaies-22 which shows a zone in the reservoir with medium storage and low capacity	87
Figure 4.45: Lorenz Plot for lithofacaies-23 which shows an excellent zone of storage and low capacity due to diagenesis effect	88
Figure 5.1: Water saturation modeling workflow used in this study.....	91
Figure 5.2: MICP curves which show the closure effect that is corrected for this study...	92
Figure 5.3: Capillary Pressure curve for all samples	94
Figure 5.4: Capillary pressure curves for all lithofacies	95
Figure 5.5: Predicted J-function plot for each lithofacies	98
Figure 5.6: Lithofacies-1 water saturation histogram with water saturation mean of 10.7%	99
Figure 5.7: Lithofacies-4 water saturation histogram with water saturation mean of 12.3%	100
Figure 5.8: Lithofacies-8 water saturation histogram with water saturation mean of 15.3%	100
Figure 5.9: Lithofacies-9 water saturation histogram with water saturation mean of 18.9%	101
Figure 5.10: Lithofacies-15 water saturation histogram with water saturation mean	

of 10.4%	101
Figure 5.11: Lithofacies-16 water saturation histogram with water saturation mean of 12.9%	102
Figure 5.12: Lithofacies-17 water saturation histogram with water saturation mean of 13.9%	102
Figure 5.13: Lithofacies-18 water saturation histogram with water saturation mean of 15.4%	103
Figure 5.14: Lithofacies-19 water saturation histogram with water saturation mean of 14.4%	103
Figure 5.15: Lithofacies-21 water saturation histogram with water saturation mean of 15.8%	104
Figure 5.16: Lithofacies-22 water saturation histogram with water saturation mean of 18%	104
Figure 5.17: Lithofacies-23 water saturation histogram with water saturation mean of 24.7%	105
Figure 5.18: Well-103 water saturation predicted (red curve -4th track-) compared to Archie water saturation (blue curve -4th track-), 6th track shows the difference between product of predicted water saturation and porosity for our method and Archie in the shaded pinkish area	108
Figure 5.19: Well-143 water saturation predicted (red curve -4th track-) compared to Archie water saturation (blue curve -4th track-), 6th track shows the difference between product of predicted water saturation and porosity for our method and Archie in the shaded pinkish area	109
Figure 5.20: Well-29 water saturation predicted (red curve -4th track-) compared to Archie water saturation (blue curve -4th track-), 6th track shows the difference between product of predicted water saturation and porosity for our method and Archie in the shaded pinkish area	110
Figure 5.21: Well-39 water saturation predicted (red curve -4th track-) compared to Archie water saturation (blue curve -4th track-), 6th track shows the difference between product of predicted water saturation and porosity for our method and Archie in the shaded pinkish area	111
Figure 5.22: Histogram of capillary pressure at reservoir conditions for all lithofacies...	112
Figure 5.23: Histogram of J-function values calculated at reservoir conditions for all lithofacies.....	113

LIST OF ABBREVIATIONS

HCPV :	Hydrocarbon pore volume
MRGC:	Multi-resolution graph-based clustering
KNN :	K-nearest neighbor
PLT :	Production logging tool
MICP :	Mercury injection capillary pressure
FWL :	Free water level
k_r :	Relative permeability
RRT :	Reservoir rock typing
CCA :	Conventional core analysis
NMR :	Neutron magnetic resonance
mD :	Milli-Darcy
Q :	Flow Rate
ΔP :	Pressure drop in the reservoir
K :	Absolute permeability
L :	Length
A :	Cross sectional Area
μ :	Viscosity
R_o :	Completely brine saturated rock
R_w :	Water resistivity
φ :	Porosity
P_c :	Capillary pressure
SCAL :	Special core analysis

PDF	:	Probability distribution functions
R^2	:	Correlation coefficient
Kh	:	Flow capacity
LP	:	Lorenz Plot
IFT	:	Interfacial tension
σ	:	Surface tension
θ	:	Contact angel
S_{wirr}	:	Irreducible water saturation
OWC	:	Oil-water contact
OOIP	:	Original Oil in Place
$P_{c\ lab}$:	Capillary pressure at the laboratory conditions (air-mercury system)
$P_{c\ res}$:	Capillary pressure at the reservoir conditions (water-oil system)
$E_{\bar{x}}$:	Error average
$E_{St.D}$:	Error standard deviation
E_{MAX}	:	maximum absolute percent relative error
AARE	:	Average absolute percent relative error
RMS	:	Root mean squares

ABSTRACT

Full Name : Meshal Ali Al-Amri

Thesis Title : Integrated Petrophysical and Reservoir Characterization Workflow to Enhance Permeability and Water Saturation Prediction

Major Field : Petroleum Engineering

Date of Degree : May 2015

Geological information from sedimentary core description is crucial in reservoir modeling. This allows a link for an enhanced petrophysical properties estimation and various reservoir layering that makes up the reservoir. Establishing a correlation between basic reservoir petrophysical information to depositional/texture environment highly assist in predicting geology based reservoir models. Eventually, high confidence in reserves estimation is obtained when saturation height functions are modeled with a direct link to geology that are related to reservoir lithofacies when distributing water saturation height models in the reservoir section.

The objective of this work is to present a robust combined workflow using geological and petrophysical properties and show how it improves the estimation of permeability and water saturation and hence hydrocarbon pore volume estimation (HCPV). The integrated efforts presented in this research proved to be accurate in predicting fundamental reservoir properties such as permeability and water saturation. Permeability prediction is carried out using pattern recognition algorithm called multi-resolution graph-based clustering (MRGC).

Incorporating geology information with respect to well logs data, core permeability and sedimentary core description assist in predicting permeability. Minimal KNN shows an excellence agreement between core and predicted permeability that has a correlation coefficient of 0.91 that is relatively great in carbonates, complex, and diagenetic environments. This has been bench marked to show the accurate predicted model against a systematic set of criteria that includes:

- Corrected core permeability.
- Transient well testing flow capacity (kh).
- Production logging tools (PLT) results.

All of the above is established for all lithofacies in this reservoir. Later, each lithofacies is dealt with independently using mercury injection capillary pressure (MICP), porosity and permeability using water saturation height modeling “Leverett J-function”. In addition, capillary pressure analysis is presented to define representative capillarity for all lithofacies that is eventually model J-function parameters (a and b) for all lithofacies. This study shows that the outcomes from this integration led to an optimistic match with conventional petrophysical analysis using wireline inputs. Therefore, more confident match to water saturation from logs is observed especially when compared to water saturation estimated by Archie in high quality rocks, however, J-function shows more initial water saturation than Archie in low quality lithofacies (diagenetic effect) which honors reservoir heterogeneity in the modeling. As a result, an enhanced hydrocarbon in place estimation is achieved that is directly linked to geology.

ملخص الرسالة

الاسم الكامل: مشعل علي احمد العمري

عنوان الرسالة: الطريقة البتروفيزيائية و وصفية المكامن المتكاملة لتعزيز تنبأ النفاذية و تشبع المياه

التخصص: هندسة نفط

تاريخ الدرجة العلمية: شعبان 1436

المعلومات الجيولوجية من وصف الصخور المسامية تعتبر اساسية في نمذجة المكامن. هي تسمح وجود صلة لتحسين تقدير الخصائص البتروفيزيائية و مختلف طبقات المكامن. إنشاء صلة ترابط معلومات المكامن الاساسية مع بيئة الترسيب تساعد بدرجة عالية في التنبؤ الجيولوجي لنماذج المكامن. في نهاية المطاف يتم الحصول على ثقة عالية في تقدير الاحتياطيات عندما تتم نمذجة تشبع الارتفاع مع وجود صلة مباشرة للجيولوجيا و السحنة الصخرية في عملية توزيع نمذجة تشبع المياه في أي جزء من المكامن.

الهدف من هذا العمل هو تقديم سير عمل متماسك و قوي باستخدام الخصائص الجيولوجية و البتروفيزيائية كي توضح كيف أنه يزيد دقة تقدير النفاذية و تشبع المياه و بالتالي تقدير افضل لحجم الزيت و الغاز. الطريقة المتكاملة في هذا البحث يمكن لها ان تتنبأ بشكل أدق للخصائص الأساسية للمكامن مثل النفاذية و تشبع المياه. يمكن حساب النفاذية بواسطة استخدام الطريقة الخوارزمية للتعرف على النمط و التي تدعى التقسيم بواسطة تعدد الوضوح المبنية على الرسوم البيانية. دمج المعلومات الجيولوجية فيما يتعلق بسجلات الآبار و نفاذية العينات و وصف الصخور الرسوبية يساعد في تنبؤ النفاذية و التي توضح اتفاق ممتاز بين نفاذية العينات و النفاذية من التنبؤ و التي من خلالها تم الحصول على معامل ارتباط يتجاوز 0.91 و التي تعتبر جيدة نسبيا في المكامن الكربونية و بيئات المكامن الناشئة متأخرا. هذا العمل تمت مقارنته بعدد من المعايير لإظهار دقة النماذج المتوقعة و تشمل الآتي:

- نفاذية العينات المصححة.
- قوة النفاذية عبر اختبار سعة الآبار.
- نتائج ادوات و معدات تسجيل الانتاج البترية.

تم تأسيس كل ما سبق لجميع السحنات الصخرية في هذا المكن. لاحقا يتم التعامل مع كل سحنة صخرية بشكل مستقل باستخدام ضغط الحقن الزنقي الشعرية بالإضافة للمسامية و النفاذية باستخدام نمذجة تشبع ارتفاع المياه المعروفة باسم معادلة ليفريت. بالإضافة إلى ذلك يتم تقديم تحليل ضغط الشعرية للتعريف بالخصائص الشعرية لكل سحنة صخرية و في نهاية المطاف يتم تجديد معاملات معادلة ليفريت (أ و ب). و تبين هذه الدراسة أن النتائج من هذا التكامل أدى إلى اتفاق نسبي مع التحاليل البتروفيزيائية التقليدية لسجلات الآبار. لذلك لوحظ ان هناك ثقة اكبر في تشبع المياه من سجلات الآبار و مقارنتها مع تشبع المياه المقدرة من قبل معادلة أرشي في الصخور ذات الجودة العالية. أما بالنسبة للصخور ذات الجودة المنخفضة فتظهر طريقة البحث تشبع اكبر للمياه و ذلك بسبب بيئة النشوء المتأخر للمكن الغير متناسق في النمذجة. و نتيجة لذلك يمكن لنا ان نحصل على تقدير أفضل لحجم للزيت و الغاز الأصلي في المكامن البتروولية عندما يتم الارتباط المباشر مع الجيولوجيا.

CHAPTER 1

INTRODUCTION

1.1 Background

The main objective of integrating petrophysical properties is to develop a reliable reservoir static models. These models consisted of various reservoir petrophysical parameters which include and not limited to porosity, permeability, relative permeabilities, and water/hydrocarbon saturations. Pore systems vary with rock type which is related to mineralogical composition and related to certain specific fluid flow characteristics. Porosity is a simple term that refers to the mathematical ratio of pore to bulk volumes that is altered by several factors and most importantly pore-size, grain density, and grains sorting that make up the rock itself. Fluid saturation oil water and gas, is defined as the percentage of pore size that is filled with a specific fluid phase. Saturation is a function of porosity, permeability, capillarity, wettability and water salinity. Most of the oil reservoirs is initially water saturated. Migration of oil into the reservoir causes drainage of water. Therefore, as the distance above the Free-Water Level (FWL) increases progressively, smaller pores are filled and oil saturation increases. Permeability can be defined as the ability of certain fluid to move within the rock matrix that is controlled by depositional environment, porosity, pore system, grains sorting and capillarity. Relative permeability (k_r) is defined as the ratio of a specific fluid phase effective permeability to the matrix static permeability (absolute permeability) which

reflects the capacity of a given rock to produce that fluid by showing the permeability of those fluids versus water saturation as shown in figure 1.1.

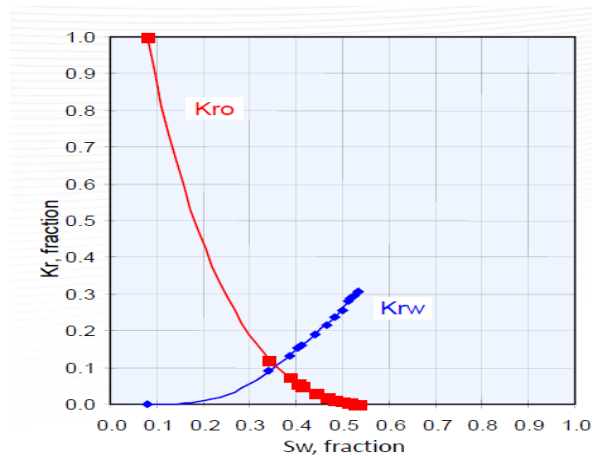


Figure 1.1: Typical Oil-Water system relative permeability curves

Laboratory techniques that use nitrogen, helium and mercury injection into core plug samples are dependable in obtaining reservoir properties. Helium is capable of filling up all connected space inside a rock sample thus giving accurate porosity values. Mercury, a fluid with very small compressibility (≈ 10 times smaller than water), is a non-wetting fluid that does not react with the rock and also possesses the ability to completely occupy pore space. Thus, measurements using mercury injection are accurate in determining pore throat sizes.

Grouping rocks into classes that have a specific range of petrophysical properties seem to be a good approach that carried out using different methods such as capillarity, reservoir rock typing (RRT) and electrofacies. These classes define a specific porosity/permeability relationships which is quite complex and challenging in carbonate

environments. Combination of different methods with lithofacies distribution in geological model that may lead to a more refined reservoir model and hence better prediction and forecasting.

1.2 Facies Determination

Classification of carbonate rocks have not been proliferated quite to the extent of sandstone classification. Nonetheless, several classifications of carbonate rocks have been published since 1960s (e.g. Power, 1962; Folk, 1962 and Dunham, 1962). The most common carbonate classification today is Dunham's classification (Dunham 1962) which simply focuses on depositional textures that were created during deposition. This classification divided the carbonate rocks into two major groups: (1) mud-supported rocks, (2) grain-supported rocks that imply if the original constituents of the limestone were or were not bound together at the time of deposition. Mud-supported limestones consists of mudstone (i.e. lime mudstones) if they contain less than 10% carbonate grains and wackstones if they contain more than 10% grains. Grain-supported limestones on the other hand consist of packstone that has 10-20% mud and grainstone that has 10% or less mud content. Dunham uses the term boundstone for limestones composed of components bound together at the time of deposition and they are larger than 2 mm.

1.3 Permeability Determination

Reserve estimation is the most used term in any reservoir simulation studies as it controls any field development plans. Reserves is the recoverable hydrocarbon volume that is

controlled by different reservoir and technological aspects such as, relative permeability, wettability, capillarity, permeability and effective porosity. Intensive work should be done to accurately quantify these rock properties. However, permeability is considered to be the highest uncertain parameter in reservoir rock evaluation. Permeability defined as ability of certain fluid to move within the rock matrix. Literature illustrates that permeability can be known from various sources such as well transient analysis, conventional core analysis (CCA), formation testers and advance logging tools (e.g. NMR).

Permeability is very essential petrophysical property that in addition to viscosity and differential pressure, it has a direct proportional effect on the fluid flow in porous media hence wells production. The permeability values can range from less than 0.01 mD to more than 1000 mD in naturally fractured reservoirs. The known Darcy's law define the fluid flow in the reservoir to the wellbore and given by:

$$Q = A \left(\frac{k}{\mu} \right) \left(\frac{\Delta P}{L} \right) \quad (1.1)$$

Darcy's Law is used to determine permeability, which is a constant when the following conditions are met:

1. Laminar fluid flow
2. No observed reaction between fluid and rock
3. Single-phase present at 100% saturation
4. Incompressible fluid type

In carbonate reservoir usually a value less than 0.01 mD is considered as the cut-off for a non-reservoir rock unless special technique is applied such as hydraulic fracturing which we call it unconventional reservoir.

In sandstone reservoirs, controlling factors on permeability include the volume and type of clay, grain size and sorting which as a result will increase the estimation uncertainty.

In figure-1.2, clean sandstone shows a perfect trend (relationship) between porosity and permeability values. On the other hand, carbonate reservoir permeability showed a cloudy relationship which is due to; dolomitization, diagenesis, vugs and fractures.

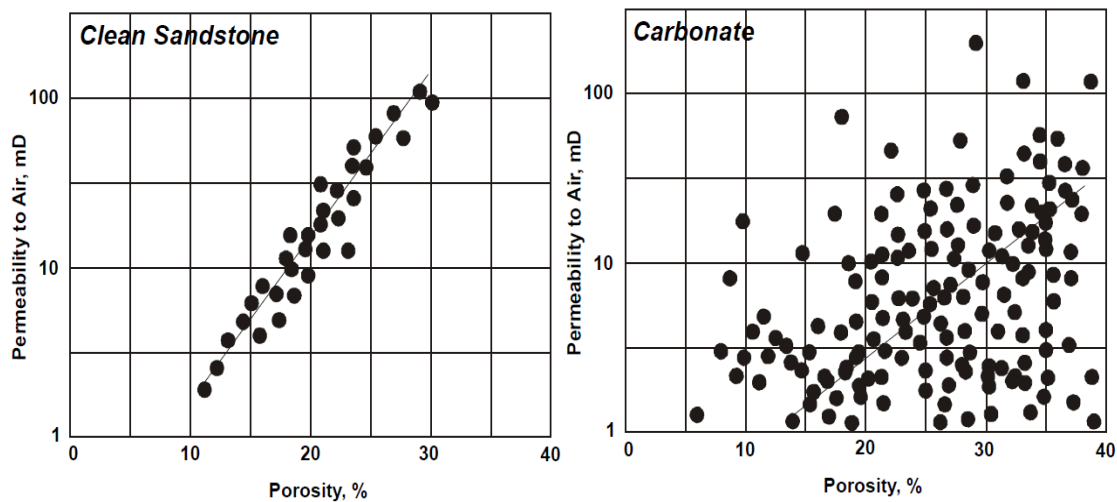


Figure 1.2: Typical porosity-permeability cross-plots

Figure-1.3 illustrates that porosity-permeability relationship varies with different pore systems and depositional environment. For a given porosity, permeability can vary from 2600 mD to 10.5 mD. This is a clear indication that lithofacies properties must be taken into consideration for an enhanced reservoir characterization. There has to be clear criteria in selecting representative core plugs that will yield to accurate basic reservoir

properties estimation. For example, core plugs should avoid vugs, fractures and moldic porosity to have a good representation of the core matrix.

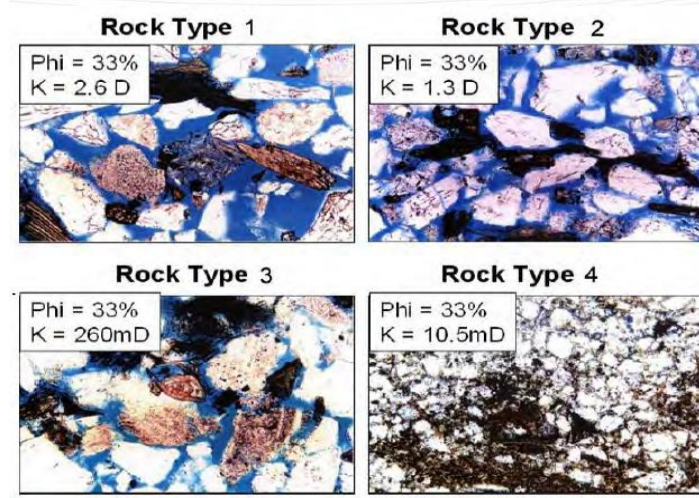


Figure 1.3: Effect of pore system on porosity-permeability relationship

1.4 Saturation Determination

Initial water saturation is an important reservoir property that helps in estimating initial hydrocarbon in place. There various methods in estimating water saturation and the known method is from logs resistivity measurements. (Archie, 1952) came up with equations using resistivity of a completely brine saturated rock (R_o), resistivity of brine (R_w), and rock actual resistivity when filled with reservoir fluid. He concluded that the formation factor (F) is correlated with porosity and certain reservoir coefficients (cementations and tortuosity) and given by:

$$F = a * \varphi^{-m} \quad (1.2)$$

$$R_t = S_w^{-n} * F * R_w \quad (1.3)$$

Other investigators estimated initial water saturation using several models. One of the most popular equation to predict water saturation that depends on capillarity is Leverett J-function that relates water saturation to permeability, porosity, wettability and capillary forces in the reservoir. He estimated water saturation by combining different rocks representing the reservoir into a single model (J-function) that converts all capillary curves to a universal one. Figure 1.4 shows that J-function for different samples that will be combined in a model that best fits them all of a power law equation derived from the below equation:

$$J(S_w) = \frac{P_c}{\sigma \cos \theta} \sqrt{\frac{k}{\phi}} \quad (1.4)$$

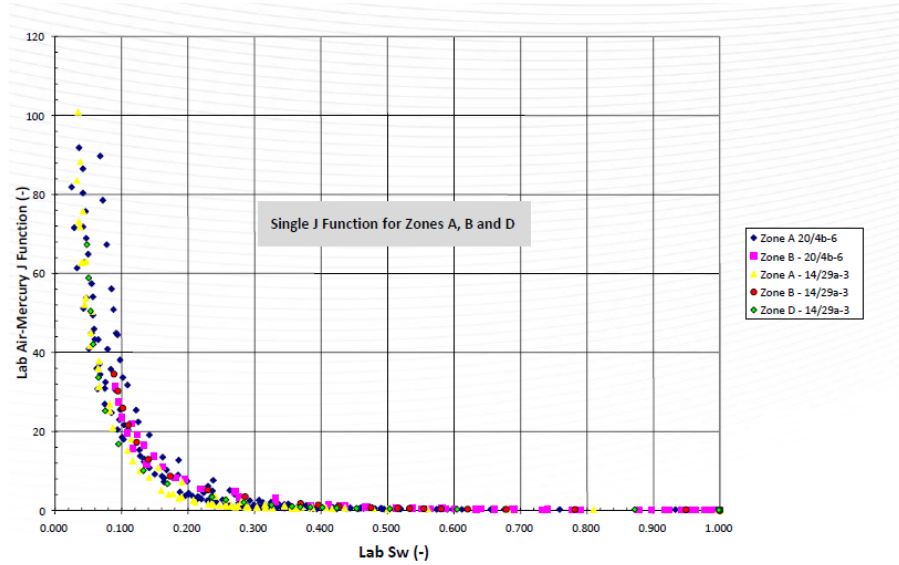


Figure 1.4: Leverett's J-function at different reservoir zones

According to Leverett, the $\cos \theta$ term was introduced to account for reservoir wettability. Capillary pressure measurement in the laboratory is conducted using different techniques such as mercury injection capillary pressure (MICP) which then can be used in the

Leverett J-function to come up with a unique model fit for each reservoir layering. J-function is then constructed and plotted using the following power law equation:

$$J = a(S_w)^b \quad (1.5)$$

The model parameters (a and b) are obtained for similar rock types and layers to define the saturation height model above the free water level. Since he recommended that layering the reservoir would greatly assist in obtaining accurate model, we will utilize this conclusion to correlate same lithofacies capillarity to examine water saturation model for each depositional environment.

1.5 Statement of the Problem

Common permeability modeling is randomly constructed using conventional core analysis (CCA) (porosity/permeability relationship) to form a non-linear relationship that will ultimately make permeability prediction as porosity transformation. In carbonate reservoirs, this relationship can be utilized to predict permeability in un-cored wells using basic log parameters. Then, a model will be constructed to extend permeability in the whole section of the reservoir. This does not take into account other important rock/reservoir properties such as grain size, sorting, tortuosity and diagenesis. In addition, pore throats play a major role in identifying accurate permeability values; this is a major challenge in Carbonate environment as there is no robust pore size identification of the pore system. The main complexity in predicting permeability is the wide variety of pore system in terms of geometry (Intergranular, Intragranular, Intercrystalline, Vuggy and Fracture) and pore sizes classes (Macro-Porosity, Meso-Porosity and Micro-Porosity).

For confident permeability characterization, coring campaign and physical core description should be planned in order to get the data from each well which is quite time consuming and need expensive laboratory measurements.

1.6 Research Objectives

The objective of this research is to implement an integrated petrophysical workflow for carbonate reservoirs to improve geological/static models in predicting permeability and saturation distribution. Reservoir permeability variation provides information on reservoir rock heterogeneity. This will be carried out using quantified geological facies model to better represent permeability family to each facie. The proposed model will be vital in characterizing reservoir matrix and improving reservoir simulation history matching for improved field strategies and enhanced reservoir engineering best practices. An attempt will be made to model saturation distribution from the constructed permeability model which will use available special core analysis SCAL (Normal Capillary Pressure and Mercury Injection Capillary Pressure, MICP) to obtain reliable saturation model for un-cored wells.

1.7 Research Methodology

The research methodology is first collecting a range of data from carbonate reservoir in Saudi Arabia which will include facies inputs, core plugs analysis, mercury injection capillary pressure data and well logs. The study will start from Geology to petrophysical modeling. The lithology facies will be built for the studied cores. Each facie will have a permeability range related to its quality. In carbonate environment, we are dealing with

Micro and Macro pore systems. The quality range is wide and each rock type is characterized by a lithofacies. The permeability model will be constructed by modeling each facie with its representative permeability range from core and link them accordingly. Finally, a saturation height model will be assigned for each facie to at most correct saturation values from well logs.

CHAPTER 2

STATE OF THE ART LITERATURE REVIEW

In this chapter, we summarize most important researches that evolved around the permeability prediction as well as water saturation using various techniques and methods. This helps in identifying the baseline for way forward for our implemented workflow. Several investigators have gone around our topic which their studies are summarized as follows:

The importance of pore texture on the physical properties in carbonates was first realized by (Archie, 1952). He first classified carbonate rocks by their pore size to get an approximation on the permeability. Porosity is subdivided into visible macro-porosity and matrix micro-porosity. The visible macroporosity is divided in pore size classes; pore size is increasing from class A with no visible macro-porosity up to class D with pore sizes larger than cutting size. Further, the matrix microporosity is divided as being in between sucrosic crystals ($>50\text{ }\mu\text{m}$ crystals), in chalky matrix ($<50\text{ }\mu\text{m}$ crystals) or in compact matrix.

(Lucia, 1983) introduced a qualitative carbonate pore type classification which is based on pore size and pore connectivity and its effect on the petrophysical properties. For example, moldic and interparticle porosity fall both in the same fabric selective pore classification after Choquette and Pray's (1970), but they show very different porosity-

permeability trends. He subdivided porosity into touching vugs porosity, separate vugs porosity and interparticle pore space. All three groups have differences in the quality of connected pores. As a result, all three groups show distinct porosity-permeability relationships.

(Usman, 1991) discussed the importance of permeability estimation and compared the measurement techniques. Three main measurement techniques were studied in this work such as wireline log, core laboratory and well testing. Several approaches were conducted under each technique. In single phase flow, well test gives the most reliable permeability values among all methods. On the other hand, wireline logs show better permeability estimation for more than phase flow. Usman suggested that permeability correlations should be integrated with available information such as wireline logs, core laboratory and well testing to enhance the accuracy of permeability values.

In the case of porosity which is solely made up of interparticle pore space, (Lucia, 1993) showed that the grain size distribution has a dominant effect on the interparticle porosity – permeability relationship. Fine grained carbonates ($<20\ \mu\text{m}$) with mud and crystal size controlling the small pore size distribution, display the lowest permeability at any given porosity. Grain dominated carbonates in which mud and grain size controls the pore size ($20 > 100\ \mu\text{m}$) and subsequently coarse grained carbonates ($>100\ \mu\text{m}$) have higher permeability at any given porosity.

Traditional methods for estimation formation permeability values have high uncertainty due to many assumptions such as linear regression and empirical inferences. (Maghsood, 1996) presented an improved method to estimate permeability values using Hydraulic Unit (HU) technique. The aim of this paper is to calculate permeability values in uncored wells. Many algorithms and graphical methods were used to support his work. Maghsood applied Bayesian Inference technique for assigning probability distribution function (PDF) of log values to each hydraulic flow units and then classify to which PDF certain set of logs most likely fit. His method was applied into two carbonate and laminated sandstone formations in which excellent results were achieved from this method and matched to permeability values from Pressure Test Analysis PTA technique. In this paper a comparison of permeability estimation provided between HU and conventional methods to show how HU method is valuable among all techniques.

(Gunter, 1997) described a technique that combines basic reservoir properties i.e. bed thickness, porosity and permeability information for flow units calculations. They applied Modified Lorenz plots (MLP) for characterization. This method of flow unit determination is quite useful because it only requires routine porosity and permeability data (from logs and/or core), is independent of facies information, and utilizes simple cross-plotting techniques. However, facies and depositional environment is essential in an integrated reservoir petrophysical modeling.

(Morris and Biggs, 1997) developed an empirical correlation to predict permeability at initial water saturation. They defined the correlation of logs calculated porosity and resistivity based saturation to estimate permeability by:

$$k^{1/2} = \frac{c\varphi^3}{S_{wi}} \quad (2.1)$$

Where c is a constant which is a function of reservoir fluid density.

(Fleury, 2002) proposed a model that included the non-Archie behavior which accounts for resistivity measurements on double DPC porosity (Dual Porosity Conductivity) or triple porosity TPC (Triple Porosity Conductivity) micritic and oolitic carbonates. The proposed model for DPC is:

$$RI \text{ (Resistivity Index)} = S_{w1}^{-n_1} \frac{1+\alpha}{1+\alpha S_{w1}^{-n_1}} \text{ for } S_w \geq S_c \quad (2.2)$$

$$RI \text{ (Resistivity Index)} = S_{w1}^{-n_1} \frac{1+\alpha}{1+\alpha S_{w1}^{-n_1}/S_{w2}^{-n_2}} \text{ for } S_w \leq S_c \quad (2.3)$$

Where: n_1 is the saturation exponent at high S_w , n_2 is the saturation exponent at low S_w , α is the ratio between micropores to macropores fraction and S_c is the average water saturation at which micropores invaded. In this model (DPC), 4 parameters have to be identified; S_c which can be determined from MICP data with some degree of uncertainty while other parameters are fitted.

(Jennings and Lucia, 2003) concluded sequence-stratigraphic framework would be more systematically organized using rock-fabric classification instead of using the direct relationship of porosity and permeability. They introduced a new parameter called rock-fabric number (λ) which is a function of two reservoir parameters above capillary

transition zones: initial water saturation and porosity.. A generalized permeability-porosity-rock fabric relationship is given by:

$$k = e^{a(\lambda)} \varphi_{ip}^{b(\lambda)} \quad (2.4)$$

$$a(\lambda) = a_0 - a_1 \ln(\lambda) \quad (2.5)$$

$$b(\lambda) = b_0 - b_1 \ln(\lambda) \quad (2.6)$$

Where $a(\lambda)$ and $b(\lambda)$ are rock fabric coefficients.

(Pablo, 2003) proposed a method to predict permeability from well log responses and conventional core analysis. First, he classified the reservoir using mathematical tools from integration of available information such as petrophysics, lithofacies, electrofacies and hydraulic flow units. Then, core permeability values mapped and calibrated with well logs data using neural networks. This shows better results than canonical methods. The disadvantage of this method is that it requires adequate number of data.

Many studies showed that estimation of permeability in carbonate formation is considered to be a very challenge task due to changes in both depositional environment and diagenesis effect on porosity/permeability relationship. (Perez, 2005) proposed a statistical tool named classification-tree analysis that classified data and separating permeability predictions from well logs based on three different approaches: electrofacies, lithofacies and HFUs. A comprehensive study conducted to compare the three approaches, electrofacies approach showed better permeability prediction compared to other approaches.

Permeability estimation in heterogeneous reservoir is a challenge work to handle accurately. Many researches tried to relate permeability and reservoir properties using complex mathematical equations in which resulted inaccurate estimation of formation permeability values. (Shokir, 2006) proposed a permeability model to predict uncored wells using Fuzzy model. Fuzzy model proves best way to model heterogeneous formations, nonlinear and multivariable petrophysical reservoir properties. One of the main advantageous of Fuzzy model is that it doesn't require prior assumptions for the measured data. Three wells were studied by using Fuzzy model and compared to other models, Fuzzy model showed excellent results with correlation coefficients about 1. Shokir recommended that, collection more data will enhance the fuzzy model and reduce the uncertainty.

(Anouk, 2007) proposed another workflow for a carbonate formation (Natih, Oman). The objective of his methodology is to gather variety of scales of heterogeneity to a field reservoir modeling. In addition, he successfully captured the heterogeneity effect on fluid displacement, vertical to horizontal permeability ratio and sweep efficiency. The study showed that the ratio of different rock types used and the 3-D classification of good to poor permeable rocks resulted in a big effect on both flow and recovery in which they should be included in reservoir simulation models.

(Maclean, 2008) presented an astonishing approach for water saturation predication based on new saturation/height model. He started to develop the model by link both depositional and diagenetic rock texture to HU. After that, he combined the obtained HU

to the zones with same capillary pressure relation.. He calculated water saturation values from three different models: Leverett J-function, FOIL and Modified FOIL functions. After that, he compared the estimated values with water saturation from core capillary experiments which is the reference in his study. The comparison study showed that the Modified FOIL is the best model that produces the highest correlation coefficient of 0.985. Since this model showed accurate results among all proposed models and doesn't need any permeability values, it can be used in uncored wells.

Several researches showed that no unique technique is available to identify reservoir properties cutoffs. (Worthington, 2008) suggested that the key factor for proper cutoffs identifications is to link conventional core analysis to a reference parameter that assist in distinguishing reservoir and non-reservoir sections. He proposed a methodology to apply in a way that follows rock typing criteria and at the same time honors different measurement sampling size.

(Yarra et. al., 2008) concluded that especially in clustering modeling training data values can be grouped based on specified associated parameters. One of them is multi-resolution graph-based clustering (MRGC). It solves dimensionality problems that usually occurs when log data is relatively constrained with few clusters. This will merge large number of clusters into a small cluster that was assigned from the geological characterization. It also reduces several drawbacks that come from conventional method.

Describing hydrocarbon productivity of certain reservoir required full understanding of reservoir characterization of that reservoir. (Mohamed, 2011) proposed a methodology called Reservoir Rock Type (RRT) that used to link petrophysical properties with lithofacies as one model. The objective to utilize RRT methodology to characterize Kharaib reservoir, which include the following criteria:

1. Each RRT has distinguished depositional environment with diagenesis effect.
2. Porosity/Permeability relationship rarely overlaps for any RRT.
3. Using capillary pressure curves, pore-size distribution is the dominating properties any RRT.
4. For any given wettability curves, RRT has similar relative permeability curves.

CHAPTER 3

DATA DESCRIPTION AND VALIDATION

In this study, 38 vertical wells have been considered with more than 4,000 core plug samples from carbonate reservoir have been used for permeability and water saturation prediction. Conventional Core Analysis (CCA) was performed for all core samples beforehand to measure porosity and permeability in laboratory conditions. In addition, lithofacies description has been carried out for cored wells to identify the number of facies in the reservoir of study as well as build a robust geological lithofacies model to be propagated in reservoir section and then improved using wireline openhole logs for uncored wells. Moreover, wireline logs were prepared as input parameters for permeability models. Intuitively, three main input sources of data are used in this study to come-up with a permeability model for each lithofacie and hence water saturation is derived which include core plug samples measurements, wireline logs measurements and lithofacies model inputs.

In this chapter, quality control of CCA data is performed to correct for laboratory conditions which includes applying overburden corrections for porosity values, Klinkenberg effect of permeability values and depth shift between core data and wireline logs. After performing the necessary overburden and Klinkenberg effects corrections, a depth shift of data is carried out by plotting core data with wireline logs. Usually, spectral gamma-ray (SGR) reading is used as a reference in depth-shifting however dealing with

carbonate reservoir making it difficult to distinguish for signatures and markers although sandstone is a perfect formation to use SGR as shale sections are differentiated by high GR. Therefore, corrected core porosity (shown as black dots) is plotted against wireline corrected porosity from neutron-density cross plot (shown as red curve) to obtain the best depth match. This was achieved with around 4 to 12 ft depth adjustment to wireline logs porosity values due to elasticity of the wireline tools. Figures 3.1 and 3.2 show the data before and after the depth shift in the highlighted sections for two wells. This resulted in an excellent depth match between core and wireline logs. In addition, both statistical and graphical representations of the filtered data are shown in figures 3.3, 3.4 and 3.5 for corrected core porosity, permeability and logarithmic values of permeability as it is believed that permeability usually logarithmically distributed. Table 3.1 shows data description for the filtered data.

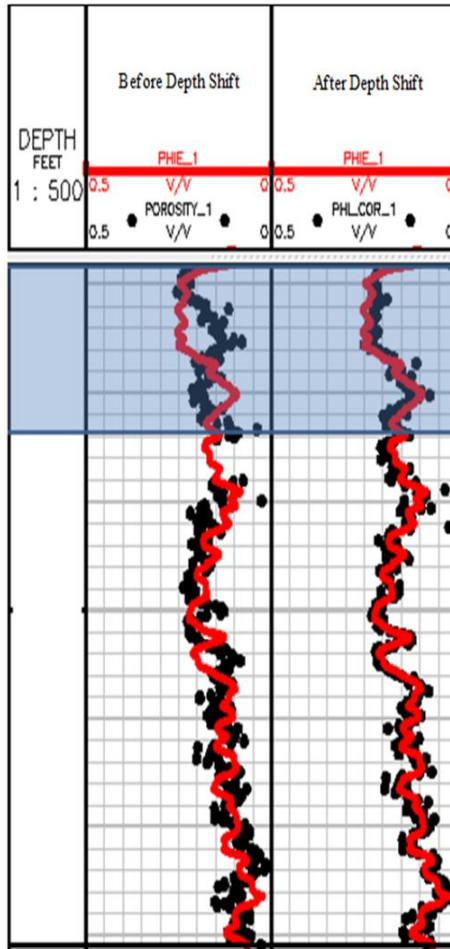


Figure 3.1: well 142 depth shift technique for data preparation

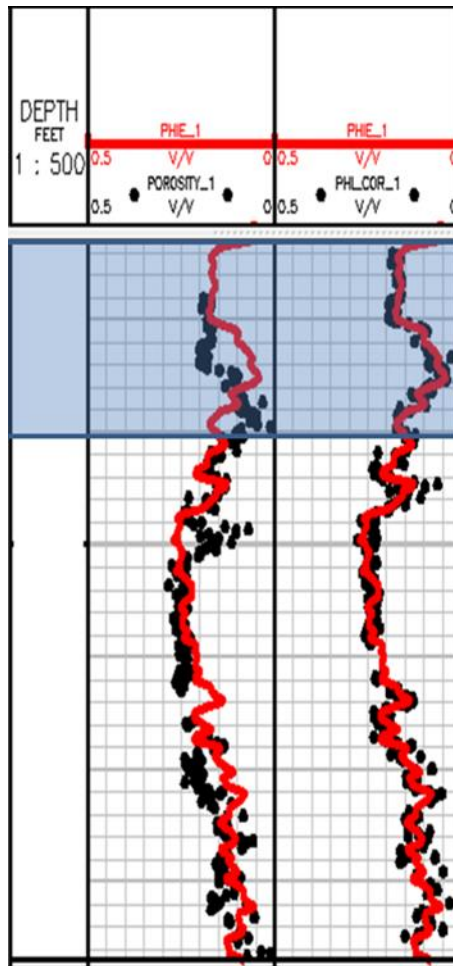


Figure 3.2: well 101 depth shift technique for data preparation

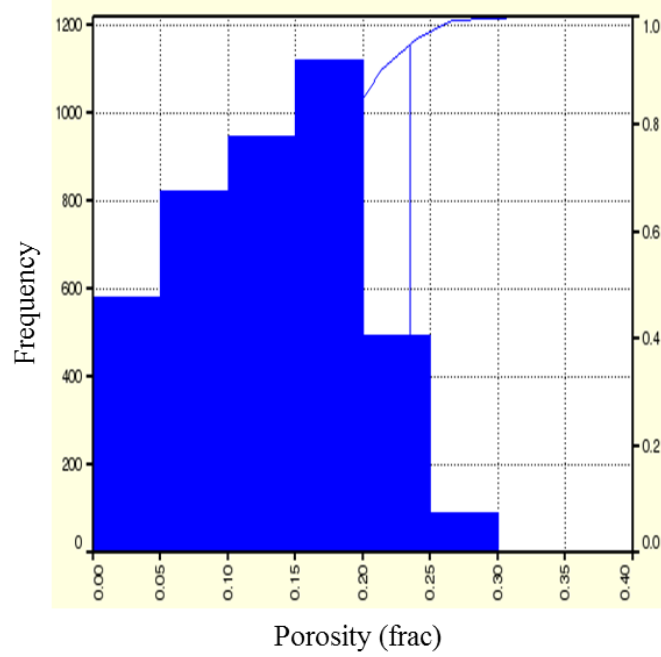


Figure 3.3: Filtered corrected core porosity histogram

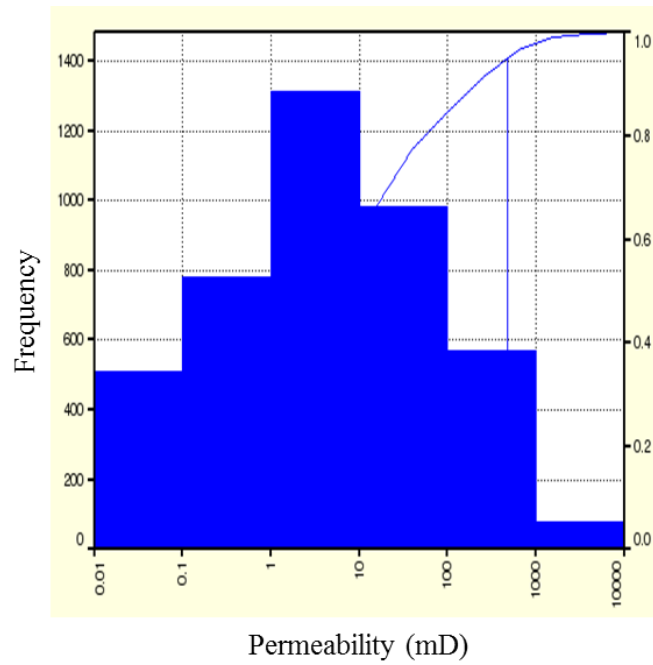


Figure 3.4: Filtered corrected core permeability histogram

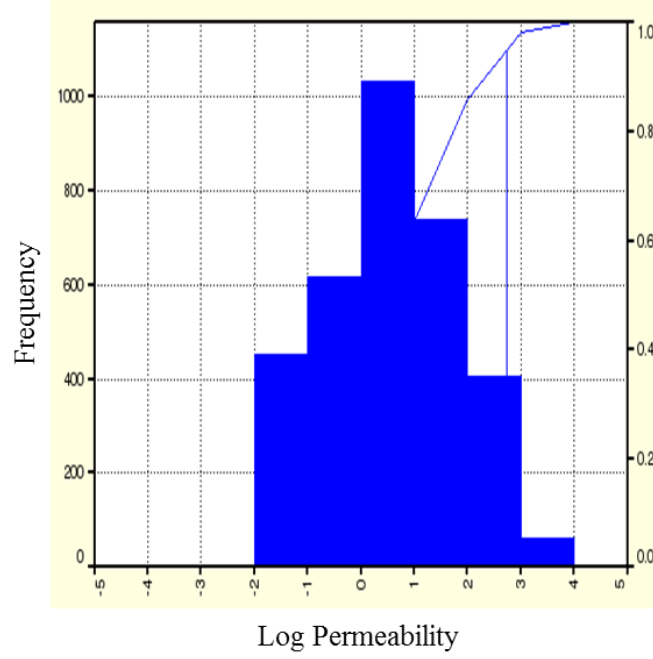


Figure 3.5: Filtered logarithmic corrected core permeability histogram

Table 3.1: Statistical data description of the core corrected porosity and permeability for filtered data.

Parameter	Min	Max	Average	St. Dev	Skewness	Kurtosis
Porosity	0.0002	0.2936	0.1293	0.0653	-0.0478	2.1106
Permeability	0.0297	4892.2197	86.8585	292.2680	7.1901	74.0382
Log Permeability	-1.5271	3.6895	0.5666	1.2176	0.1006	2.2751

After performing the depth shift, a systematic approach for data filtration was followed to define which data set is considered for this study to eliminate introducing unknown factors in the modeling. Using standard deviation of corrected porosity difference, it is then applied to the absolute difference between the corrected core porosity and wireline log porosity to filter the data that exceed the standard deviation of the absolute difference. The absolute difference should not exceed the standard deviation of the corrected core porosity to include all relevant data at this specific depth whereas high absolute difference of more than the standard deviation is considered as a bad data point which in this context is neglected to ensure high level of confidence on the final selected set of data. This does not mean that removed data set is outliers however, more investigation needs to be carried out to assess the measurements deviation, which is not part of the study scope, which could be due to different measurement sizes between logs and core data. In addition, some of the porosity measured in the laboratory exhibited low grain density which in turn results in wrong porosity calculations. Figure 3.6 shows an example of data points fall outside the standard deviation of the absolute difference of porosities. Standard deviation is high when more scattered the data. Figures 3.7 and 3.8 show graphical description and histogram of all 38 wells absolute difference between core samples porosity and wireline logs porosity and difference between porosities, respectively which give a standard deviation of 0.0201 porosity units (pu). A statistical description of the data utilized in the data filtration is shown in Tables 3.2 and 3.3. As a result of the filtration process, 4299 data points are within the above set criteria which have been considered for permeability modeling. Figures 3.9 and 3.10 show neglected

data from permeability modeling in red dots while the black dots are the values included in the following analysis.

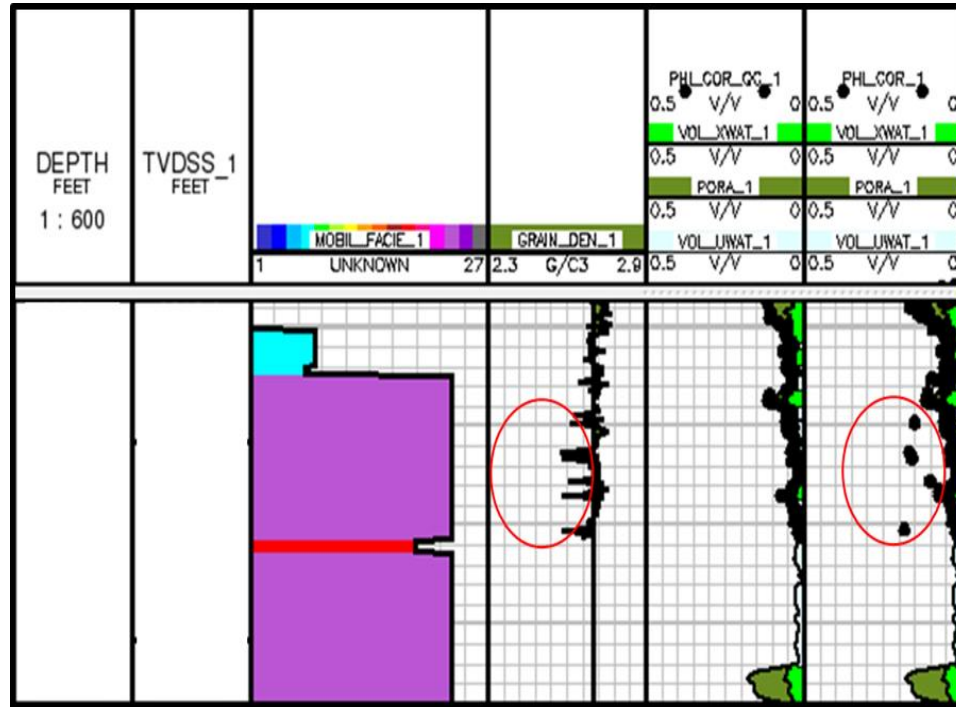


Figure 3.6: Well-115 showing process of data removal using grain density measurement.
(6th and 5th tracks show porosity before and after data filtration, respectively)

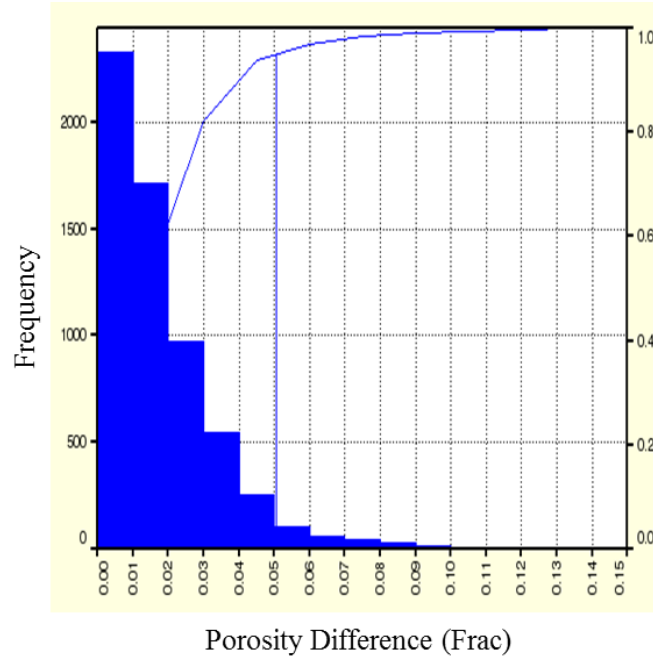


Figure 3.7: Histogram of absolute difference between corrected core porosity and neutron-density values

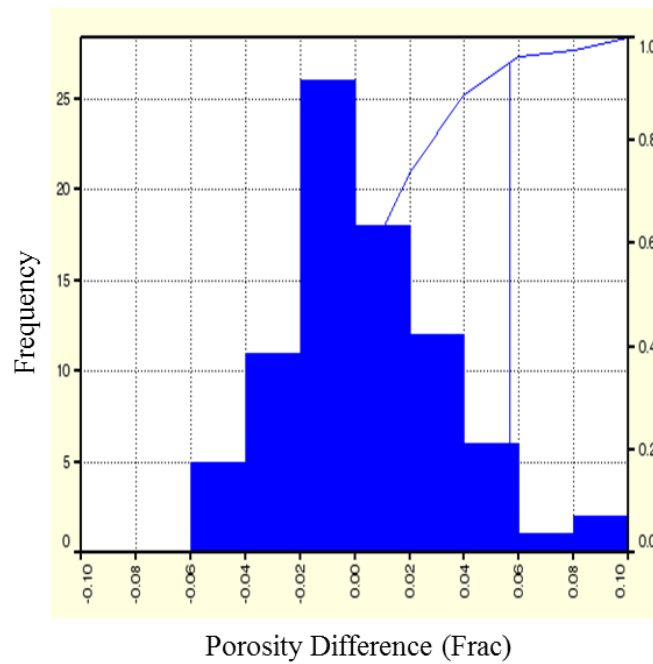


Figure 3.8: Histogram of difference between corrected core porosity and neutron-density values

Table 3.2: Statistical data description of the absolute difference between core porosity and wireline logs porosity.

Parameter	Min	Max	Average	St. Dev	Skewness	Kurtosis
Value	0	0.1551	0.0174	0.0201	2.2340	11.5904

Table 3.3: Statistical data description of the difference between corrected core porosity and wireline logs porosity.

Parameter	Min	Max	Average	St. Dev	Skewness	Kurtosis
Value	-0.1352	0.1551	0.0006	0.0201	-0.2901	6.3191

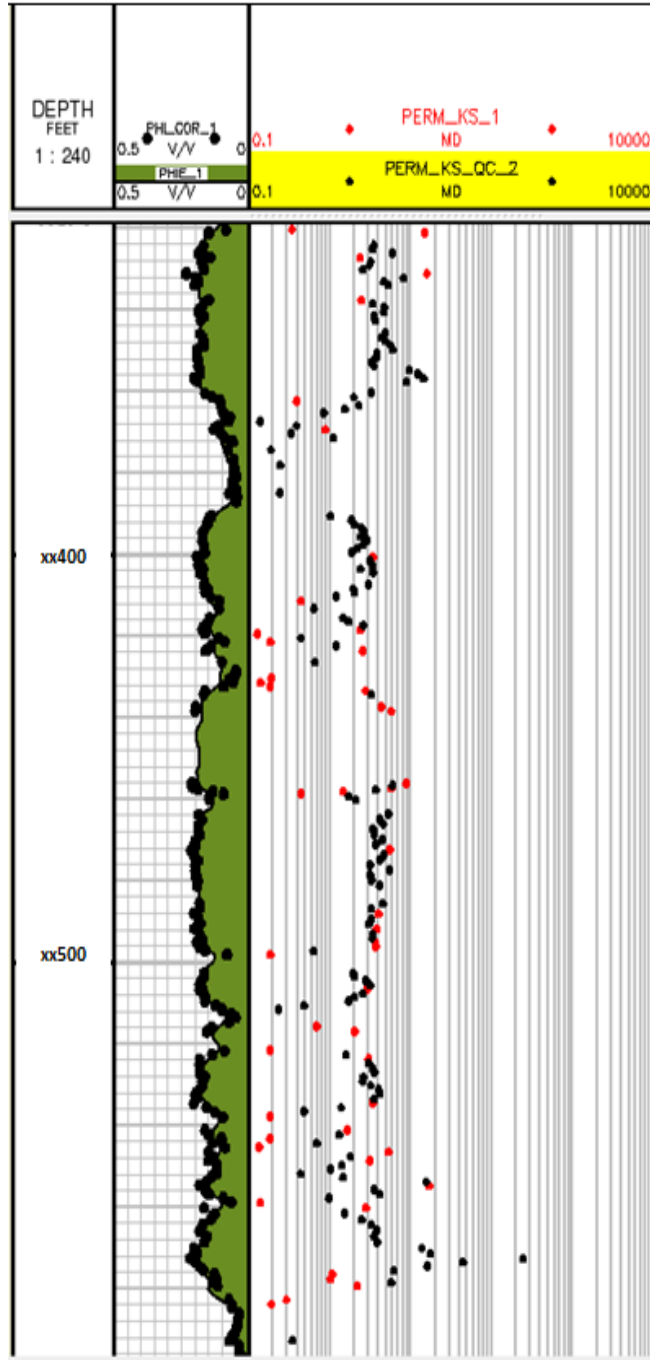


Figure 3.9: well 143 removed permeability values in red which falls outside the recommended range for porosity standard deviation.

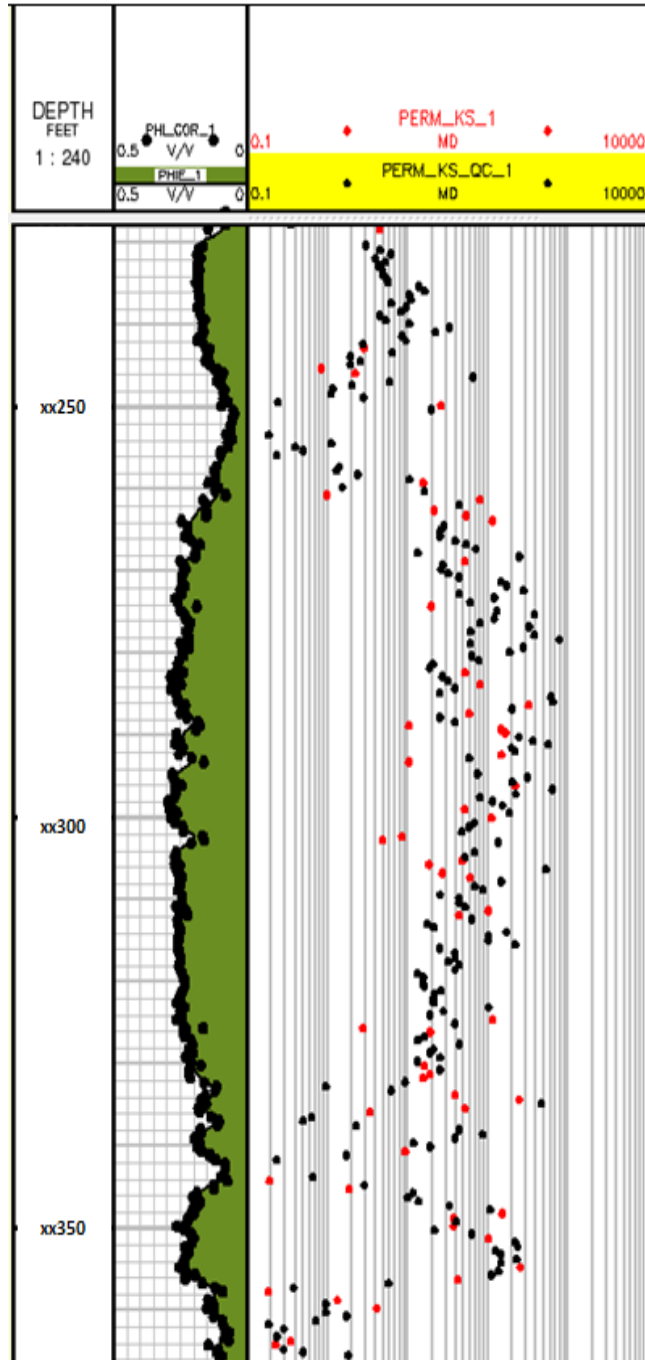


Figure 3.10: well 182 removed permeability values in red which falls outside the recommended range for permeability standard deviation.

Lithofacies description has been completed beforehand for the selected 38 vertical wells. 17 lithofacies have been identified that represent the various depositional environments of the understudy reservoir. Every lithofacie has a range of permeability values depending on the depositional cyclicity. Depositional cyclicity is a common characteristic of carbonate platform sequences, which is evident in this reservoir at a variety of scales ranging from centimeter and decimeter scale bedforms to larger scale packages of sediment approaching 15 feet to 30 feet in thickness. Recognition and interpretation of these larger scale cycles provides the basis for defining chronostratigraphic surfaces, identifying time-equivalent facies, and constructing a depositional and sequence-stratigraphic framework for the reservoir section. This unified framework describes the three-dimensional geometry of the reservoir and provides a means for evaluating historical fluid movement and overall reservoir performance. Detailed facies mapping within each cycle of deposition allows the sequential development of the reservoir.

Late Jurassic carbonates (algal and skeletal grainstones) were deposited on a gently sloping ramp between shallow-marine, high energy Rimthan Platform to the north, and the deeper marine, low-energy Arabian Basin to the south. Vertically, the reservoir carbonates generally exhibit coarsening upward sequence. The reservoir grainstones, in turn, are overlain by low-energy, organic-rich lime mudstones. Laterally, reservoir carbonates form a wedge-shaped sedimentary body that varies in thickness from about 230 feet in the north to about 50 feet in the south. The high to moderate energy grainstone facies in the north become finer grained to the south by being gradually replaced down ramp. Reconstruction of the reservoir depositional profile indicates that sedimentation occurred on a gently-inclined, essentially homoclinal ramp, exhibiting between 0.06 and

0.5 degrees dip. It's noteworthy that absence of lagoonal or peritidal deposits along with absence of exposure surfaces, suggests that subaqueous marine conditions were largely maintained across the ramp and throughout the reservoir deposition.

Lithofacies ranges of permeability and logarithmic of permeability are summarized in tables 3.4 and 3.5, respectively with basic statistical data description for all lithofacies. In addition, permeability and logarithmic histograms are shown for every lithofacies from figure 3.11 to figure 3.26. Lithofacies geological description is also provided in table 3.6.

Table 3.4: Statistical data description of permeability values for each lithofacie.

Parameter	# of data	Min	Max	Average	St. Dev	Skewness	kurtosis
F#1	766	0.0312	4892.2197	428.9388	600.0280	3.2421	17.3608
F#2	66	0.0882	1287.5479	288.4902	406.7406	1.1505	2.9370
F#4	308	0.0328	212.8918	6.3759	13.7143	11.9970	172.8986
F#7	165	0.0327	2691.9016	167.1754	398.6231	4.0234	21.5218
F#8	245	0.0301	2610.6423	34.8726	198.7767	10.0689	121.1613
F#9	33	0.0300	14.0905	1.5520	2.7866	3.1526	13.8216
F#10	44	0.0312	18.5210	0.9215	2.8000	5.8378	37.1549
F#11	14	10.0580	3932.6348	632.6297	1130.4022	2.0831	6.3170
F#15	670	0.0304	2510.4165	56.0915	161.4986	10.9471	154.7965
F#16	498	0.0305	778.2294	34.7678	83.2302	5.0945	34.6333
F#17	89	0.0330	254.1680	9.1040	32.9276	6.0000	40.7016
F#18	59	0.0308	87.3956	5.9691	12.6331	5.0000	31.03229
F#19	312	0.0314	567.5065	23.3077	63.9905	5.4568	38.7586
F#20	170	0.0298	468.19427	11.88838	41.19430	8.61107	91.24420
F#21	87	0.0313	37.63947	3.51082	5.67810	4.68879	25.41664
F#22	40	0.0315	5.83300	1.11019	1.19964	1.76726	7.06455
F#23	726	0.0297	466.06104	5.94396	29.97790	8.64373	99.84715

Table 3.5: Statistical data description of logarithmic of permeability for each lithofacie.

Parameter	# of data	Min	Max	Average	St. Dev	Skewness	kurtosis
F#1	766	-1.5053	3.6895	2.0603	1.0240	-1.3514	4.6544
F#2	66	1.0546	3.1098	1.1645	1.4332	-0.01422	1.5424
F#4	308	-1.4845	2.3282	0.5646	0.4822	-0.8079	5.6482
F#7	165	-1.4855	2.6644	0.8038	1.2632	-0.2745	1.6327
F#8	245	-1.5149	3.4168	-0.4380	1.0652	1.0269	3.6209
F#9	33	-1.4819	1.1489	-0.3545	0.7818	0.0586	1.8364
F#10	44	-1.5062	0.3696	-0.7101	0.5732	0.3593	2.1085
F#11	14	1.0025	3.5947	2.0794	0.9828	0.2058	1.4962
F#15	670	-1.5084	3.3998	1.1532	0.8181	-0.5314	3.3657
F#16	498	-1.5158	2.8911	0.8157	0.8762	-0.1605	2.7048
F#17	89	-1.4820	2.4051	0.4370	0.5470	0.3572	7.4109
F#18	59	-1.5114	1.9411	0.3528	0.65082	-0.6111	4.2926
F#19	312	-1.5031	2.7540	0.5195	0.9867	-0.0724	2.3365
F#20	170	-1.4952	2.6704	0.1080	1.0268	0.2298	2.1333
F#21	87	-1.5051	1.5756	0.2334	0.6463	-1.1662	4.2900
F#22	40	-1.5012	0.7859	-0.2355	0.6665	-0.6859	2.2622
F#23	726	-1.5241	2.6684	-0.5706	0.9105	1.2137	4.2056

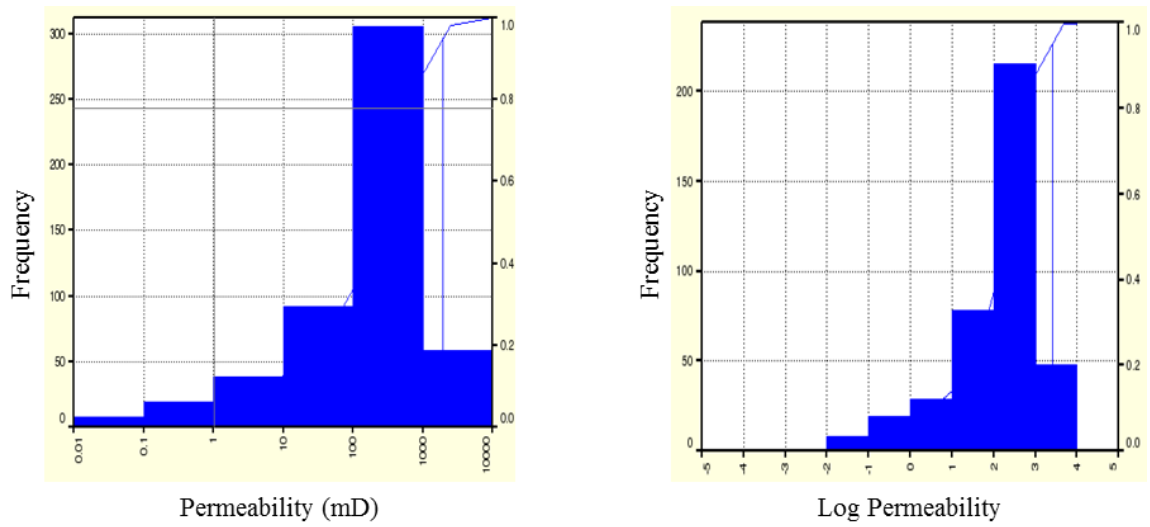


Figure 3.11: Lithofacie-1 permeability and logarithmic of permeability histogram

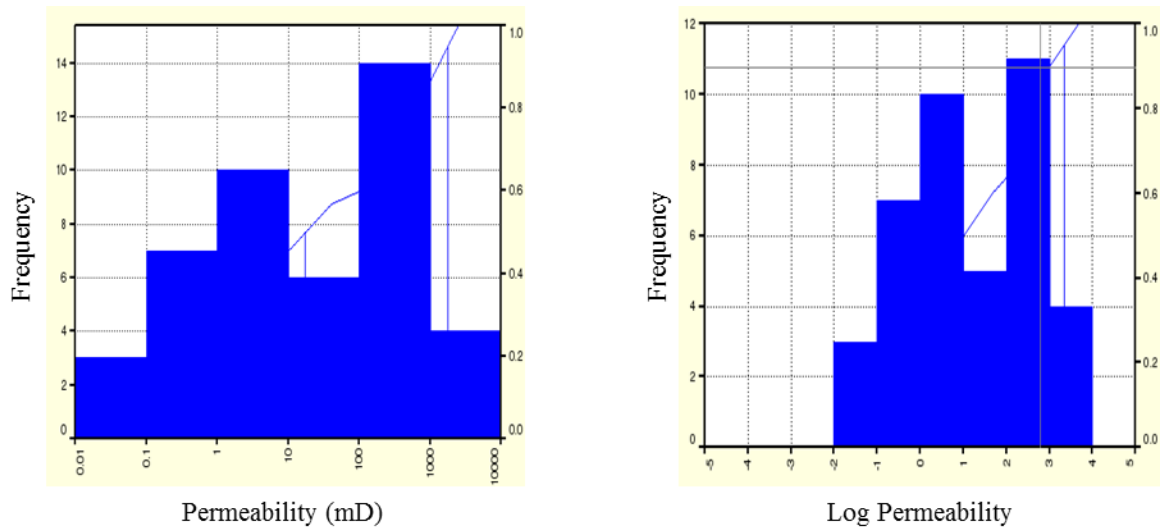


Figure 3.12: Lithofacie-2 permeability and logarithmic of permeability histogram

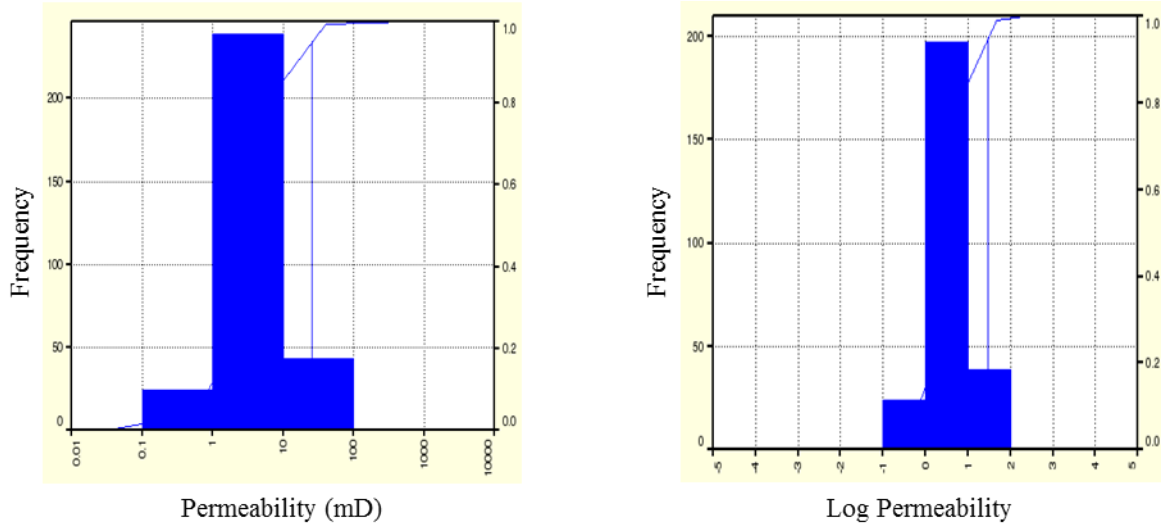


Figure 3.13: Lithofacie-4 permeability and logarithmic of permeability histogram

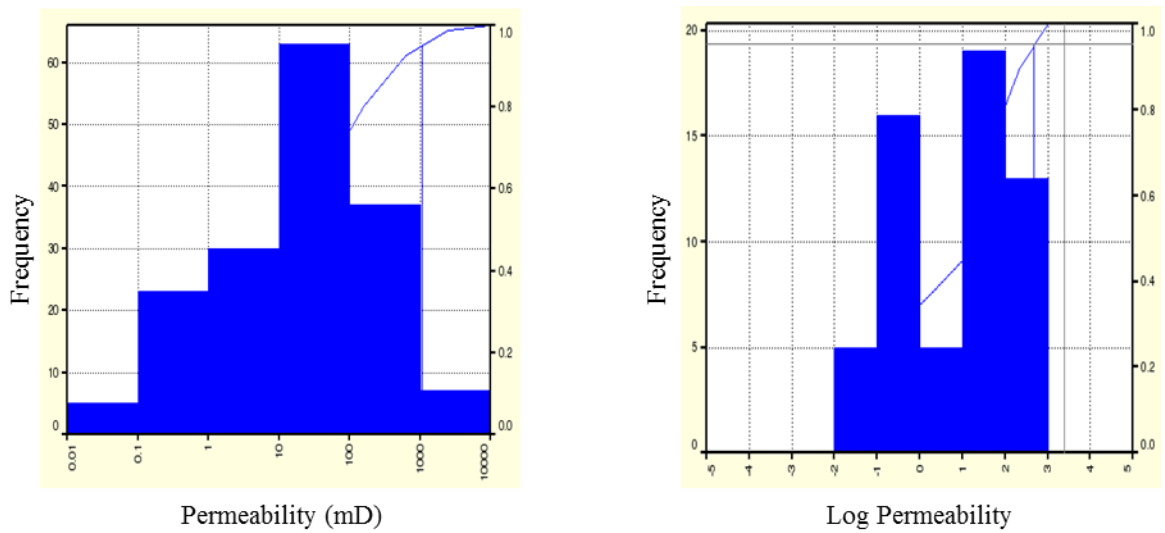


Figure 3.14: Lithofacie-7 permeability and logarithmic of permeability histogram

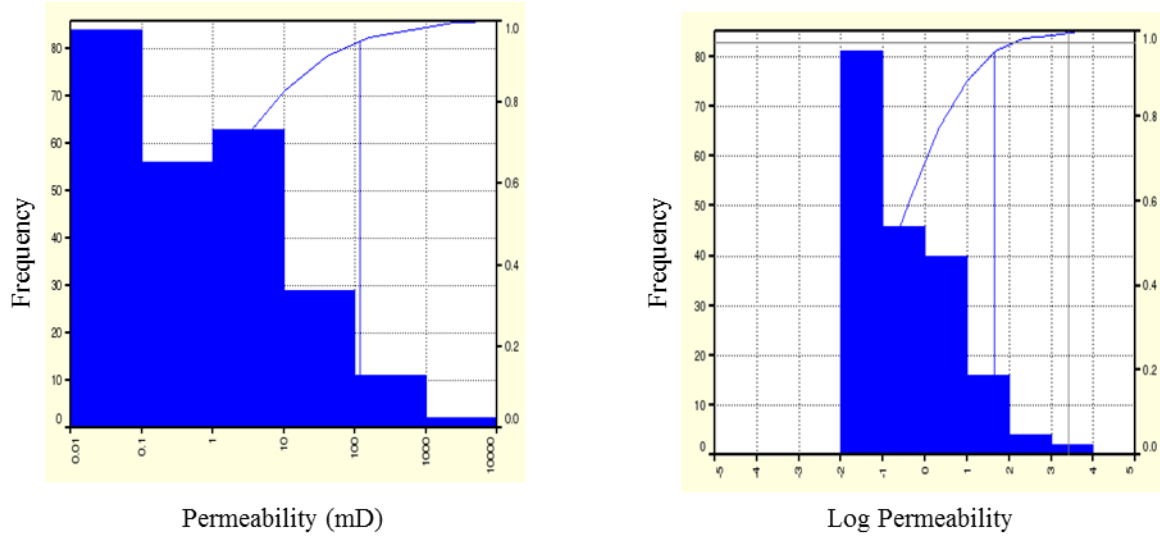


Figure 3.15: Lithofacie-8 permeability and logarithmic of permeability histogram

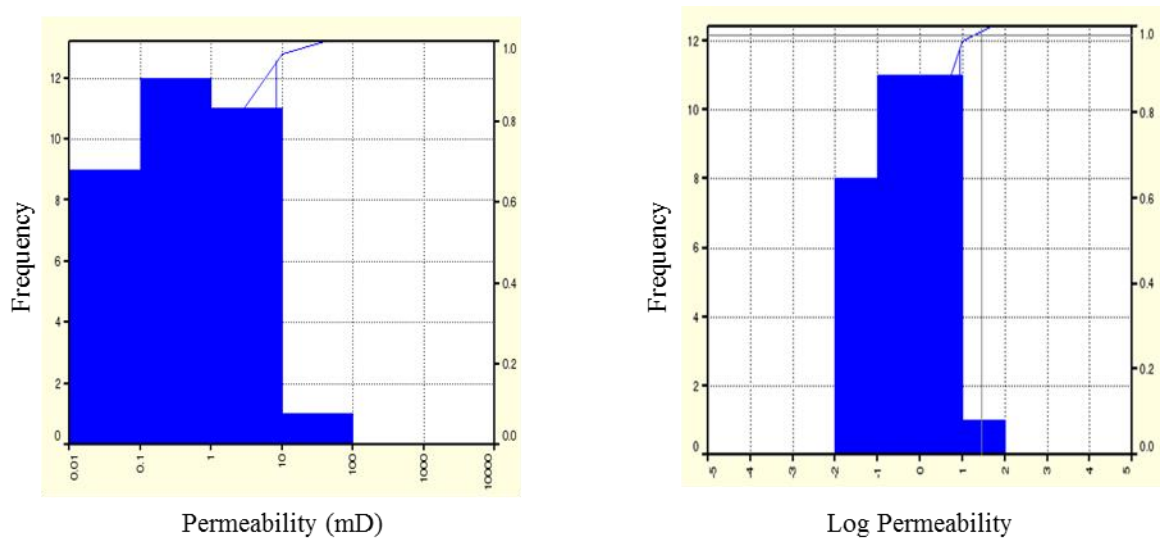


Figure 3.16: Lithofacie-9 permeability and logarithmic of permeability histogram

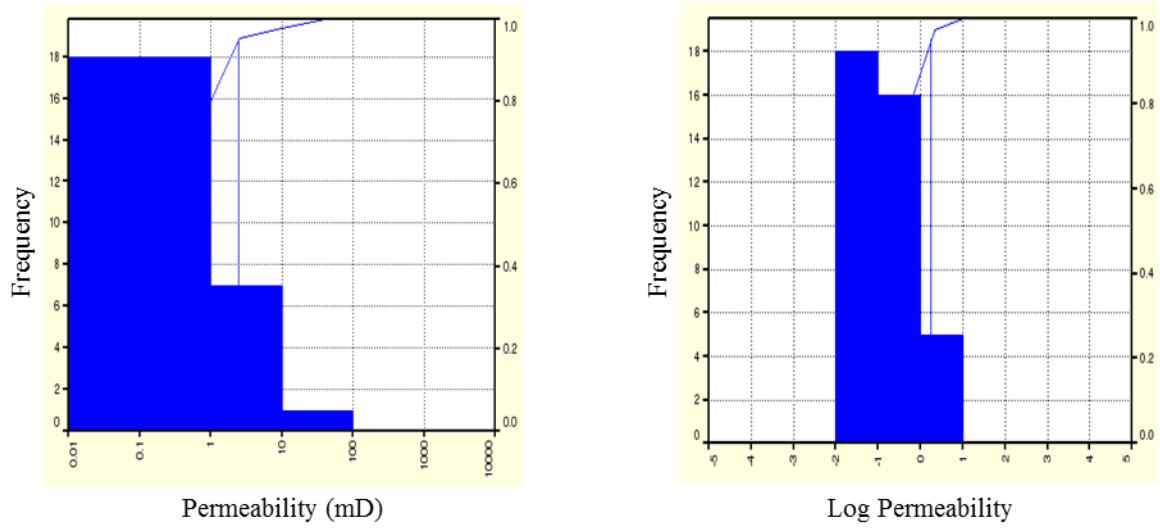


Figure 3.17: Lithofacie-10 permeability and logarithmic of permeability histogram

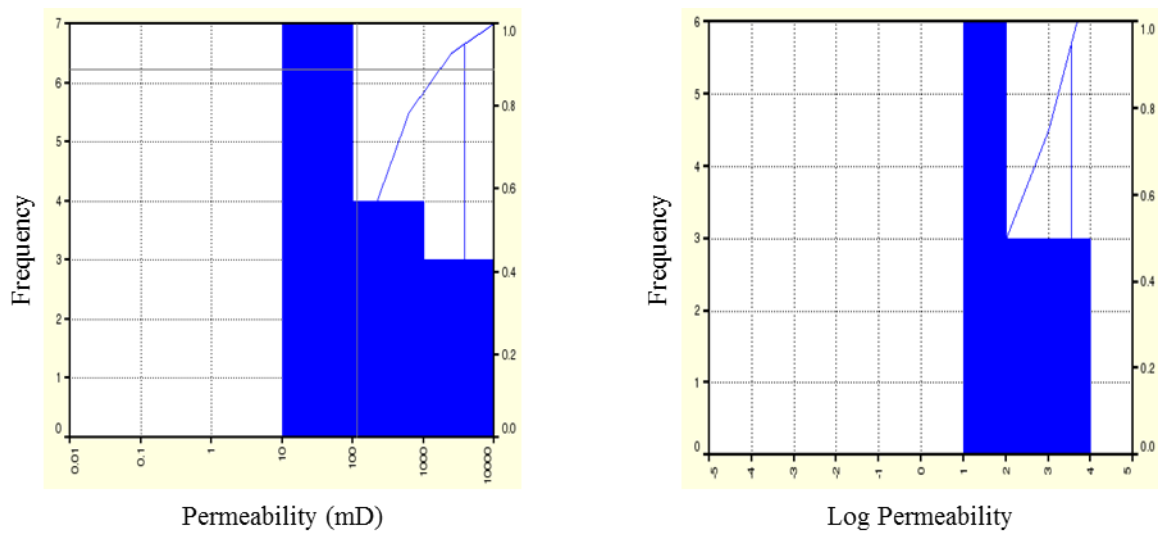


Figure 3.18: Lithofacie-11 permeability and logarithmic of permeability histogram

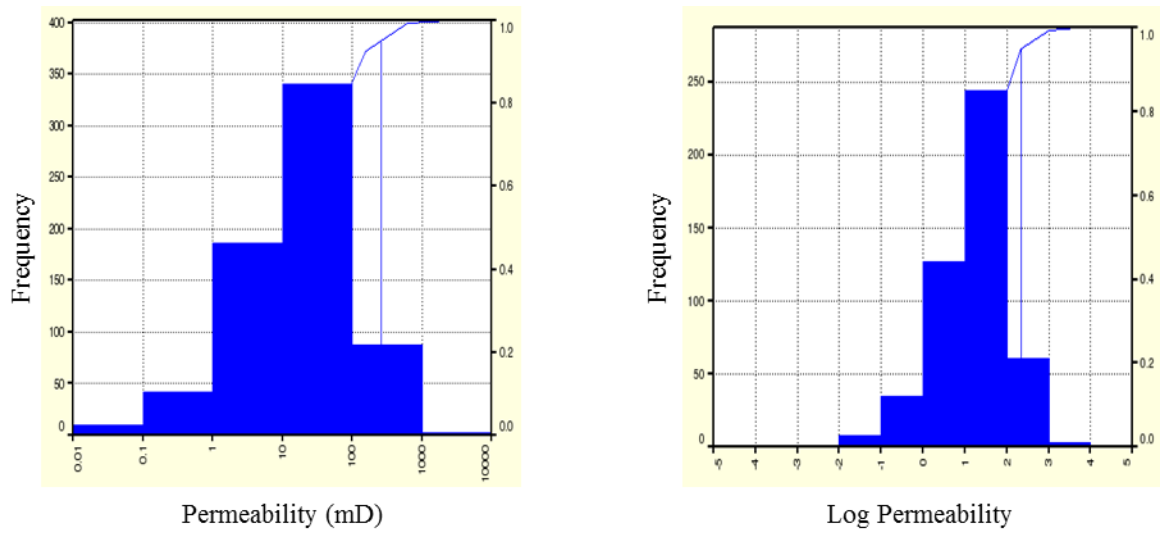


Figure 3.19: Lithofacie-15 permeability and logarithmic of permeability histogram

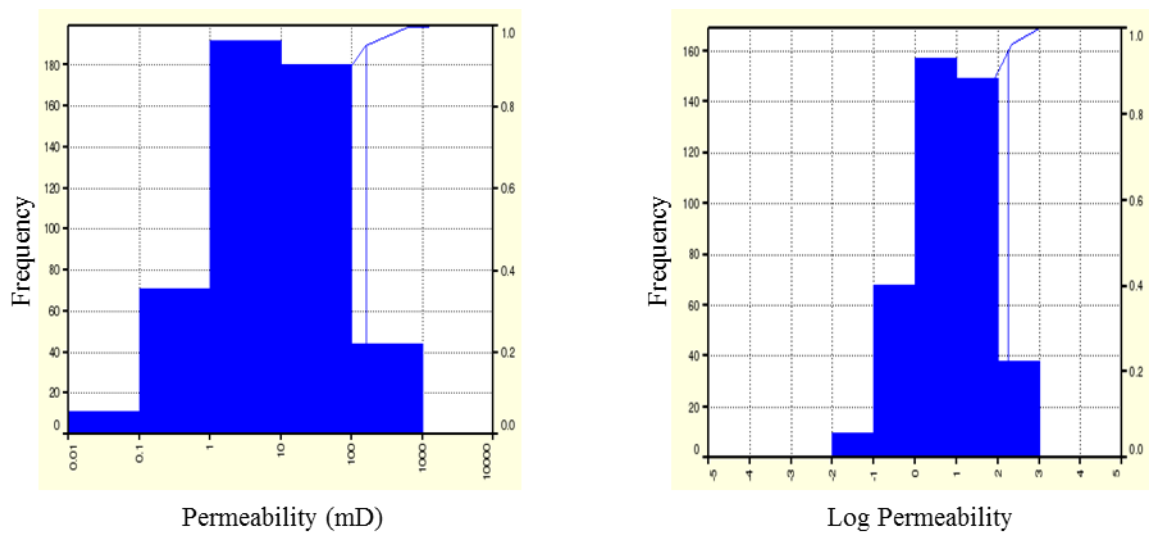


Figure 3.20: Lithofacie-16 permeability and logarithmic of permeability histogram

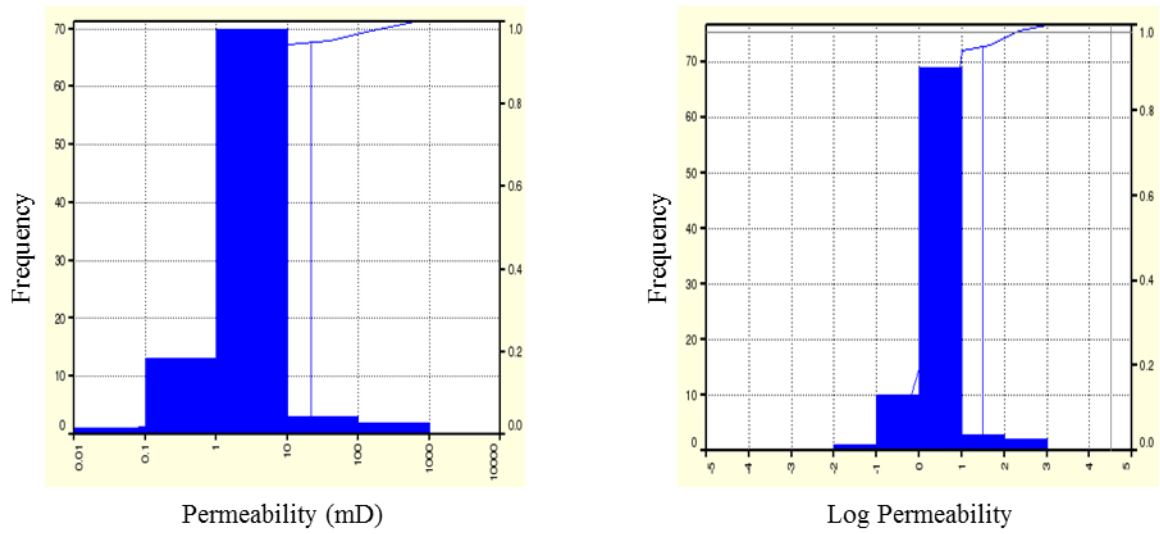


Figure 3.21: Lithofacie-17 permeability and logarithmic of permeability histogram

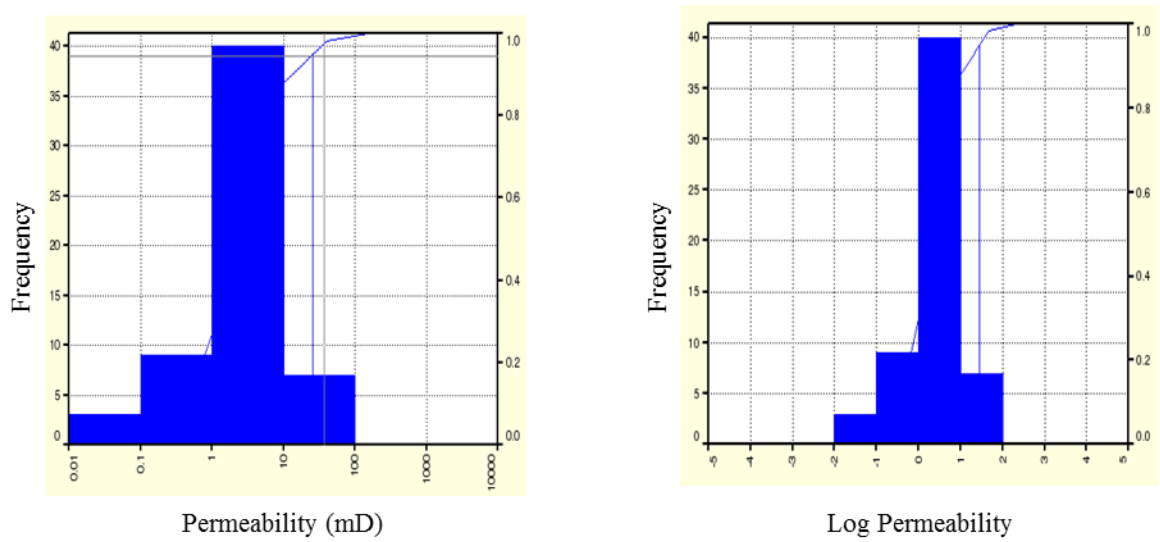


Figure 3.22: Lithofacie-18 permeability and logarithmic of permeability histogram

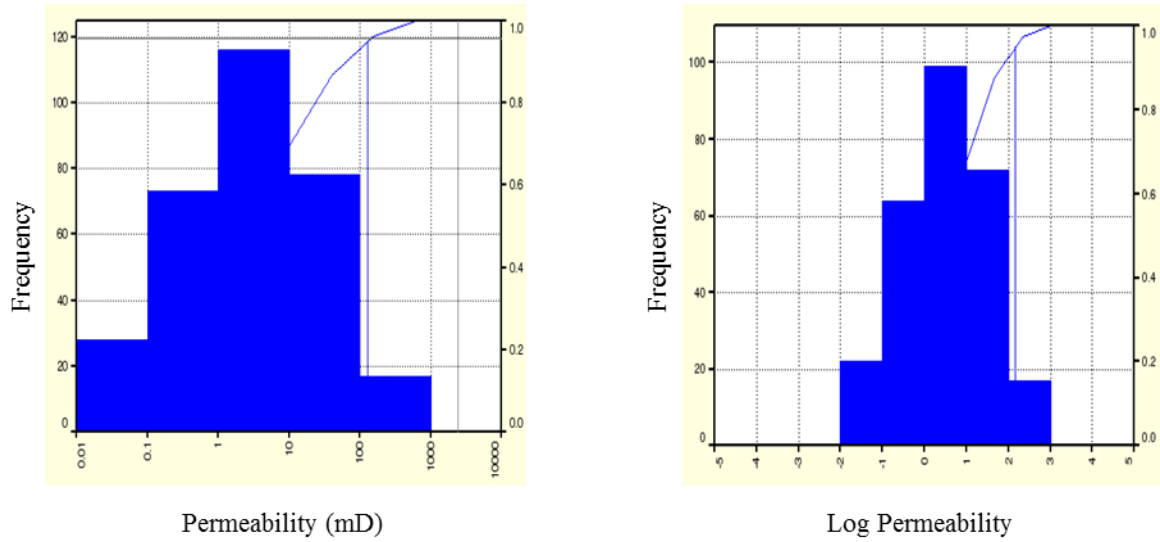


Figure 3.23: Lithofacie-19 permeability and logarithmic of permeability histogram

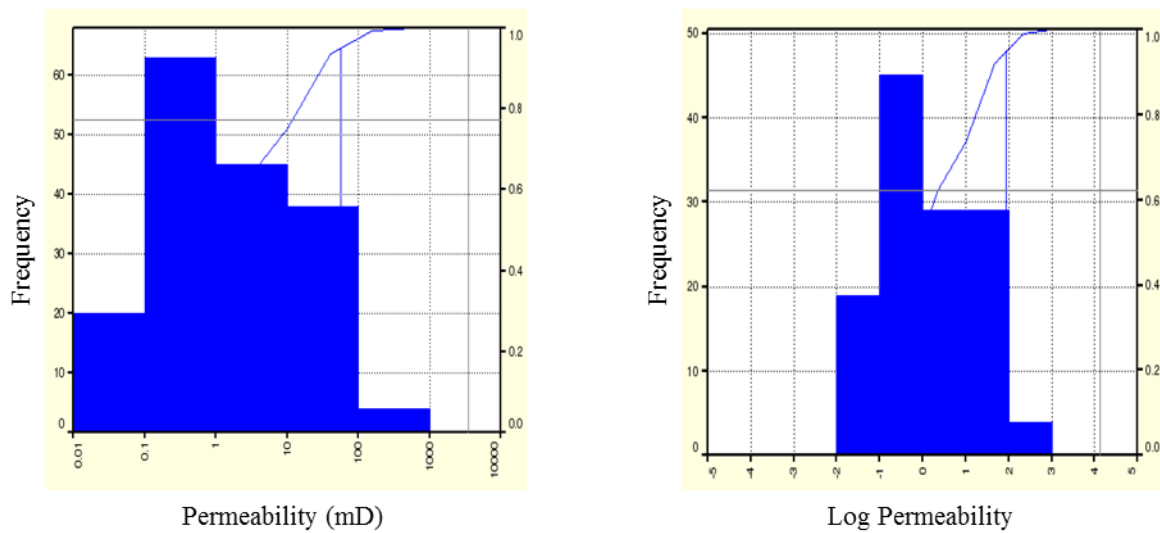


Figure 3.24: Lithofacie-20 permeability and logarithmic of permeability histogram

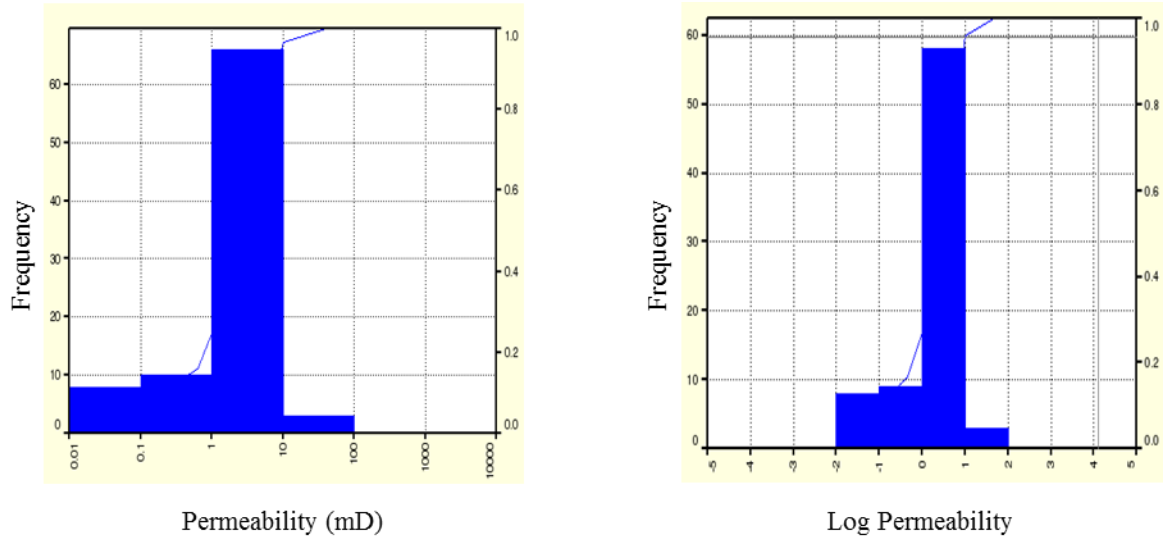


Figure 3.25: Lithofacie-21 permeability and logarithmic of permeability histogram

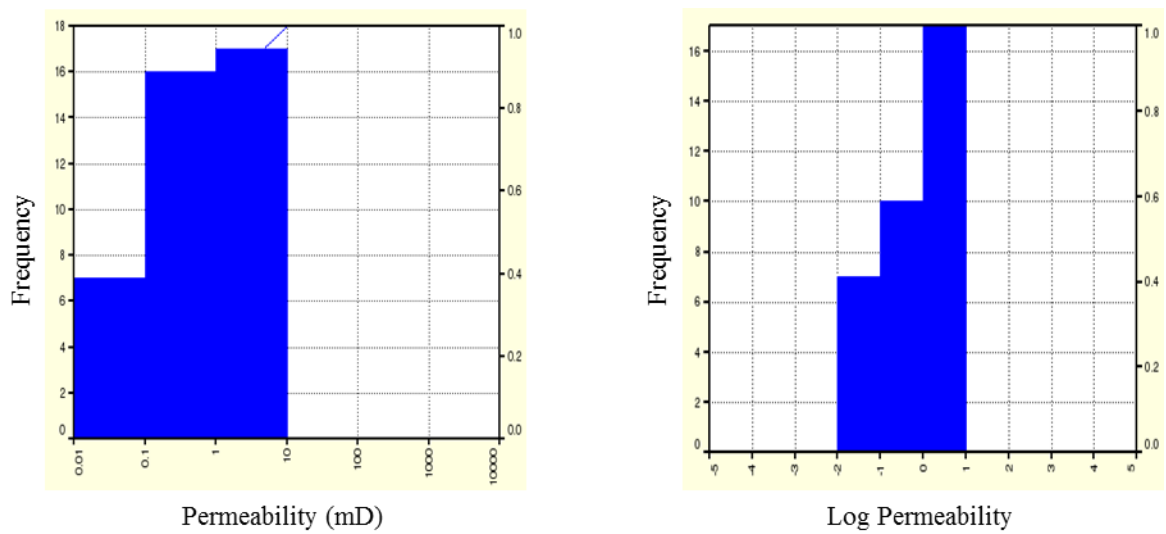


Figure 3.26: Lithofacie-22 permeability and logarithmic of permeability histogram

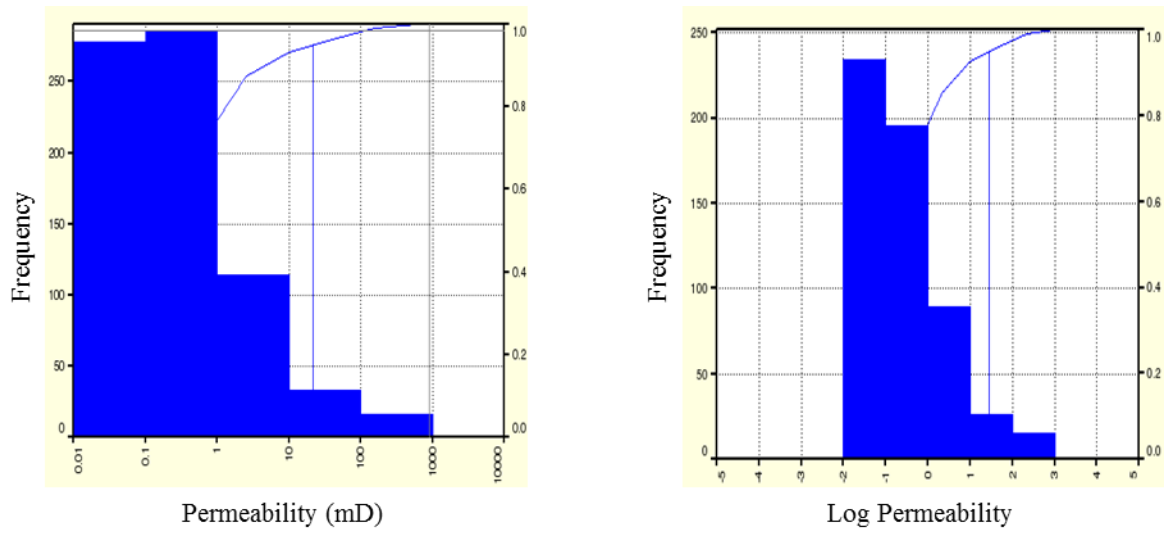


Figure 3.27: Lithofacie-23 permeability and logarithmic of permeability histogram

Table 3.6: Depositional environment of the reservoir lithofacies.

Lithofacies#	Depositional Environment lithofacies
F-1	Coarse to very coarse-grained lithocodium grainstones
F-2	Cemented very coarse to coarse-grained lithocodium grainstones
F-4	Cemented and microporous coarse-grained lithocodium grainstones
F-7	Fine to medium skeletal grainstones
F-8	Cemented fine to medium grainstones
F-9	Microporous fine to medium grainstones
F-10	Cemented and microporous medium grainstones
F-11	Oolitic skeletal grainstones
F-15	High interlayered coarse and fine peloidal grainstones
F-16	Cemented high interlayered coarse and fine peloidal grainstones
F-17	Microporous cemented high interlayered coarse and fine peloidal grainstones
F-18	Cemented and microporous coarse to fine grainstones
F-19	Moderately interlayered fine grainstones to packstones
F-20	Cemented moderately interlayered fine grainstones to packstones
F-21	Microporous moderately interlayered fine grainstones to packstones
F-22	Cemented and microporous moderately interlayered fine grainstones to packstones
F-23	Skeletal packstones

It is obvious from the above table and histograms that lithofacies have different permeability ranges which require different permeability modeling to come-up with a satisfactory correlation coefficient. It is also clear that some lithofacies have a wider range of permeability which may not be part of that specific lithofacies however due to contact/boundaries between two lithofacies, some discrepancies is observed as a result of lithofacies uncertainty. In this study, lithofacies is the guide to determine the diagenesis and quality of different layers. Therefore, secondary porosity (moldic porosity and microporosity) is also accounted in this analysis when model is propagated in uncored wells to have an extra tool in differentiating between different lithofacies characteristics utilizing sonic logs. Lithofacies is a primary input that will link depositional environment to the core permeability and this will assist greatly in predicting permeability for uncored wells. Figures 3.27 and 3.28 show permeability trends with different lithofacies.

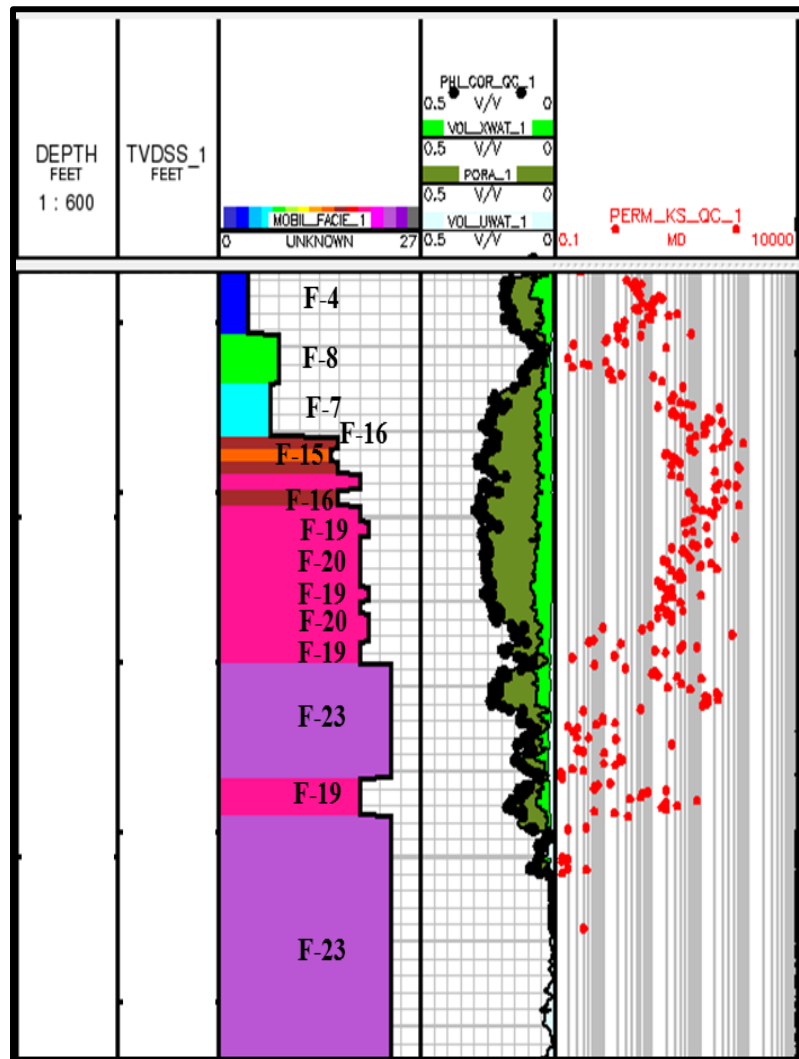


Figure 3.28: well 182 lithofacies versus core permeability

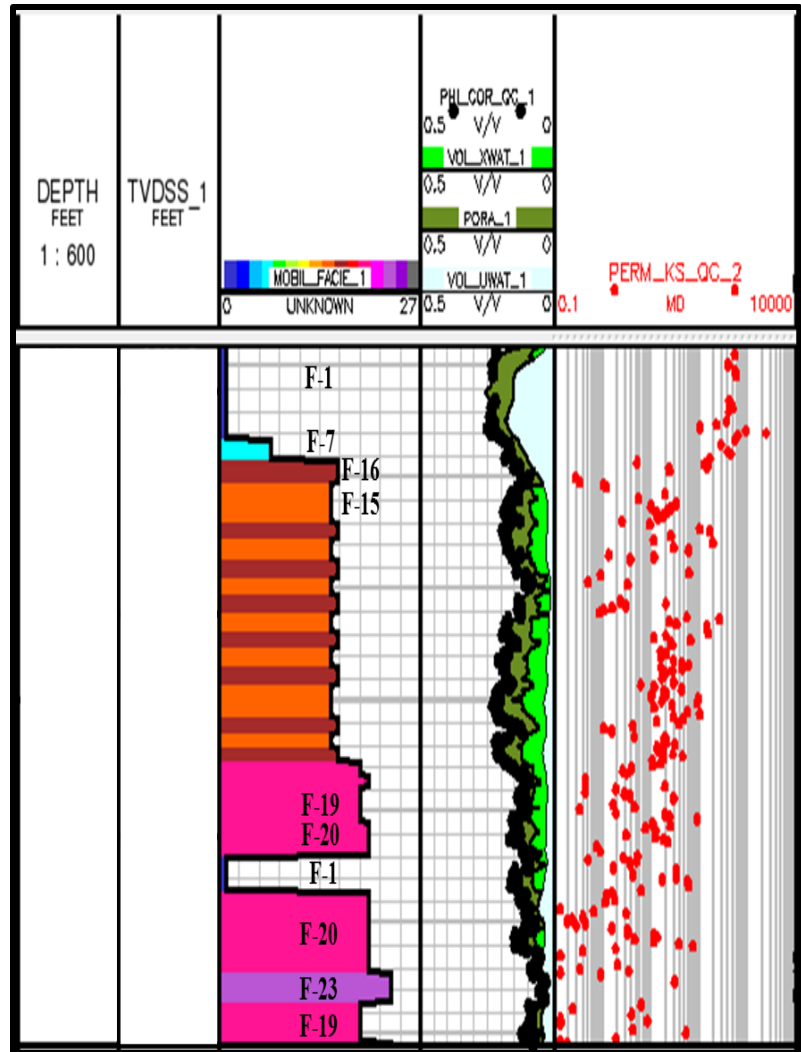


Figure 3.29: well 142 lithofacies versus core permeability

The microporosity identification is interpreted using sonic logs which is usually responds to the porous media volume (porosity) that is controlled by several factors such as: formation lithology, rock texture, overburden/pore pressure and fractures. In the understudy reservoir, lithology is relatively uniform mainly Calcite, scanty fractures and no gas trapped. Therefore, the two remaining factors are porosity and rock texture (lithofacies). Therefore, a technique using wireline logs to detect microporosity presence is included in this study to distinguish low permeability rocks from high quality ones when both have the same high porosity range which is a common phenomenon in carbonates (Figure 3.29). This technique increased our confidence in detecting microporosity zones from logs which agreed to core measurements. Core description (lithofacies determination) also proved to be in agreement with log-derived microporosity prediction. Hence, quality rocks typically lead to a satisfactory agreement between sonic and density-neutron porosities whereas the difference is an indication of poor quality rocks. Figures 3.30 and 31 demonstrate that the higher the separation between sonic porosity and density-neutron porosity the more microporosity is encountered. The addition of this technique as input parameter will strengthen permeability prediction. For instant, lithofacies-1, 2 and 4 fall under the same depositional environment of coarse to very coarse-grained grainstones, however, F-2 and F-4 have gone through a diagenetic process which transferred them to cemented and microporous lithofacies, respectively that eventually impact the petrophysical quality. As shown in figure 3.30, F-4 shows excellent porosity zone with low permeability which needs to be captured to improve uncored wells permeability modeling.

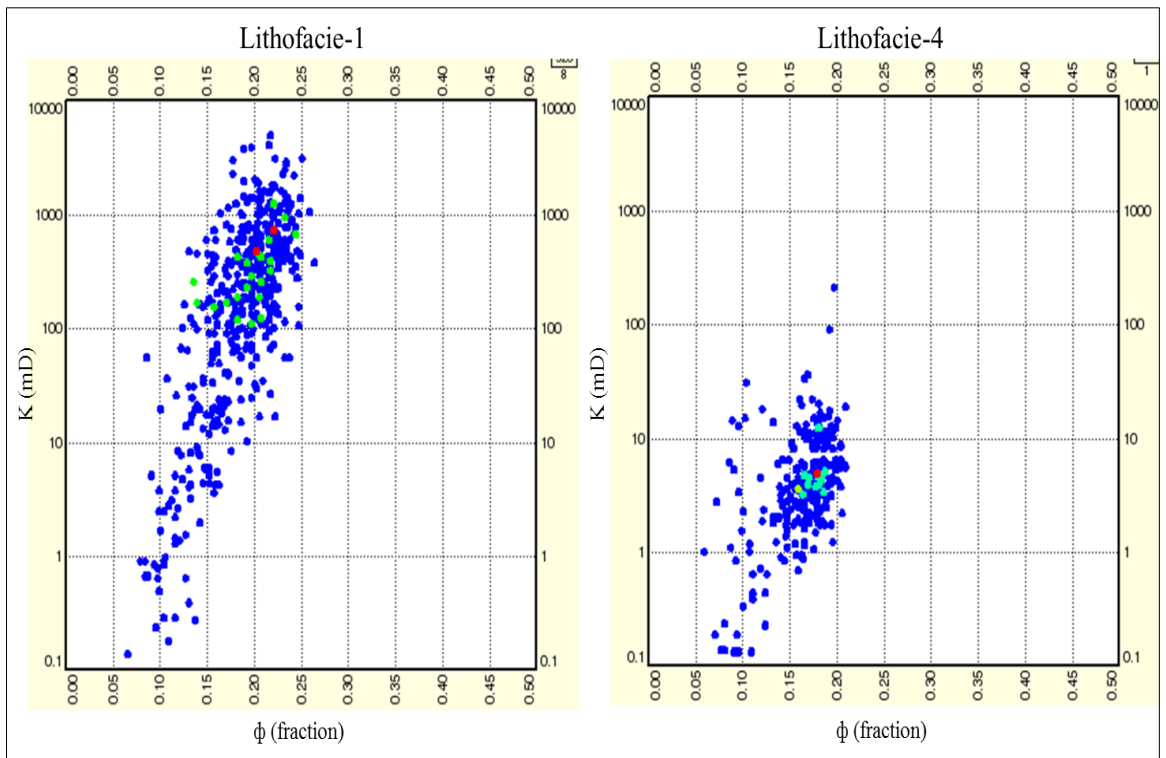


Figure 3.30: Lithofacies-1 and 4 porosity-permeability relationship

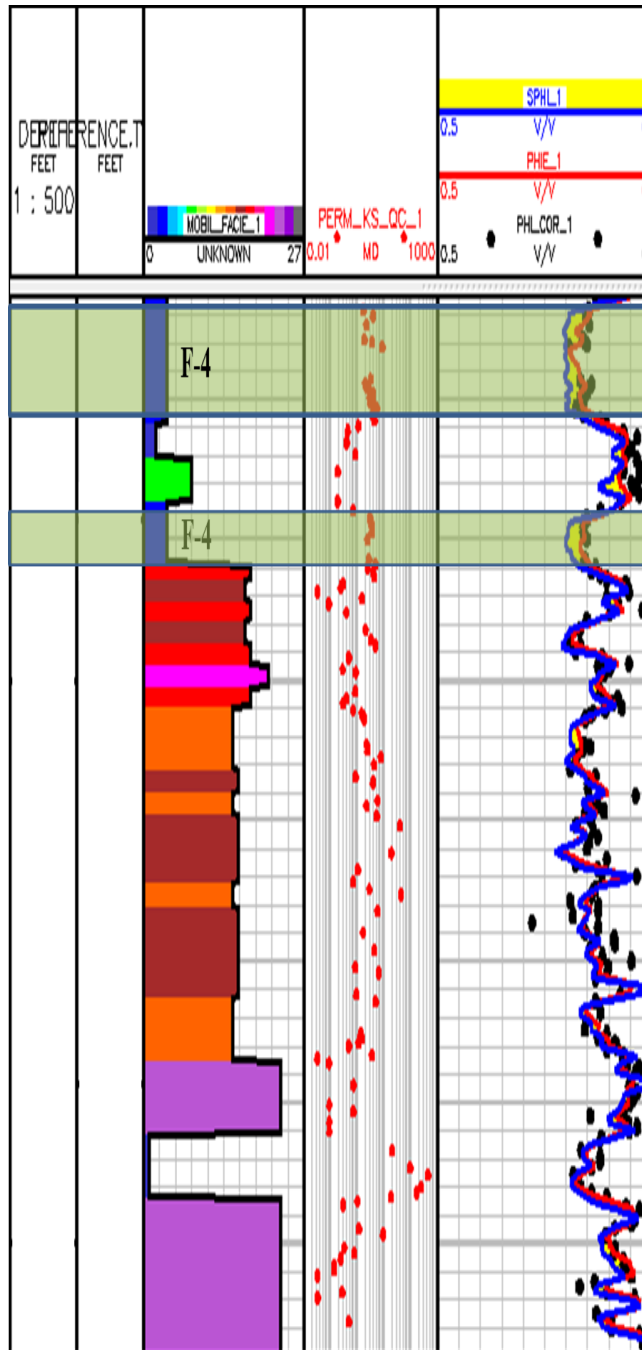


Figure 3.31: well-64 microporosity interpretation using cores, sonic and neutron/density data

CHAPTER 4

PERMEABILITY MODELING

4.1 Model Inputs

Integration of geological and petrophysical information will greatly assist in providing accurate permeability modeling. The main intent of this chapter is to come up with a robust modeling workflow using lithological and petrophysical inputs to enhance the permeability prediction accuracy in uncored wells. This involves incorporating lithological facies and wireline logs in addition to developed techniques that supports linking logs and pore network systems. Lithofacies, wireline logs and developed diagenesis algorithm tools are included in the training of data against core permeability. These major inputs are then implemented in the geological/reservoir modeling.

We will use Facimage technique which is one of the latest cutting edge tools of workflow that employs neural network and pattern recognition algorithm known as Multi-resolution graph-based clustering (MRGC) that has been known as a statistical non-parametric technique that solves dimensionality problems. It also derives valuable information about the geological lithofacies from the structure of the data itself. One of the most important advantages of non-parametric techniques is it can predict without the need to provide any information about the data distribution.

(Shin-Ju and Philippe, 2000) MRGC is a combination of two well-known techniques: K-nearest neighbor (KNN) and graphical representation of the data which takes advantages of both methods of capturing data classes or clusters for any set of data structure. KNN methods propose to have a specific number of neighbors where probability distribution functions (PDF) is estimated using the fixed neighbors for the area of the points. KNN approach has more advantages with respect to others; it is easy to formulate and set up; adjusting the number of neighbors is less critical than adjusting the grid window size. However this method takes a long time for processing that is not a good characteristic. On the other hand, the graphical methods try to relate points according to their proximity. With the help of heuristic rules, one tries to eliminate inconsistent arcs and break the graph into several connected sub-graphs that are recognized as clusters. This method is efficient to process data of small dimensions and small sizes which is generally insensitive to the different sizes among clusters. The MRGC method is utilized in this study for the following reasons:

- It is capable of capturing the structure lithofacies within the set of core description and logs data.
- It doesn't need to know the data structure beforehand.
- It detects the optimal number of clusters.
- It has stable parameters and results while values of parameters vary.
- It can run unlimited number of input parameters.

As discussed in chapter 3, cored wells are used initially to build the model and train the data set to provide a recognized form from set of logs. For applying the MRGC method in this study, GEOLOG in Linux environment is used. The workflow (Figure 4.1) of permeability prediction is simply consisted of:

1. Input sets which include: Lithofacies, density, neutron, sonic and difference of (density-neutron and sonic).
2. Associated set of corrected permeability from core measurements.
3. Output sets which defines the predicted permeability.

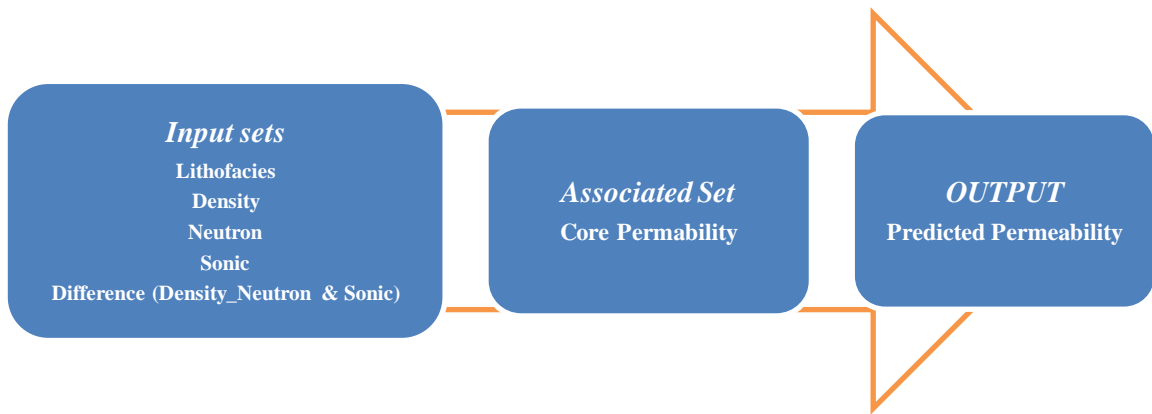


Figure 4.1: A systematic workflow used in in this study to predict permeability with the training data set

4.2 Data Training

The Lithofacies are essential for distinguishing reservoir quality and thus provide a recognized pattern for permeability range which helps in projection to uncored wells. While training the data, cross plots of input sets and, core permeability and logarithmic value of core permeability provide useful information and visuals in the form of correlations that link directly to permeability and logarithmic value of permeability as shown in figures 4.2 to 4.6.

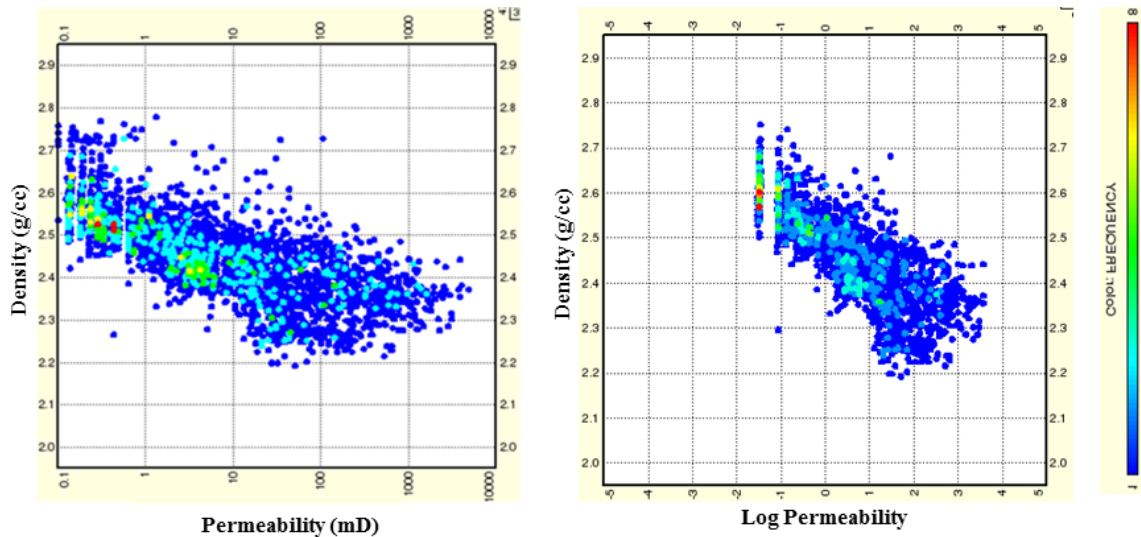


Figure 4.2: Cross –correlations show trend between density log and core permeability and logarithmic value of permeability

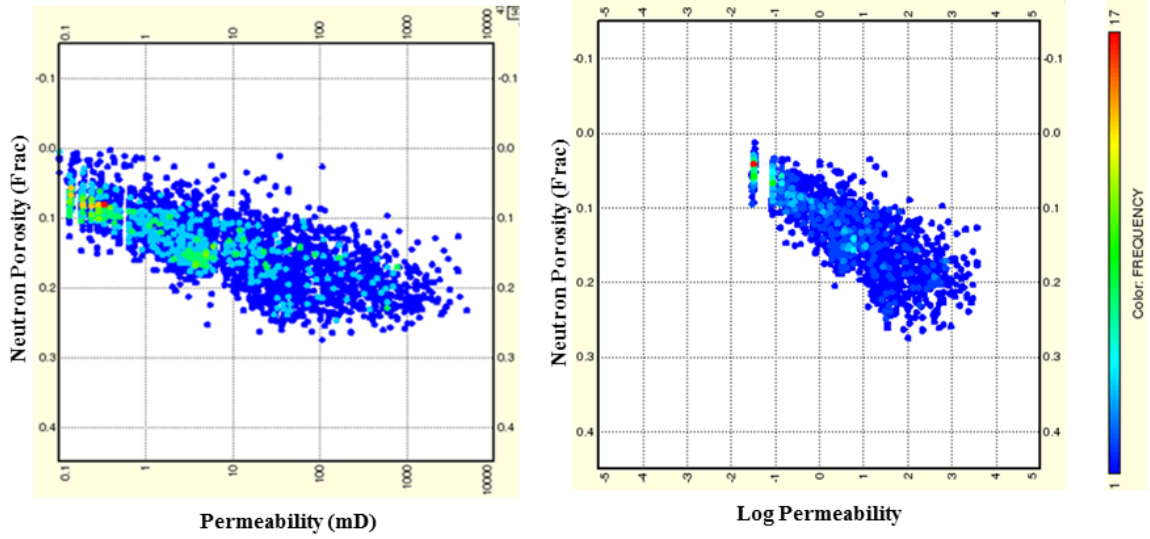


Figure 4.3: Cross –correlations show trend between neutron log and core permeability and logarithmic value of permeability

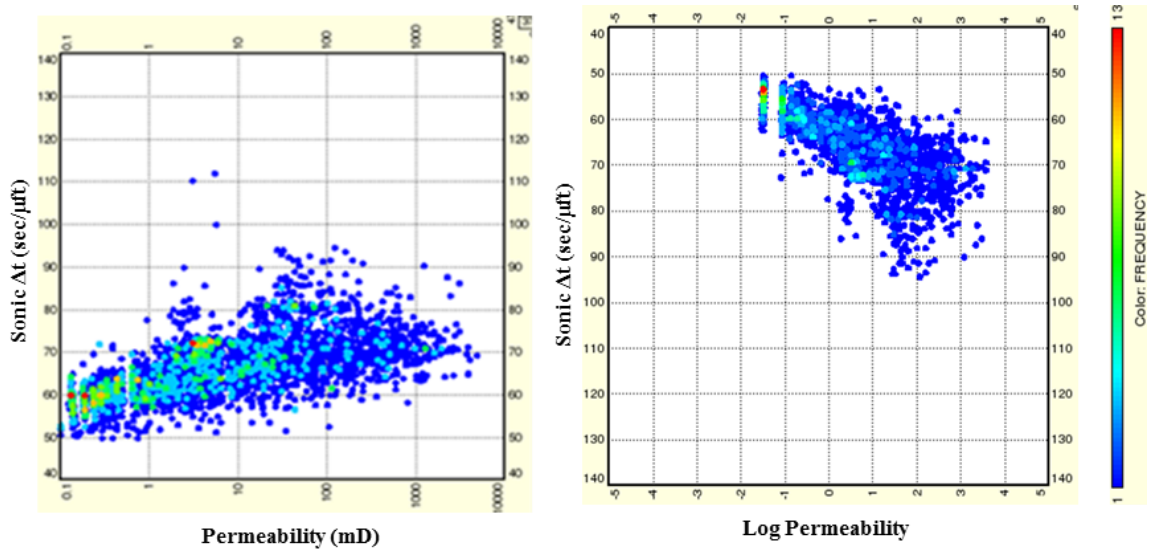


Figure 4.4: Cross –correlations show trend between sonic log and core permeability and logarithmic value of permeability

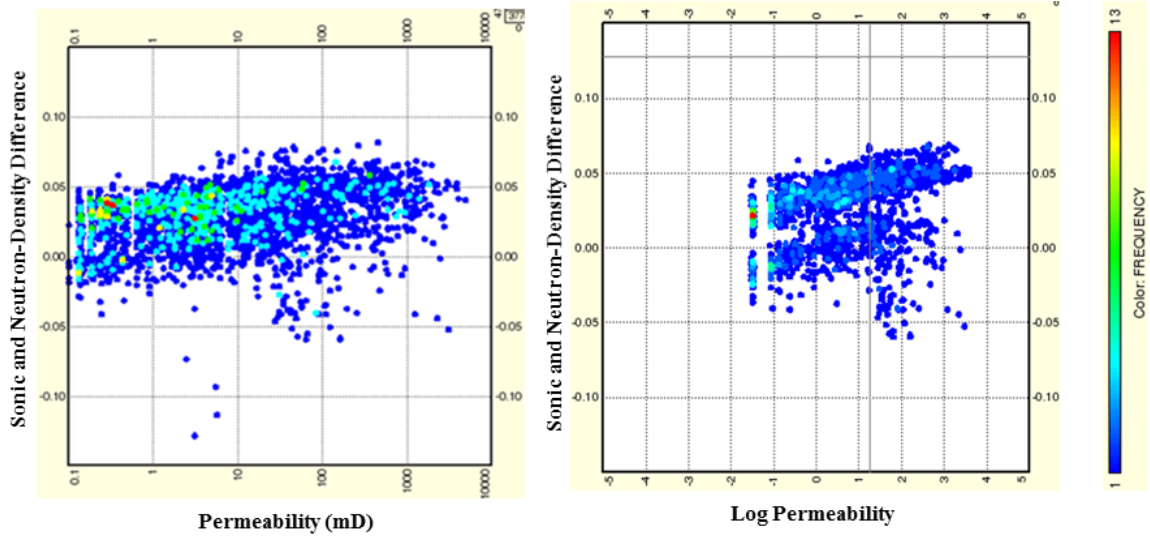


Figure 4.5: Cross –correlations show trend between the differences between sonic and density-neutron, and core permeability and logarithmic value of permeability to include diagenesis effect in the model training

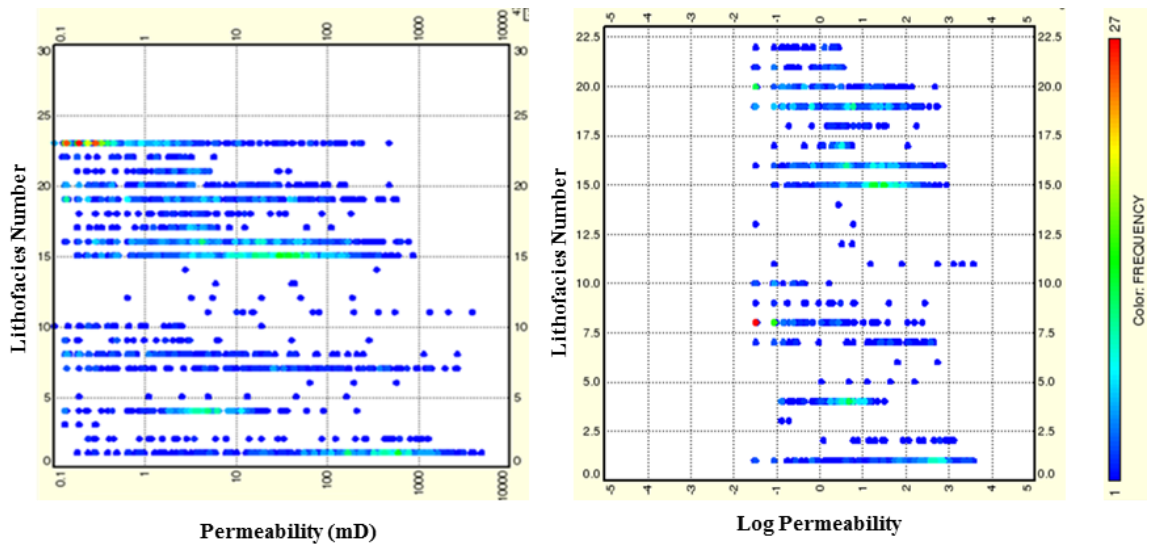


Figure 4.6: Cross –correlations show core permeability and logarithmic value of permeability ranges for each lithofacies

4.3 Prediction Sensitivity

Once all of these correlations are validated and supervised, permeability prediction starts using cluster analysis which assigns the number of nearest neighbors. The prediction is then applied on 50% of cored wells just to test the quality of predicted permeability against core data. If log prediction is good then apply the model to the wells of interest either cored or uncored wells. In order to come up with an optimum nearest neighbor number (KNN), the model is tested against three different values of KNN which are KNN = 2, 3 and 4 respectively.

To support selecting the optimum number of nearest neighbor, two data visualization techniques cross-plots and histograms are utilized to ensure that the most representative KNN value is selected to model propagation on data set level for all wells. The first technique is to compare the model for different KNN values on well level to check how the model is preserving permeability trends. The first technique is to use the cross-plot of permeability values obtained from the trained model for each KNN value and corrected core permeability and then select the best correlation coefficient for reservoir level as demonstrated in figures 4.7 through 4.9 that show all KNN values are good however KNN = 2 with $R^2 = 0.91$ is the optimum number as KNN increases the model starts to degrade. The second technique is to use histogram visualization tool to check the permeability distribution per lithofacies from the model versus the core permeability. Figures 4.10 to 4.15 show the comparison of permeability histograms from the model and core data along with the mean value from each histogram for KNN=2. This confirms that the model is preserving the core permeability with good match. In addition, a well level assessment is carried out to confirm the optimum KNN number. Figure 4.16 shows that

KNN = 2 is the best model as it captures both low and high sides of permeability ranges whereas KNN = 3 and 4 are unable to capture high permeability ends, although all KNN show excellent correlation coefficient on a reservoir level. Therefore and since the fit coefficient ($R^2 = 0.91$) of KNN = 2 is the best which is excellent in carbonate reservoirs, all above mentioned techniques suggest a KNN value of 2 in the model propagation to the remaining cored and uncored wells. In addition, a model from logarithmic value of permeability is constructed to examine the accuracy especially in the low permeability ranges. Table 4.1 shows the statistical assessment between predicted permeability model and predicted logarithmic value of permeability model.

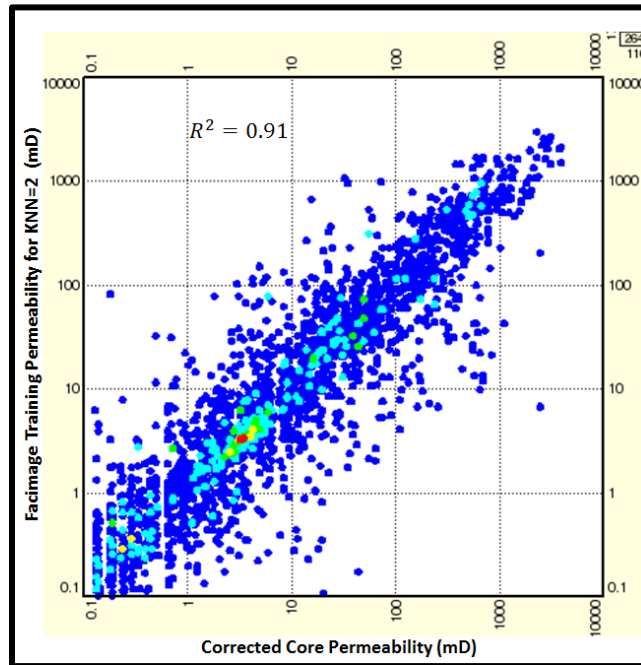


Figure 4.7: Cross-plot of predicted model permeability versus corrected core permeability for

KNN=2

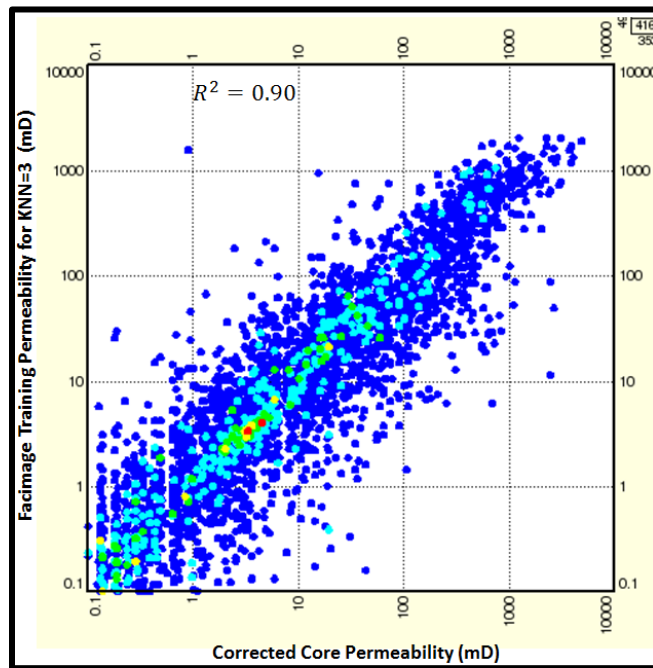


Figure 4.8: Cross-plot of predicted model permeability versus corrected core permeability for

KNN=3

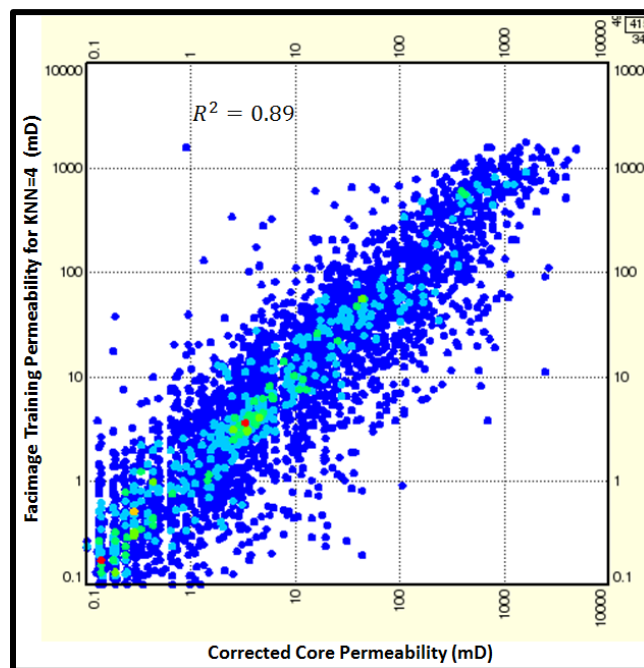


Figure 4.9: Cross-plot of predicted model permeability versus corrected core permeability for

KNN=4

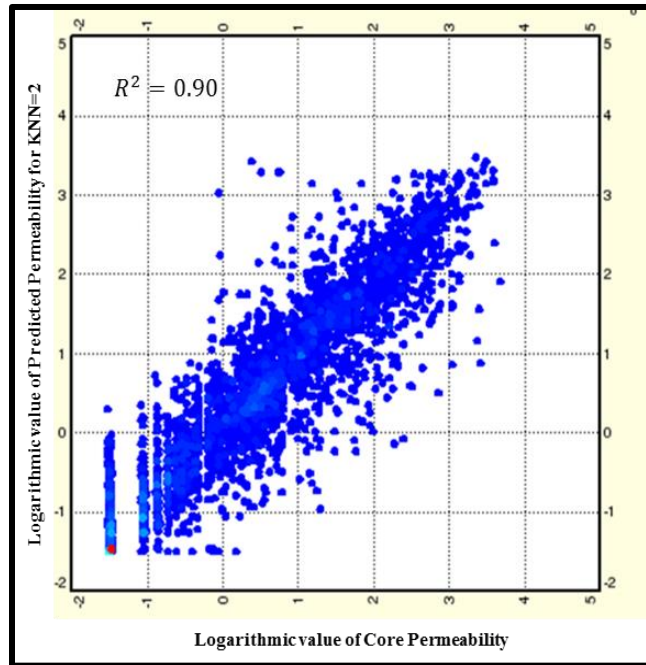


Figure 4.9: Cross-plot for predicted logarithmic value of permeability versus logarithmic value of corrected core permeability for KNN=2

Table 4.1: Statistical Assessment for predicted permeability and predicted logarithmic value of permeability at KNN=2

Parameters	Value
n	4147
Average Error Difference from Permeability Predicted	27.7
Average Error Difference from Anti Log(Permeability Predicted)	18.3
Standard Deviation Error from Permeability Predicted	1.76
Standard Deviation Error from Anti Log(Permeability Predicted)	1.93
AARE from Permeability Predicted	3376.5
AARE from Anti Log(Permeability Predicted)	257.8
Correlation Coefficient (R) from Permeability Predicted	0.75
Correlation Coefficient (R) from Anti Log(Permeability Predicted)	0.59
Root Mean Squares (RMS) from Permeability Predicted	201.6
Root Mean Squares (RMS) from Anti Log(Permeability Predicted)	241.6

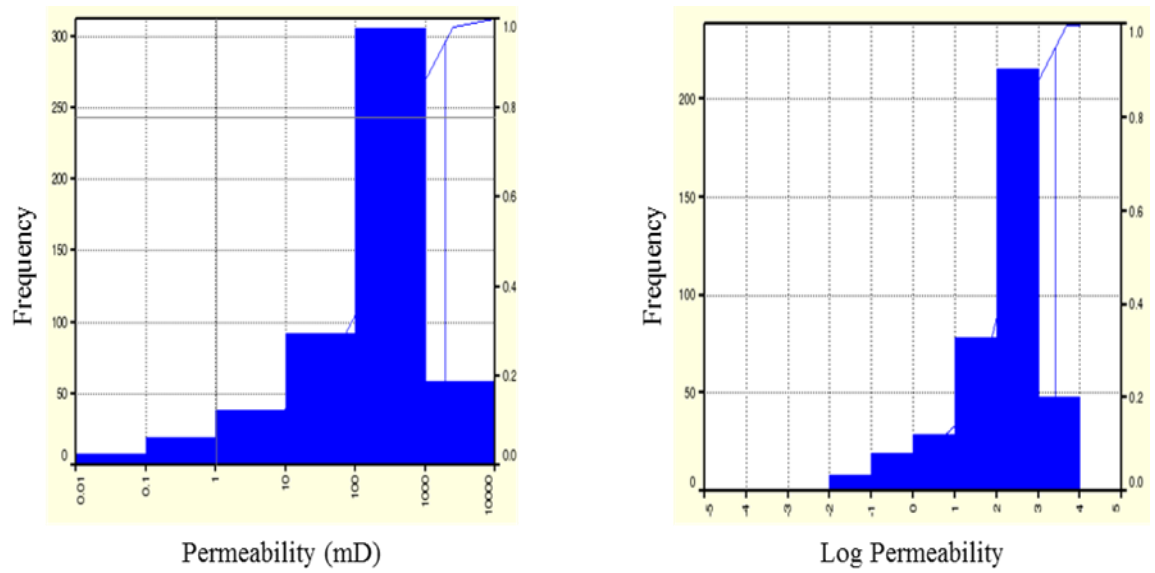


Figure 4.10: Lithofacies-1 permeability distribution from core data which exhibit a permeability mean of 428.94 mD

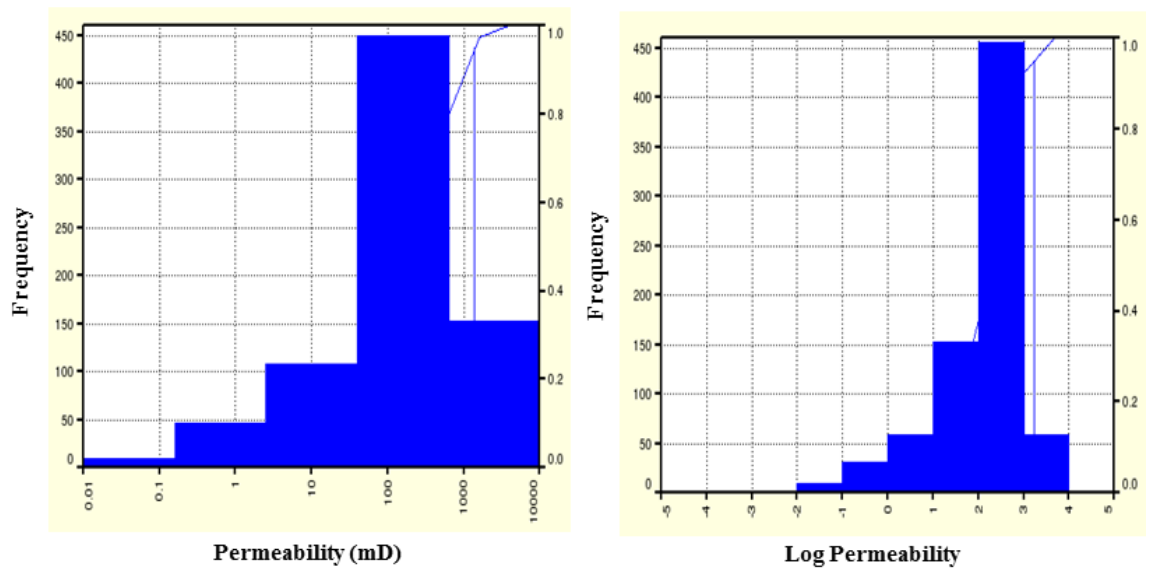


Figure 4.11: Lithofacies-1 permeability and logarithmic value of permeability distribution from the prediction model which exhibit a permeability mean of 333.47 mD

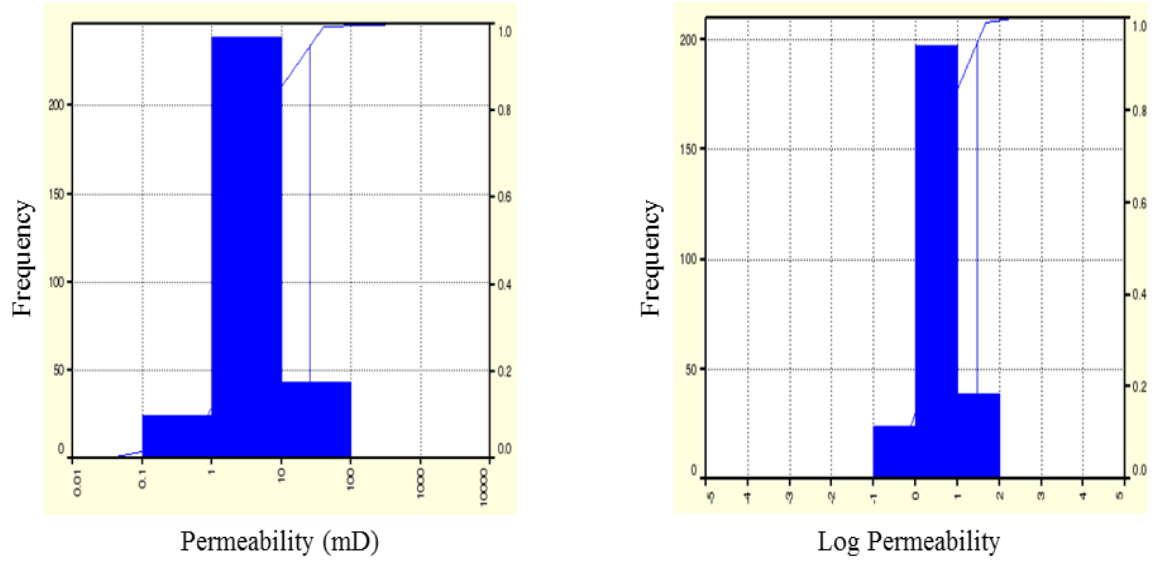


Figure 4.12: Lithofacies-4 permeability distribution from core data which exhibit a permeability mean of 6.28 mD

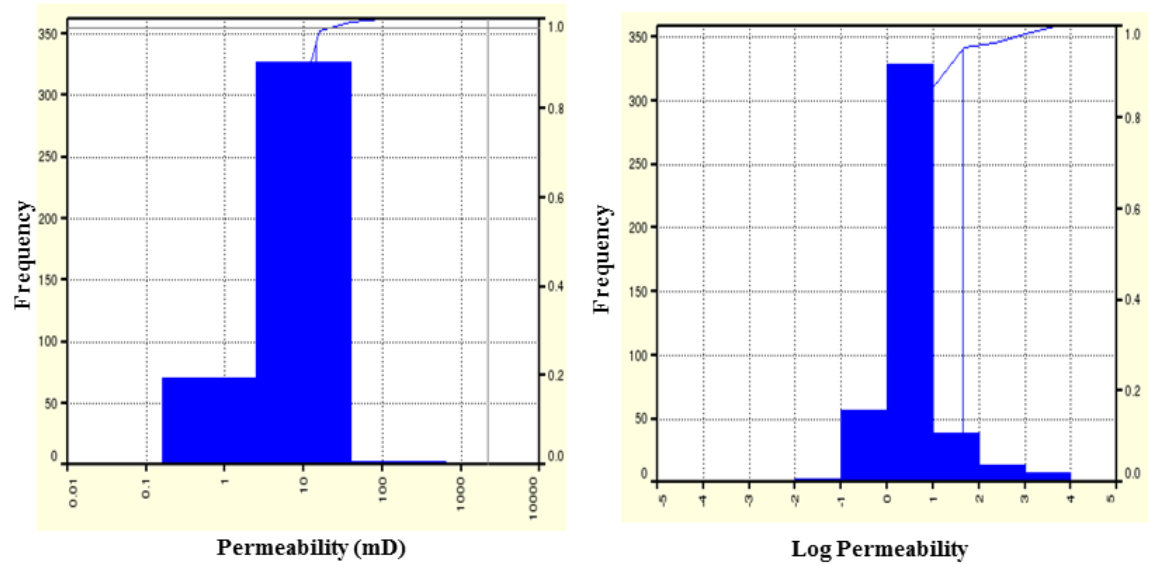


Figure 4.13: Lithofacies-4 permeability distribution from core data which exhibit a permeability mean of 6.37 mD

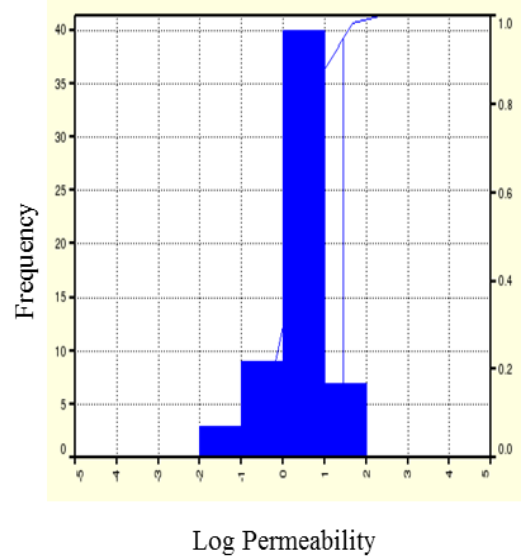
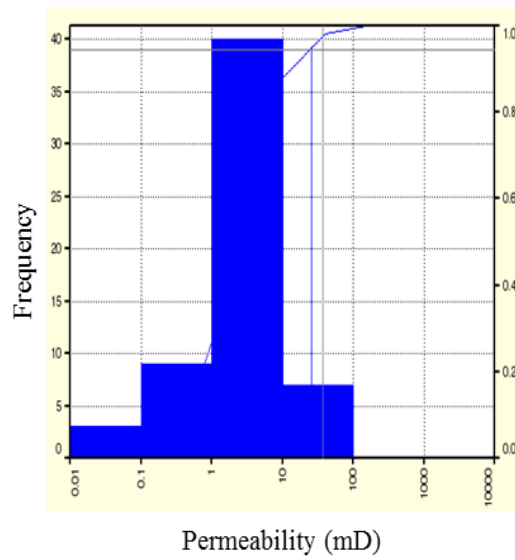


Figure 4.14: Lithofacies-18 permeability distribution from core data which exhibit a permeability mean of 5.14 mD

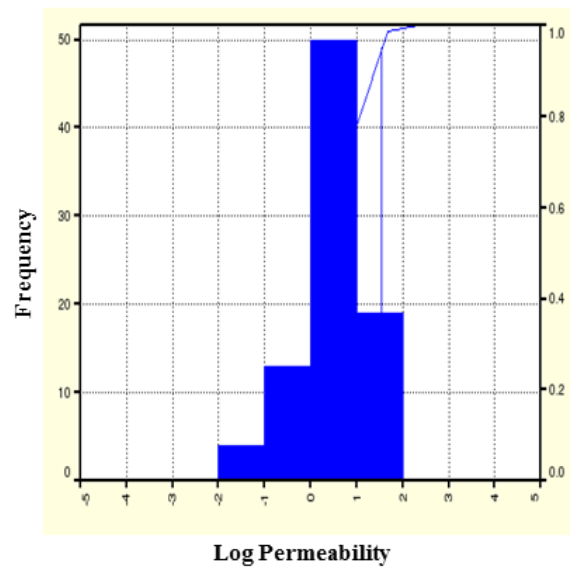
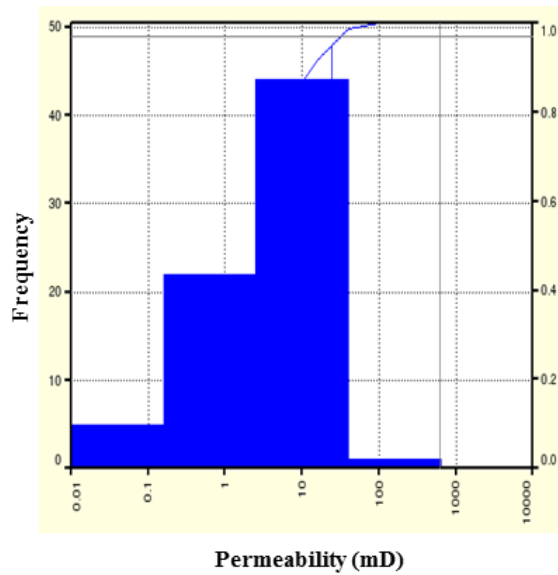


Figure 4.15: Lithofacies-18 permeability distribution from core data which exhibit a permeability mean of 5.97 mD

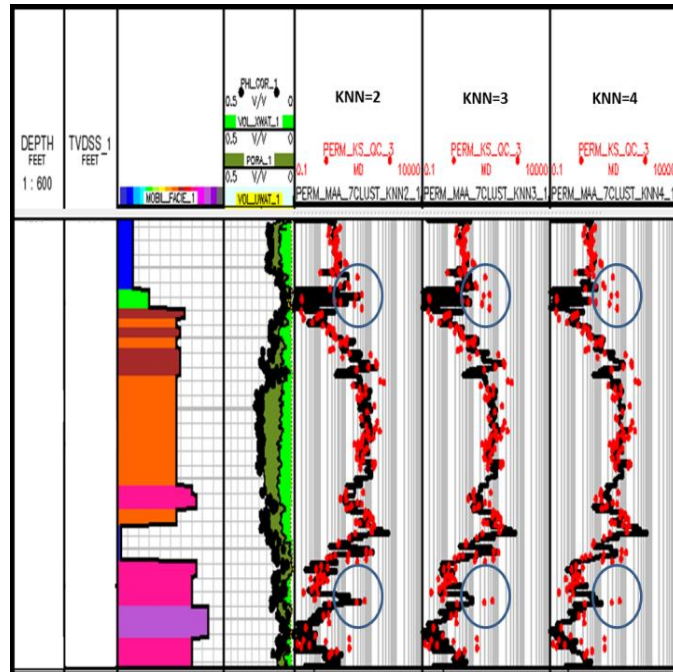


Figure 4.16: Well 101 predicted permeability (black curve) over the corrected core permeability (red dots) for KNN = 2, 3 and 4

4.4 Permeability Prediction

After a thorough study of the modeling parameters, a quality model is then propagated to all cored and uncored wells. In section 4.3, confidence is achieved across different verification techniques which enable predicting permeability in uncored wells with good accuracy. In addition, the model is compared to another model using the same approach but without incorporating lithofacies inputs which shows a very good enhancement in permeability modeling against corrected core permeability. Figure 4.17 shows an example of one well with an improved permeability prediction by introducing geology (depositional environment) into the modeling. Figure 4.18 shows permeability prediction in uncored oil producer which clearly follow the same permeability trend for each facie e.g. F-1 high permeability range which is a characteristics of this facies. In addition, Figures 4.19 and 4.20 represent the permeability prediction in uncored water injectors. Having accurate prediction enables reservoir engineers to selectively choose the preferred zones of production/injection. This is the most important tool, permeability, especially in reservoir modeling and simulation. The model in turn has a limitation in providing accurate permeability modeling per cluster/lithofacies when no enough data is provided for a specific facie as not all lithofacies are uniformly distributed in the reservoir.

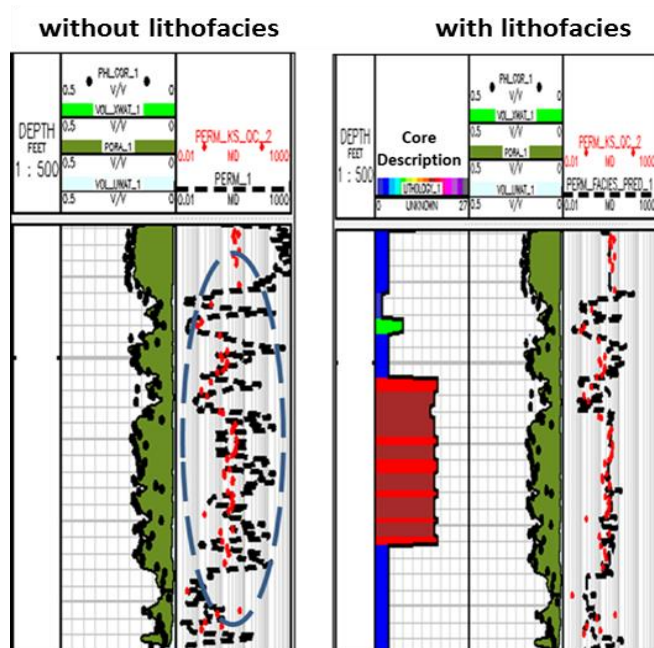


Figure 4.17: comparison between with and without lithofacies inputs predicted permeability for well-43. Lithofacies inputs clearly enhanced prediction of permeability.

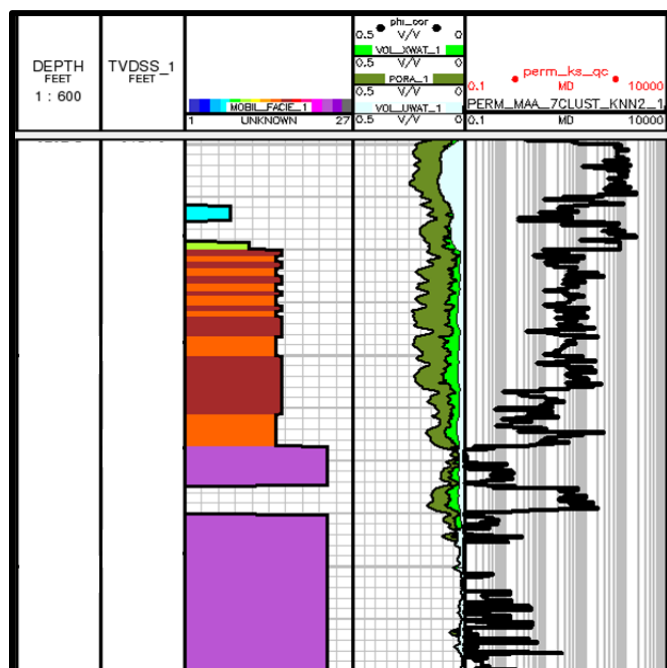


Figure 4.18: Permeability prediction in well-121, oil producer, from the model.

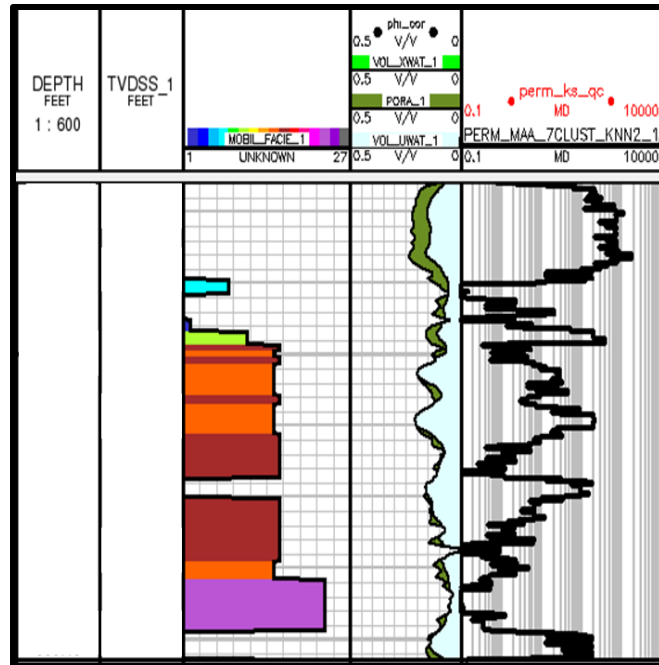


Figure 4.19: Permeability prediction in well-219, water injector, from the model.

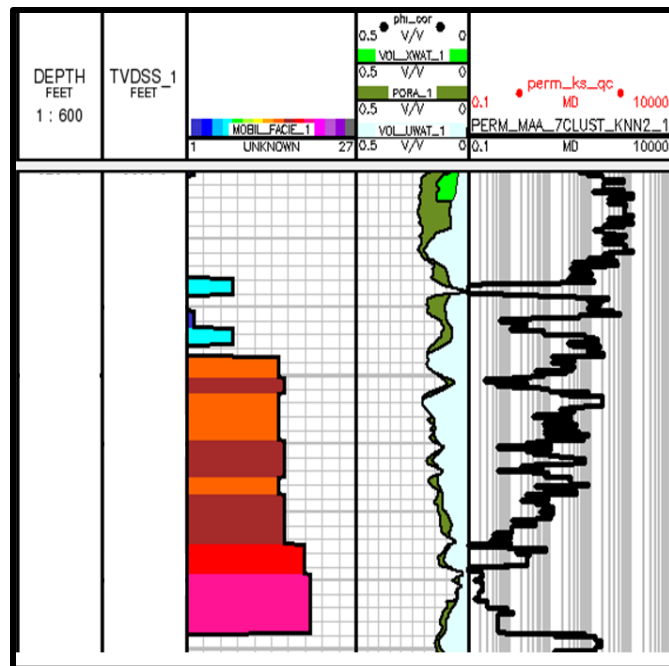


Figure 4.20: Permeability prediction in well-221, water injector, from proposed model.

4.5 Validating Permeability Model

The above systematic approach of predicting permeability is also supported by transient pressure buildup/falloff analysis to obtain the kh value for a specific well. This information assists in achieving a higher level of confidence when used in uncored wells. This validating mechanism is used to compare kh value from core data, modeling and well transient test data. A good match is observed as shown in figure 4.21 between all three measurements of flow capacity. For uncored wells, figures 4.22 to 4.24 also exhibit good match between buildup/falloff test and predicted permeability. This is an additional tool to confirm a valid model even when compared to well test results.

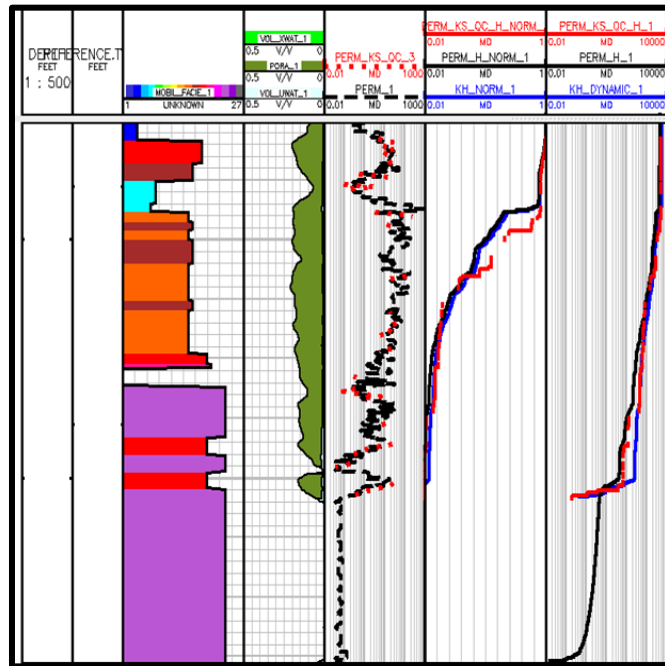


Figure 4.21: Validating modeling permeability using kh value from modeling (black curve), buildup test (blue curve) and core measurements (red curve) in cored well-19 (observation key well) which demonstrate a good match among three different validation mechanisms

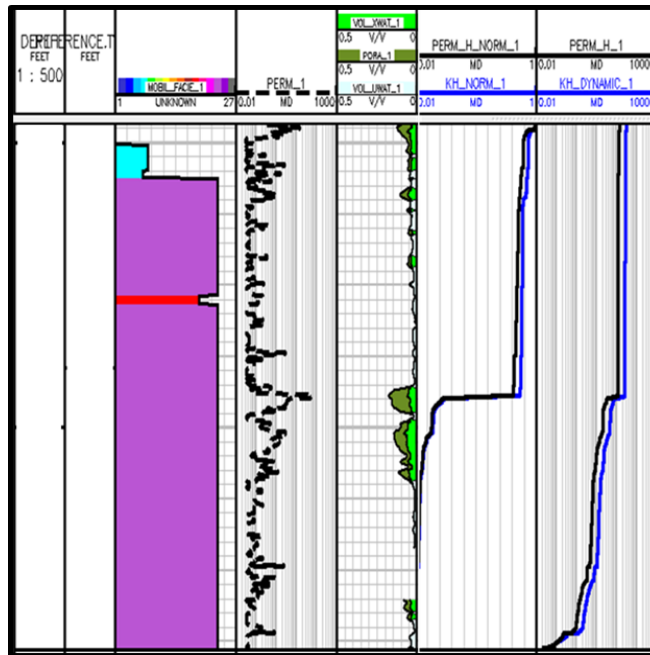


Figure 4.22: Validating modeling permeability using kh value from modeling (black curve) and buildup test (blue curve) in well-115 (oil producer) which demonstrate a good observed match

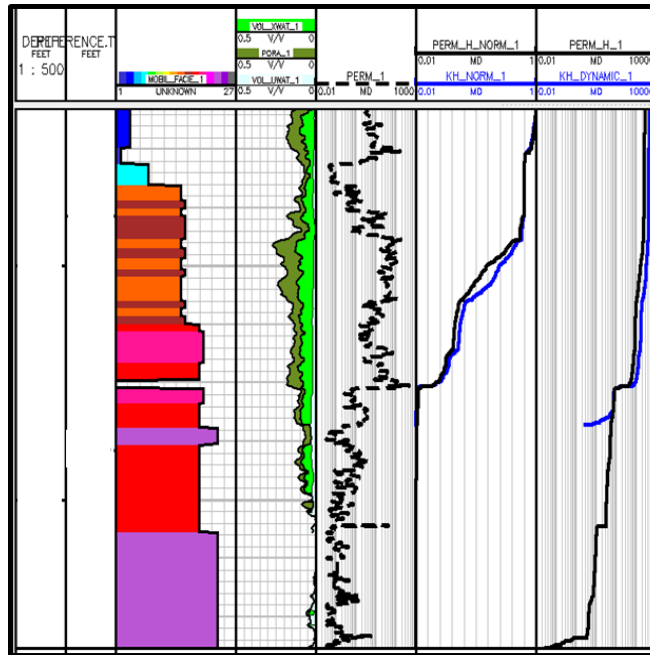


Figure 4.23: Validating modeling permeability using kh value from modeling (black curve) and buildup test (blue curve) in well-64 (oil producer) which demonstrate a good observed match

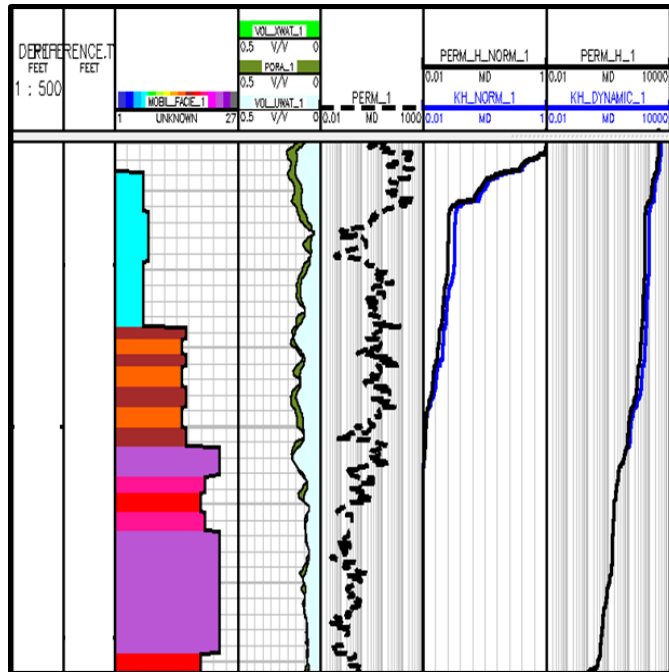


Figure 4.24: Validating modeling permeability using kh value from modeling (black curve) and falloff test (blue curve) in well-215 (water injector) which demonstrate a good observed match

4.6 Dynamic Permeability Integration

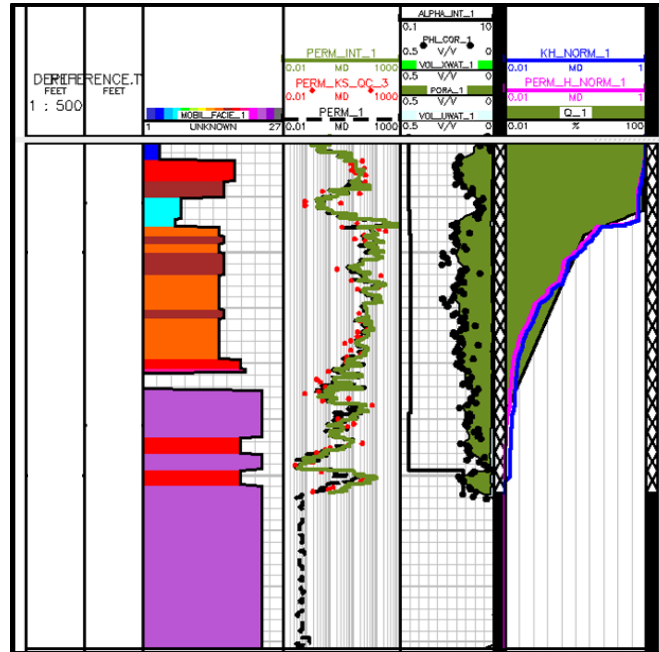
Dynamic permeability from pressure buildup/falloff analysis is utilized and integrated with flow meters analysis (from production logging tool -PLT-) to convert static permeability to dynamic in each lithofacies which in current practices achieved by using multiplier to be used in simulation models. The provided kh from well test provide information about reservoir quality and potential in both injector and producer wells. The static permeability provided by the model is linked to the dynamic permeability via a multiplier for a particular zone. Only open-hole completed wells is used in this section to establish a relationship due to limitations of cased-hole completion accessing only a certain zone or some zones. A soft code is used here to translate the flow meter contribution per 0.5 foot and multiply it by the magnitude of kh provided from well test. The resultant multiplication provides a continuous log that can be compared to the one from static permeability (modeling). Figures 4.25 and 4.26 show that minimal multiplier is needed to convert static permeability to dynamic permeability which almost no multiplier in figure 4.25. This tool can also be used as a validation mechanism of well transient testing as it provides a tool to revisit well test analysis although permeability across second and third perforations are almost matching as illustrated in figure 4.27.

Furthermore, the result is then utilized to build a dynamic permeability model from both static permeability for all reservoir zones. This information provides insight on the magnitude and variations of permeability distribution from injectors to producers. This model is used to convert static permeability (modeling) to dynamic through a nonlinear regression of static and dynamic permeability. Figure 4.28 shows the dynamic permeability model that can be used in the reservoir simulation modeling which provides

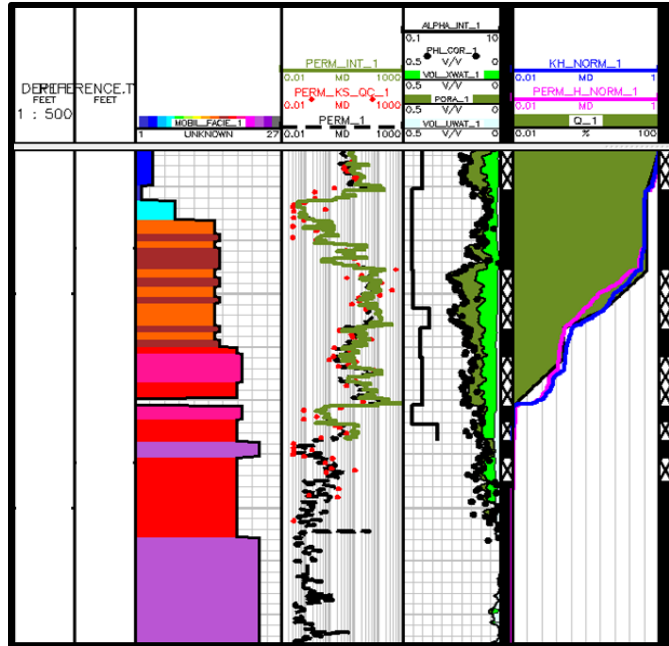
an educated multiplier instead of guessing the needed multiplier. For the understudy reservoir, the following is proposed for reservoir simulation:

$$\log(\text{Dynamic } K) = 0.190 + 0.814\log(\text{Static } K) \quad (4.1)$$

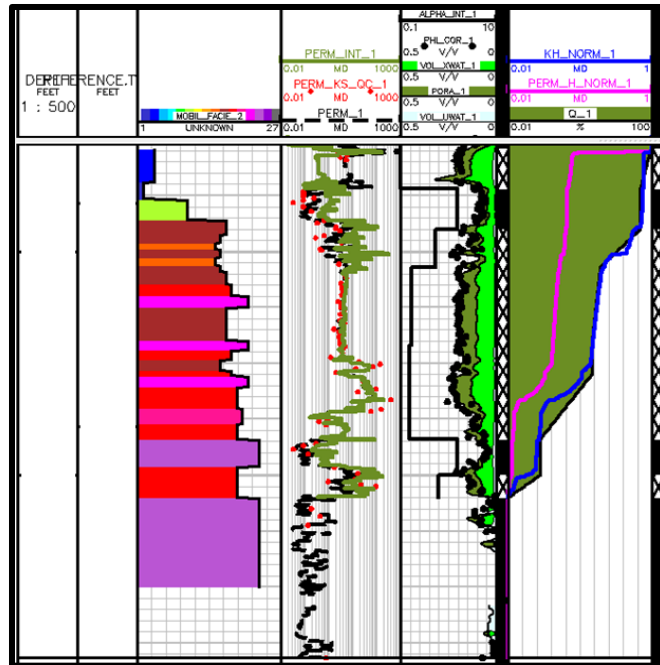
This implies that the effective permeability from well test is smaller than the absolute permeability form core measurements.



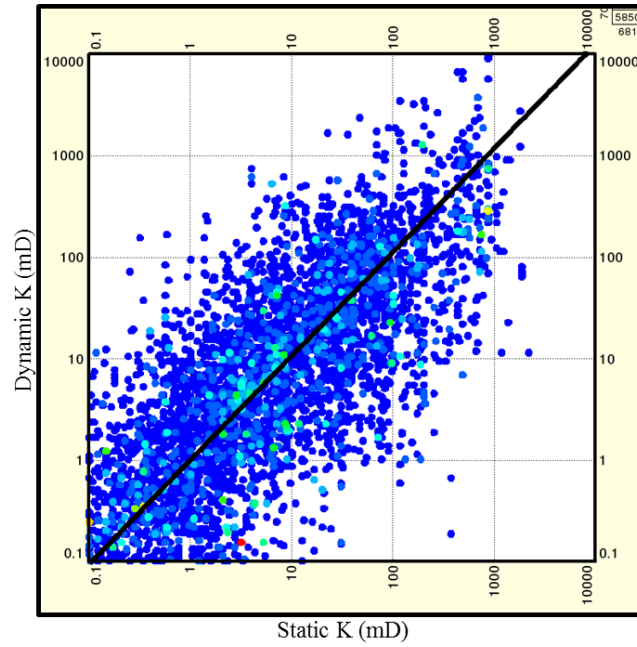
4.25: Converting static permeability (modeling) to dynamic permeability in well-19 (observation key well) with almost no required multiplier (5th track black curve).



4.26: Converting static permeability (modeling) to dynamic permeability in well-79 (observation well) with almost minimal required multiplier (5th track black curve).



4.27: Converting static permeability (modeling) to dynamic permeability in well-92 (observation well) with almost matching model and PLT Kh however well test Kh value require further investigation.



4.28: Converting static permeability (modeling) to dynamic permeability for the understudy reservoir with $R^2 = 0.73$

4.7 Reservoir Baffles-Communication Identification

The predicted permeability and the log calculated porosity from all wells is further used to calculate the storage capacity (porosity) and flow capacity (permeability). The analysis from this plot helps to identify potential flow conduits, baffles and reservoir compartments. This information is crucial for modeling fluid flow and potentially allows dynamic modeling of reservoir fluid flow in the reservoir leading to good history match. According to geology and lithofacies, some of the reservoir zones are classified as barriers that prevent vertical communication. Lorenz plot (LP) approach is defined as a tool describes reservoir heterogeneity using flow capacity versus storage capacity. (Michael and Kameron, 2009) concluded that LP is the most robust heterogeneity indicator. Porosity/Permeability relationships appear to be insufficient tool to articulate the reservoir zonation flow and storage capacity which we need to tackle it using LP that eventually emphasizes on poor and good layers. Lorenz plot analysis is provided for reservoir section to show all observed flow mechanisms per lithofacies in figures 4.29 to 4.45). From LP analysis, it confirms the study findings that the best lithofacies is F-1.

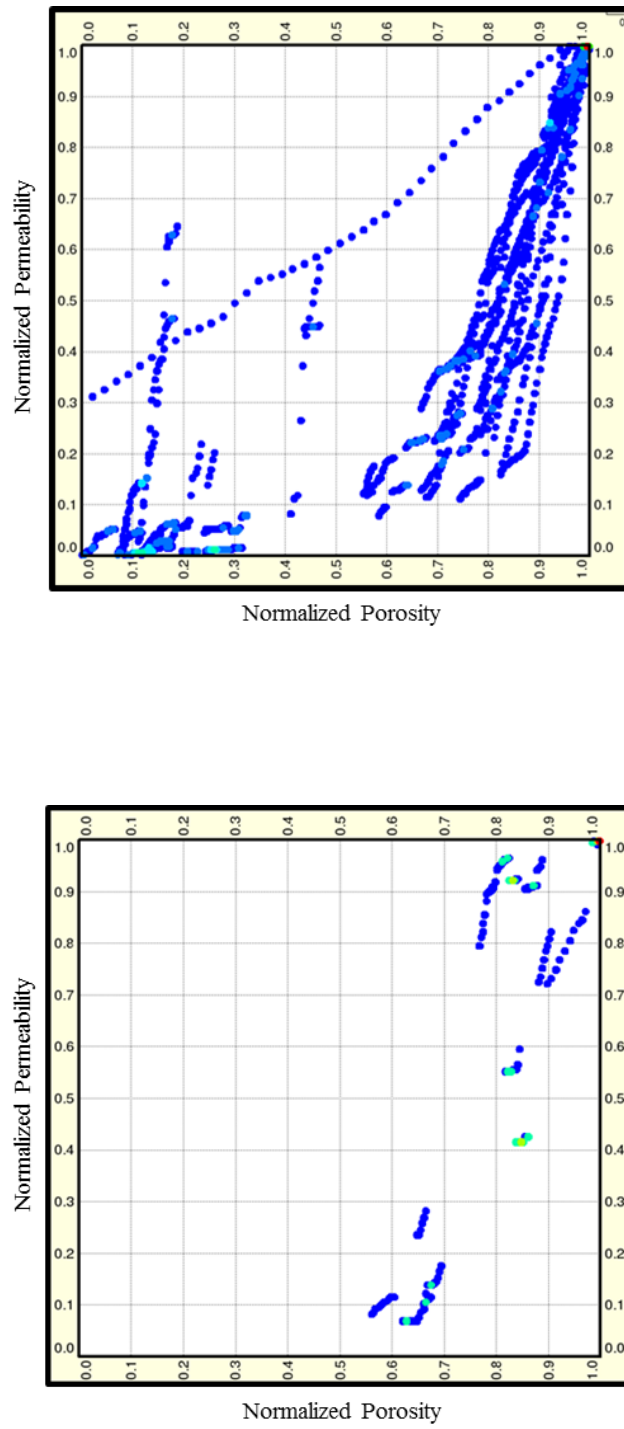


Figure 4.30: Lorenz Plot for lithofacies-2 which shows a good zone in the reservoir with high storage and low capacity due to diagenesis

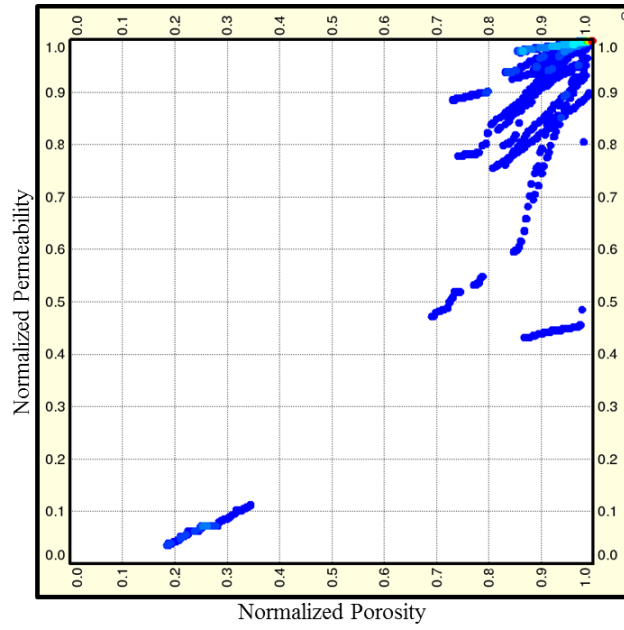


Figure 4.31: Lorenz Plot for lithofacies-4 which shows a good zone in the reservoir with high storage and low capacity due to diagenesis

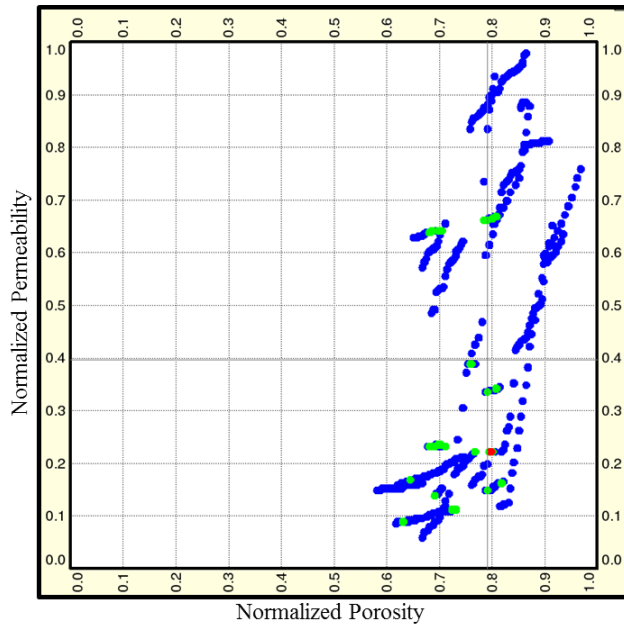


Figure 4.32: Lorenz Plot for lithofacies-7 which shows a good zone in the reservoir with medium storage and good capacity

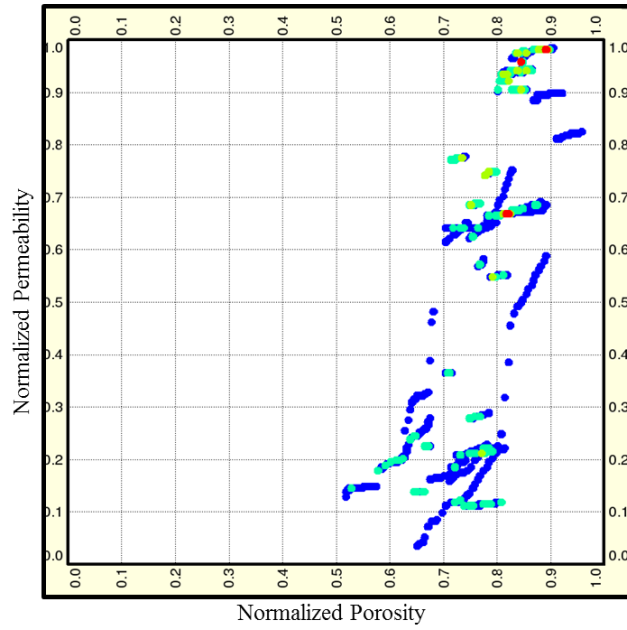


Figure 4.33: Lorenz Plot for lithofacies-8 which shows a good zone in the reservoir with medium storage and low capacity

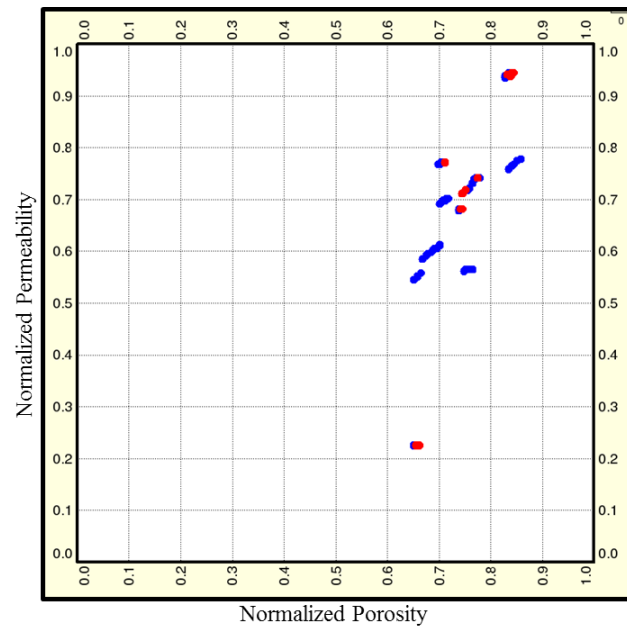


Figure 4.34: Lorenz Plot for lithofacies-9 which shows a baffle zone in the reservoir with low storage and very low capacity

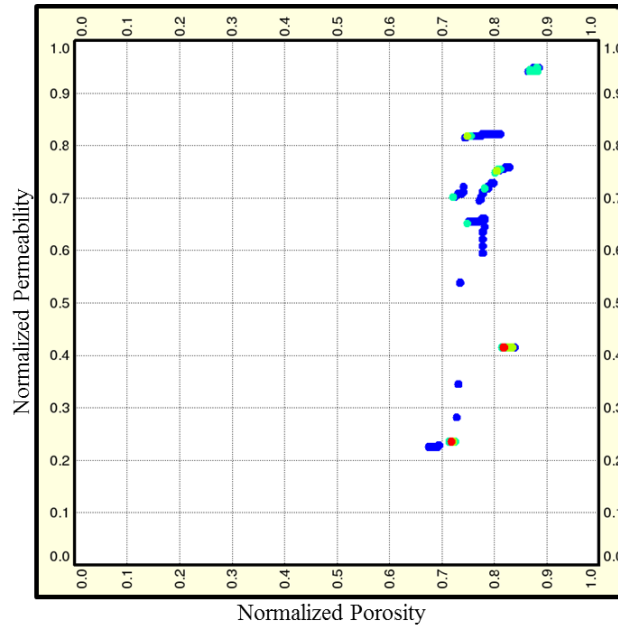


Figure 4.35: Lorenz Plot for lithofacies-10 which shows a baffle zone in the reservoir with low storage and very low capacity

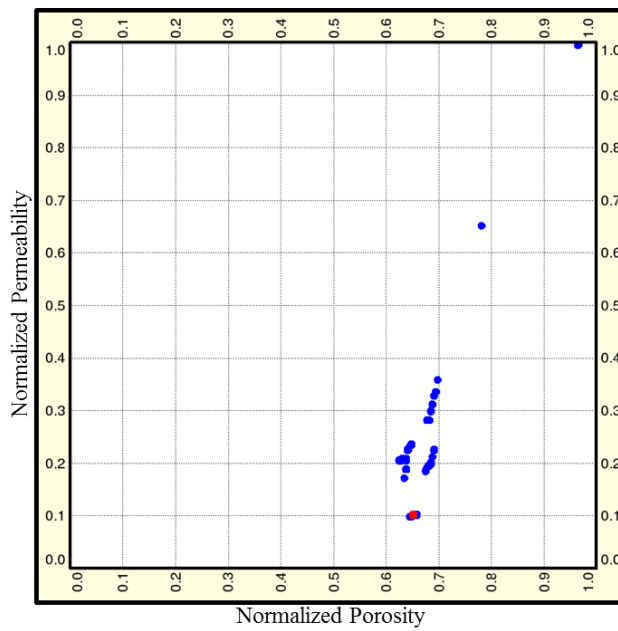


Figure 4.36: Lorenz Plot for lithofacies-11 which shows a zone in the reservoir with low storage and medium capacity

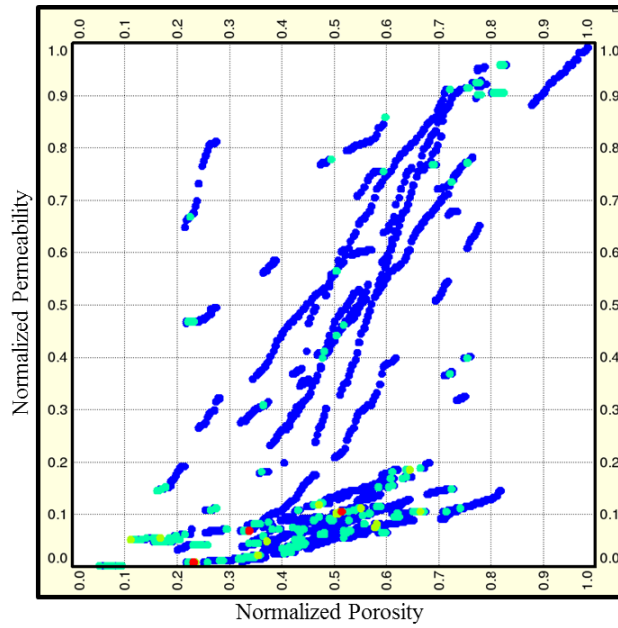


Figure 4.37: Lorenz Plot for lithofacies-15 which shows an excellent zone in the reservoir for both production and injection with storage and high capacity

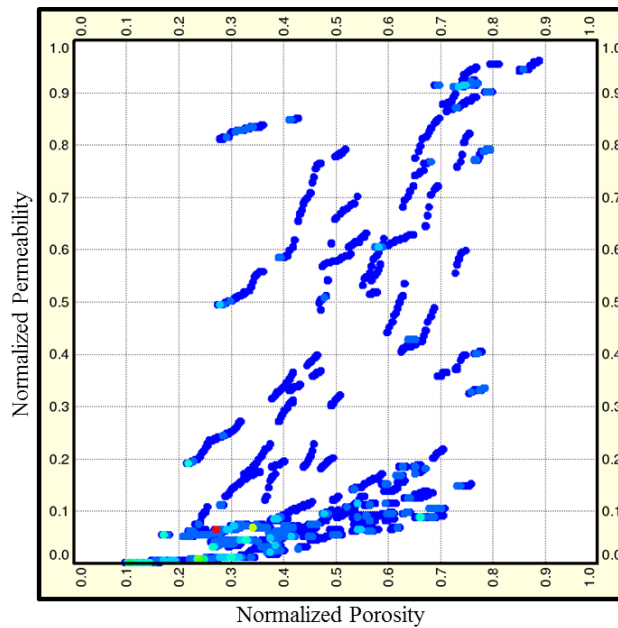


Figure 4.38: Lorenz Plot for lithofacies-16 which shows a good zone in the reservoir with medium storage and good capacity

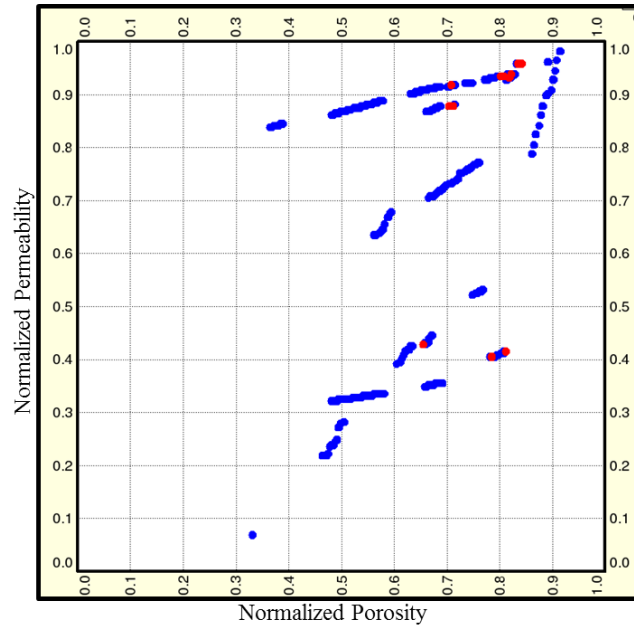


Figure 4.39: Lorenz Plot for lithofacies-17 which shows a good zone in the reservoir with high storage and good capacity

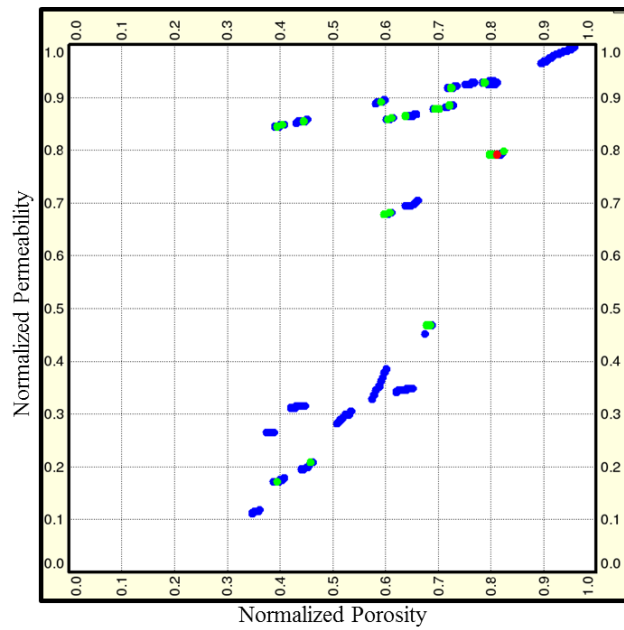


Figure 4.40: Lorenz Plot for lithofacies-18 which shows a zone in the reservoir with low storage and medium capacity

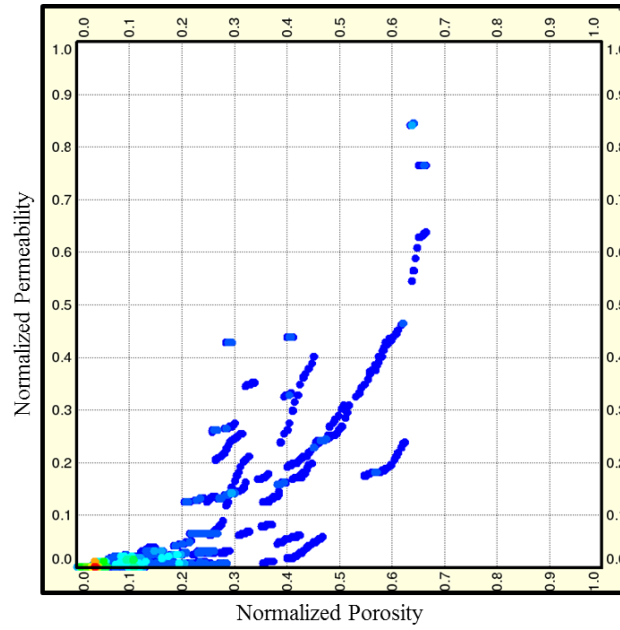


Figure 4.41: Lorenz Plot for lithofacies-19 which shows a good zone in the reservoir with medium storage and high capacity

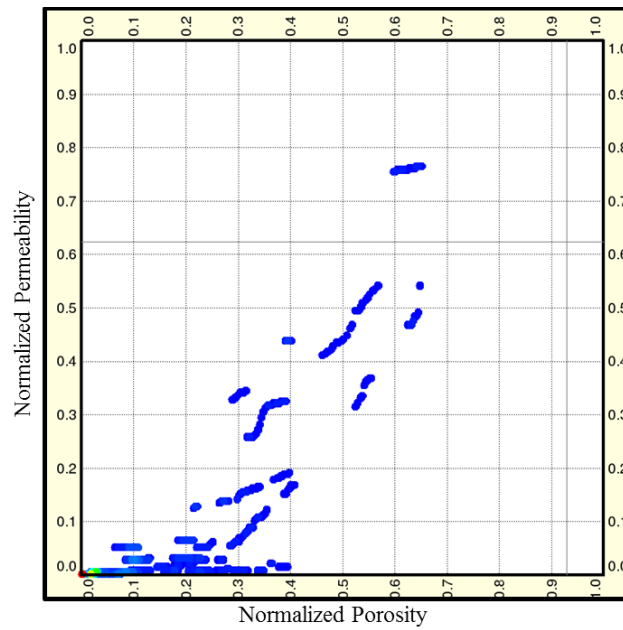


Figure 4.42: Lorenz Plot for lithofacies-20 which shows a zone in the reservoir with medium storage and medium capacity

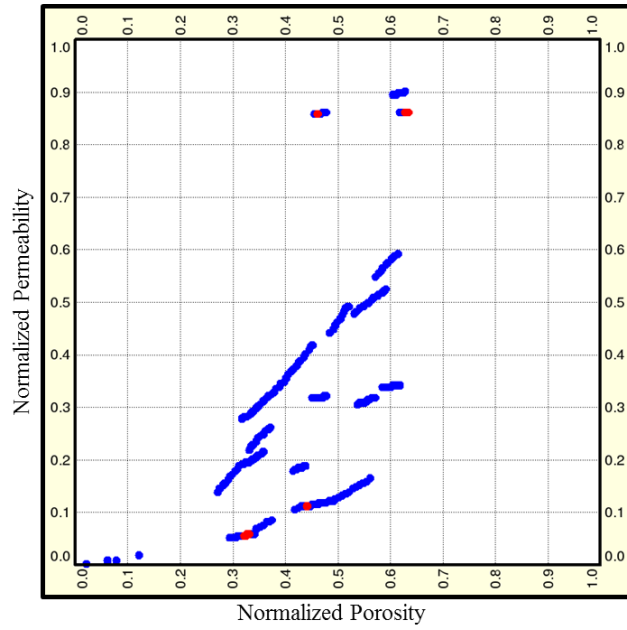


Figure 4.43: Lorenz Plot for lithofacies-21 which shows a zone in the reservoir with high storage and medium capacity

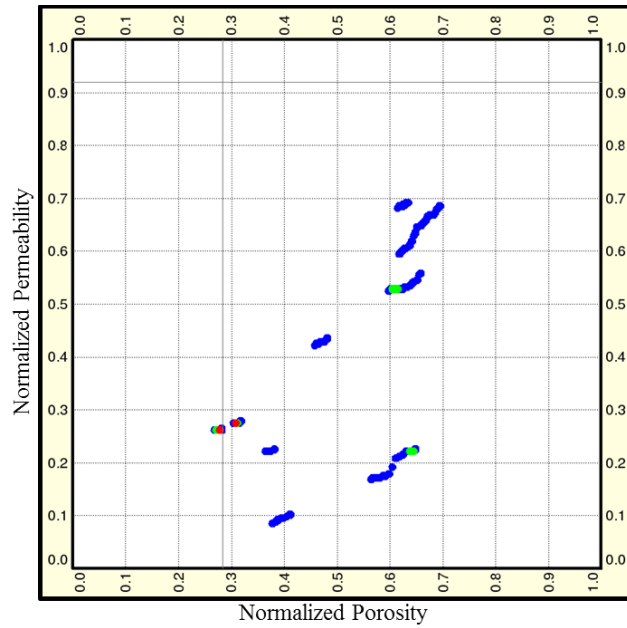


Figure 4.44: Lorenz Plot for lithofacies-22 which shows a zone in the reservoir with medium storage and low capacity

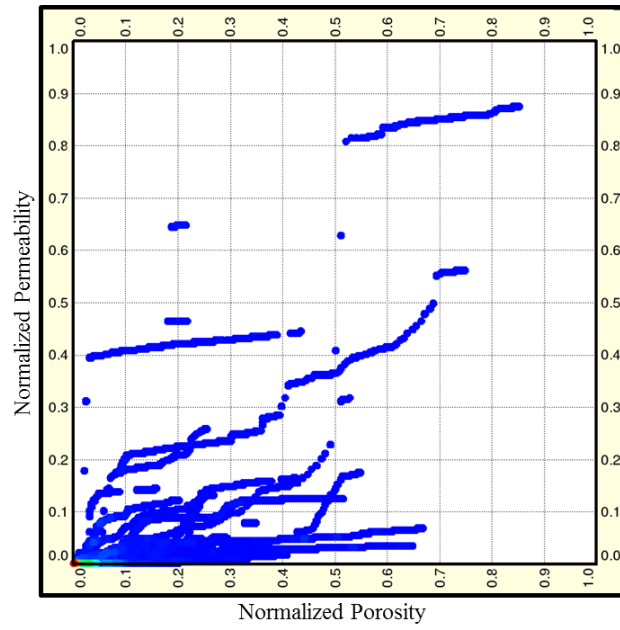


Figure 4.45: Lorenz Plot for lithofacies-23 which shows an excellent zone of storage and low capacity due to diagenesis effect

CHAPTER 5

WATER SATURATION MODELING

5.1 Saturation Model Inputs

Modeling of water saturation height functions is crucial in determining the hydrocarbon reserves in the reservoir. The change in water saturation due to production of the reservoir is continuously assessed via well logging. These changes are due to depletion of some reservoir zones that are most permeable and thus contain considerable hydrocarbon reserves. We aim in this chapter to model the saturation height of the reservoir prior to any effects using Leverett J-model to estimate lithofacies based water saturation which is simply expressed as:

$$J = \frac{0.2166 \times P_c \times \sqrt{k/\phi}}{\sigma \times \cos \theta} \quad (5.1)$$

Saturation height functions (SHF) for the understudy carbonate reservoir provide a robust saturation profile for all lithofacies to capture saturation calculations for the heterogeneous reservoir environment. This should provide the wide ranges of irreducible water saturation (S_{wirr}) for all types of lithofacies and results will be bench marked against the saturation calculated using Archie equation from wireline logs. Ultimately, hydrocarbon in place volumes will be more accurate represented by these lithofacies. Typically, high quality rocks will tend to have lower irreducible water saturation and S_{wirr} will elevate as quality of the rock degrades (Leverett, 1941).

In order to come up with representative saturation height models, we need to acquire representative capillary pressure (P_c) measurements on these various types of lithofacies. The only available source of data that has P_c curves is the mercury injection capillary pressure (MICP) which is conducted on more than 36 core plugs covering most of the reservoir lithofacies. In this chapter, water saturation from Leverett J-function is used to apply the same technique shown in chapter 4 where introducing geology into the modeling enhanced our results. Water saturation is modeled using the same concept to showcase that geology is an important part of any petrophysical/reservoir integrated studies.

5.2 Methodology

We utilized all inputs from well levels (permeability, porosity, height, and interfacial tension data) and calculate J-function based on MICP curves for each lithofacies and compare it with water saturation from Archie equation. It is recommended that only pre-production wells are used when applying modeling saturation from logs to capture the original water saturation that is not altered by production. The models from J-function is mainly controlled by the permeability and height above FWL/OWC. Archie equation is given by:

$$S_w^n = \frac{a \times R_w}{\phi^m \times R_t} \quad (5.2)$$

We initiate the saturation modeling by calculating the height above free water level which is simply obtained using this equation:

$$(HAFWL) = \frac{0.433 \times \Delta \rho x}{P_c} \quad (5.3)$$

Where HAFWL is the height above free water level.

Following that, the saturation models built for all rock type/Lithofacies are executed accordingly. As a result, lithofacies based saturation height models are built-up and used for saturation calculations. J-function value is calculated and compared against the MICP saturation conditioned for each lithofacies to wells above FWL on logarithmic scale and a regression is established to obtain the correlation between the two parameters. This power law correlation is used to calculate S_w as a function of J for all wells which define the oil column and thus OOIP. Figure 5.1 illustrates the followed methodology to predict water saturations.

$$S_w = \frac{a}{J^b} \quad (5.4)$$

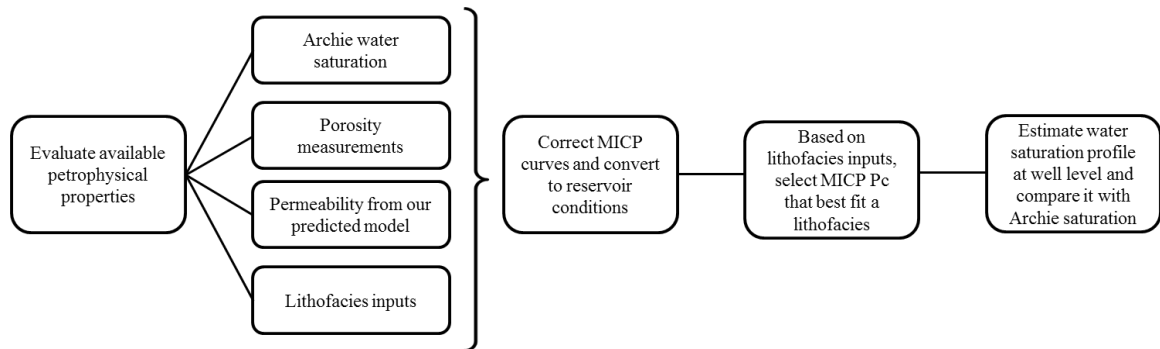


Figure 5.1: Water saturation modeling workflow used in this study

5.3 MICP Result

Mercury injection is utilized in this study to come up with a distinct capillary pressure curves for each lithofacies. Common reservoir rock typing (RRT) methods recommended the use of MICP data to categorize different petrophysical behaviors for certain reservoirs (Ali, 2011). In this study, we used geology to group MICP curves in accordance to their lithofacies. The P_c obtained from MICP experiments is corrected after converting it to reservoir conditions using the below equation to eliminate the closure effect of entry pressure at the beginning of mercury injection that is occurred during mercury injection which is defined as the pressure at which mercury starts to enter the core plug.

$$P_{c\ res} = P_{c\ lab} \frac{IFT_{res}}{IFT_{lab}} \quad (5.5)$$

Where IFT is the interfacial tension expressed by $\sigma \times \cos \theta$.

In this study, $IFT_{res} = 18.6$ and $IFT_{lab} = 368$ dynes/cm².

Figure 5.2 illustrate the correction required for P_c form MICP experiments. The summary of MICP P_c curves correction is carried out as the following:

- Convert laboratory condition to reservoir equivalent conditions
- Entry pressure effect removal
- Cap P_c to the maximum value at the reservoir pressure which represent the highest point from FWL at the crest.

P_c curves is capped to the maximum value at the reservoir condition using the below equation:

$$P_c = \Delta\rho gh = 0.433 \times \Delta\rho \times (HAFWL)$$

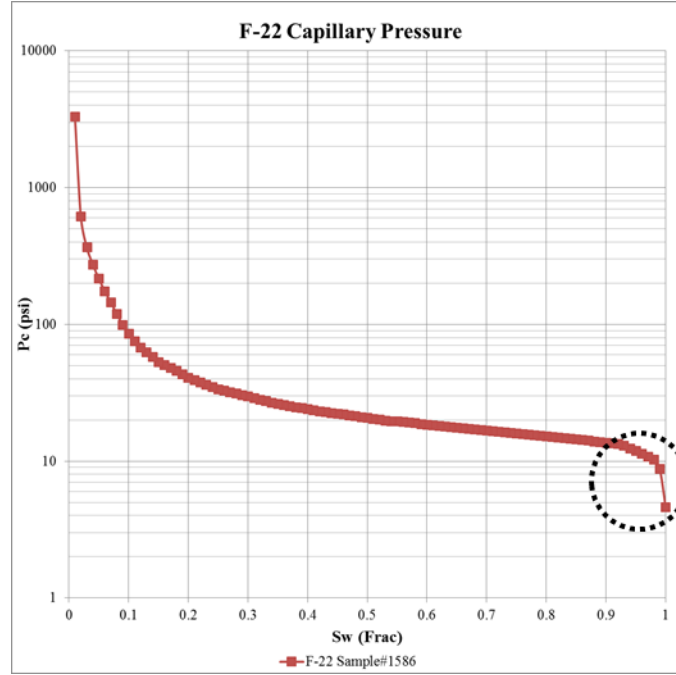


Figure 5.2: MICP curves which show the closure effect that is corrected for this study

Once all curves are corrected for closure effects, J value is calculated using Leverette J-function presented at section 5.1 in this study which uses the core plug porosity and permeability, P_c value from the above equation, and IFT which is known for this reservoir. The J value is generated for all core plugs per lithofacies which are plotted versus water saturation obtained from MICP conversion to reservoir condition (oil-brine system). A mathematical relationship is obtained for each lithofacies which is in the power law form:

$$S_w = \frac{a}{J^b} \quad (5.6)$$

This relationship will provide the SHF parameters for each lithofacies which will be used to calculate the initial water saturation. Many researchers utilized MICP data to calculate

water saturation (Wunderlich 1985, Tomutsa et al. 1990, Smith et al. 2002 and Seth and Morrow 2006). However, (Greder et al., 1997) suggested that MICP fluids (mercury-air system) is equivalent to oil-brine system when converted to reservoir conditions for purely water wet system. The below equation is used to derive the P_c at the reservoir condition from laboratory tests:

$$P_{c\ res} = P_{c\ lab} \frac{IFT_{res}}{IFT_{lab}} \quad (5.7)$$

All plug samples are corrected and then their P_c and water saturation are plotted to visualize the wide range of samples that require further classification by grouping samples with the same lithofacies family. Figure 5.3 illustrates that further grouping of MICP data is needed. As discussed in methodology section, capillary pressure curves will be generated for all lithofacies. Figure 5.4 shows the grouping of P_c curves for each lithofacies.

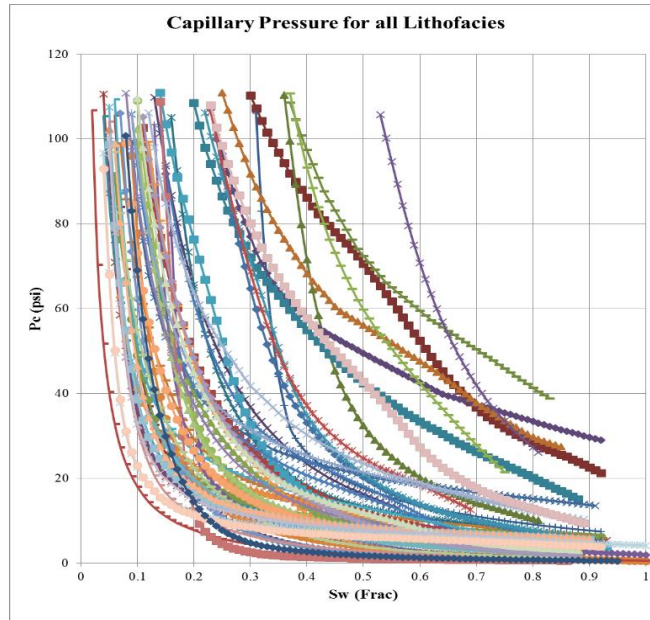


Figure 5.3: Capillary Pressure curve for all samples

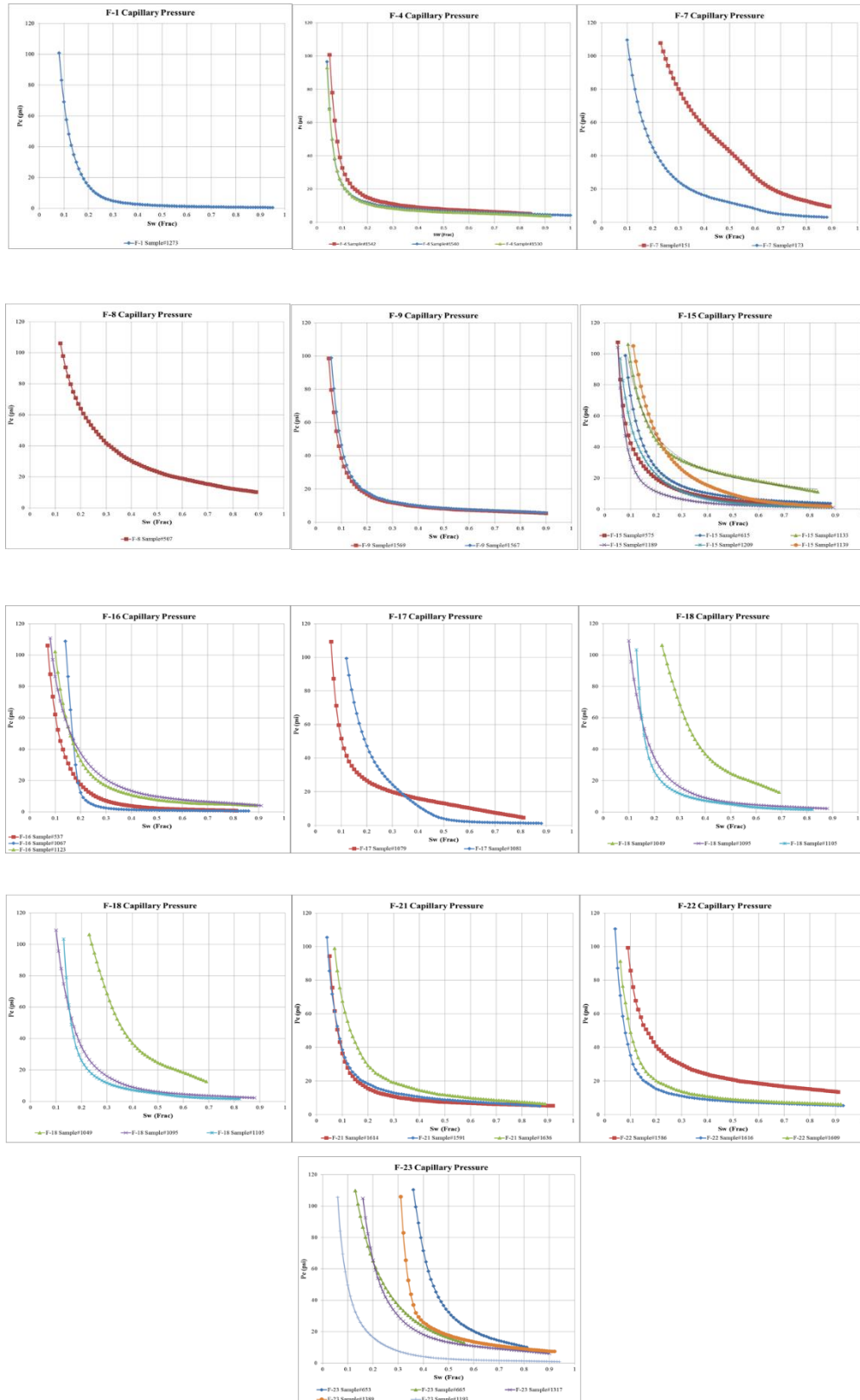


Figure 5.4: Capillary pressure curves for all lithofacies

The following table 5.1 summarizes the implementation of lithofacies grouping for MICP data which resulted in identifying different J-junction parameters to be used in predicting water saturation in all wells depending on their predicted lithofacies. It is clear from a and b values that lithofacies having poor petrophysical quality produces higher transition zones in the P_c curve. These values are generated by plotting S_{wir} versus J values for each samples within each lithofacies and then a representative curve that fits most of the data points is suggested with a typical a and b for a specific lithofacies to carry out the model propagation for all cored and uncored wells. Figure 5.5 shows the J-function curves for all lithofacies.

Table 5.1: J-Function parameters for different lithofacies

Lithofacies	a	b	Power Law Model
1	0.31	0.47	$S_w = \frac{0.31}{J^{0.47}}$
4	0.15	1.12	$S_w = \frac{0.15}{J^{1.12}}$
8	0.21	0.86	$S_w = \frac{0.21}{J^{0.86}}$
9	0.15	1.07	$S_w = \frac{0.15}{J^{1.07}}$
15	0.31	0.71	$S_w = \frac{0.31}{J^{0.71}}$
16	0.30	0.57	$S_w = \frac{0.30}{J^{0.57}}$
17	0.48	0.66	$S_w = \frac{0.48}{J^{0.66}}$
18	0.30	0.50	$S_w = \frac{0.30}{J^{0.50}}$
19	0.43	0.49	$S_w = \frac{0.43}{J^{0.49}}$
21	0.17	1.05	$S_w = \frac{0.17}{J^{1.05}}$
22	0.17	1.12	$S_w = \frac{0.17}{J^{1.12}}$
23	0.43	0.55	$S_w = \frac{0.43}{J^{0.55}}$

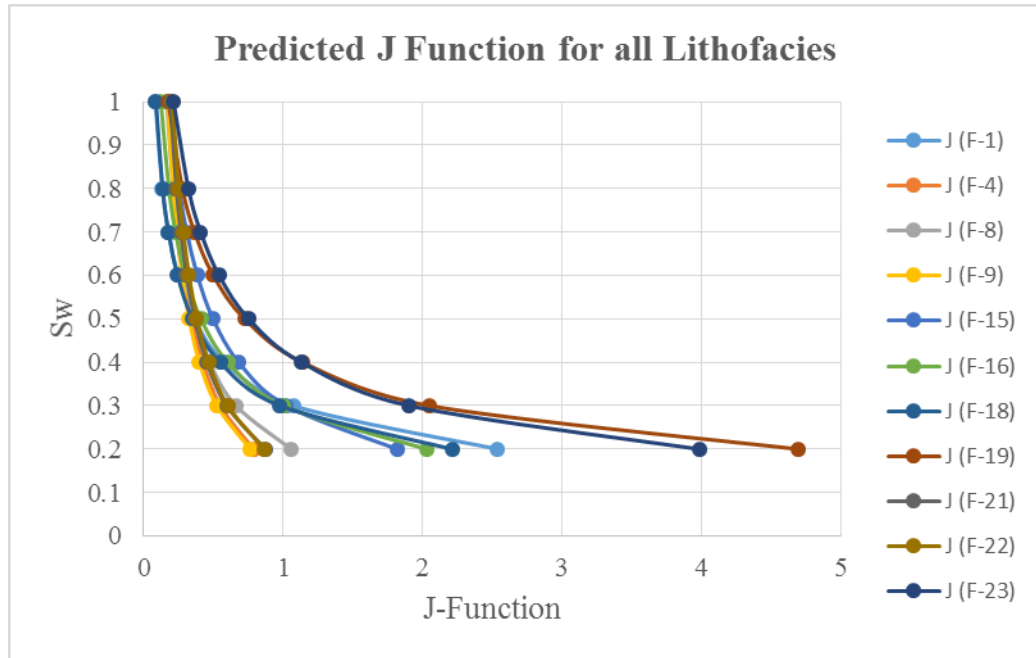


Figure 5.5: Predicted J-function plot for each lithofacies

5.4 Water Saturation Prediction

Water saturation is calculated using the obtained Leverette J-function parameters for all lithofacies which we have generated a distinct a and b per lithofacie. As a result, initial water saturation is obtained using histogram visualization tool to assess and evaluate the representative initial water saturation for all lithofacies. This is carried out from Figure 5.6 to 5.17 which is summarized in table 5.2. This information is related to the rock quality as more initial water saturation observed the more the quality degraded. In other words, high quality lithofacies represents the minimum initial water saturation. These results show the optimum utilization of the Leverette lithofacies based J-function as it was initially (Leverette, 1941) developed for certain similar rock dynamic behaviors which is now linked to geology in this study.

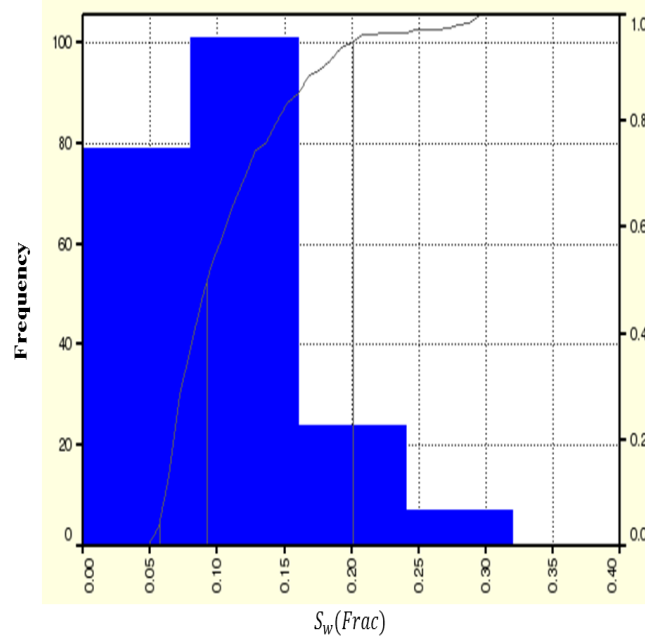


Figure 5.6: Lithofacies-1 water saturation histogram with water saturation mean of 10.7%

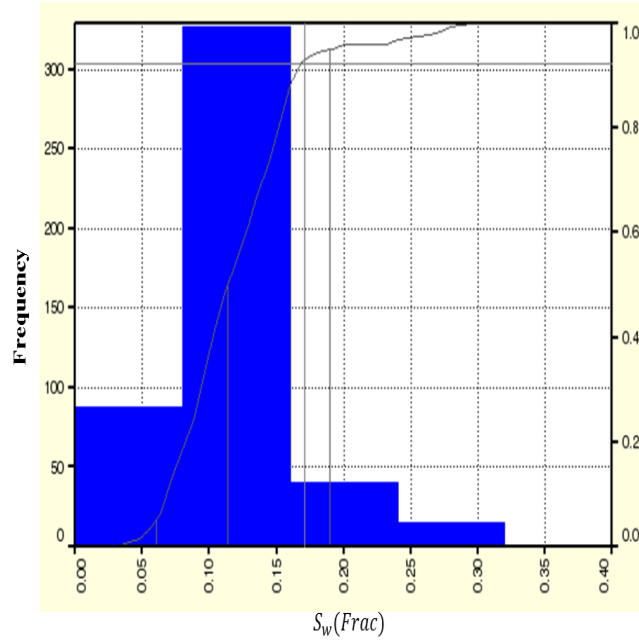


Figure 5.7: Lithofacies-4 water saturation histogram with water saturation mean of 12.3%

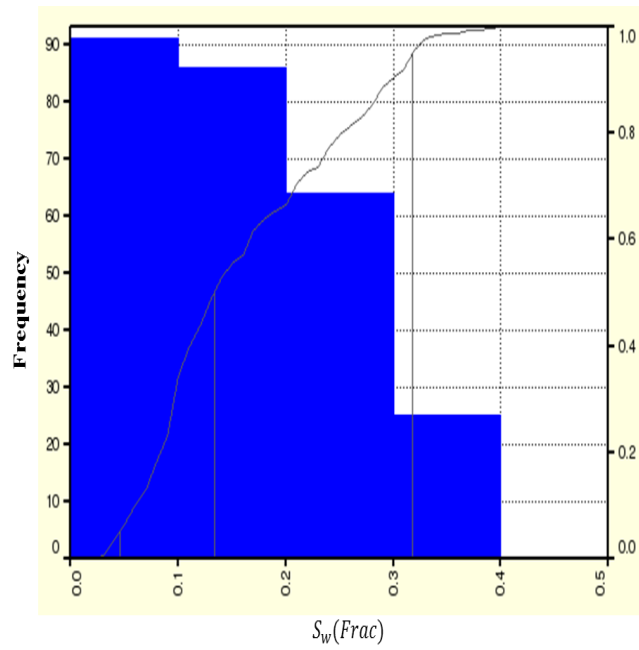


Figure 5.8: Lithofacies-8 water saturation histogram with water saturation mean of 15.3%

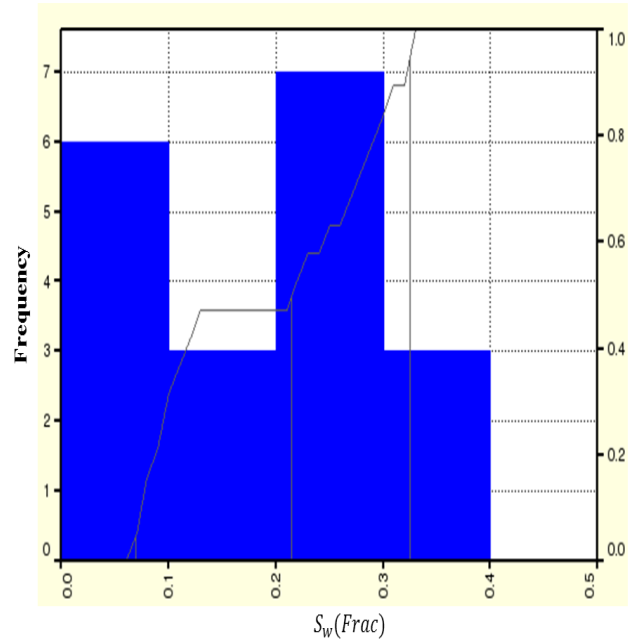


Figure 5.9: Lithofacies-9 water saturation histogram with water saturation mean of 18.9%

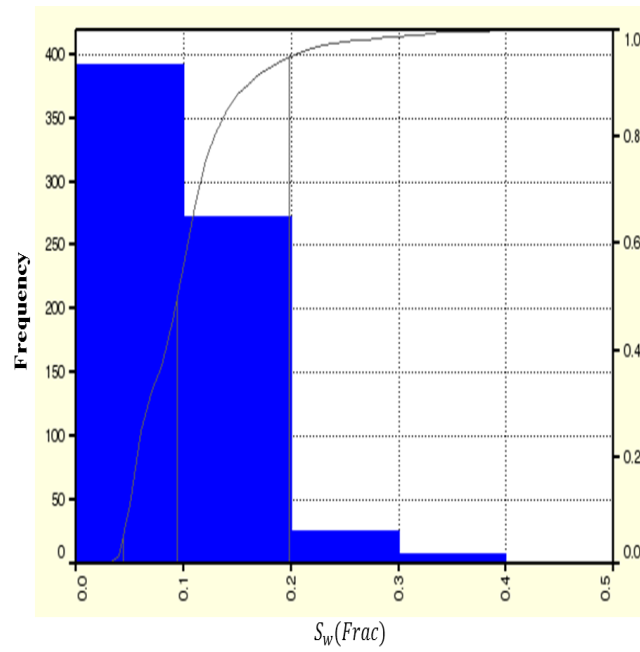


Figure 5.10: Lithofacies-15 water saturation histogram with water saturation mean of 10.4%

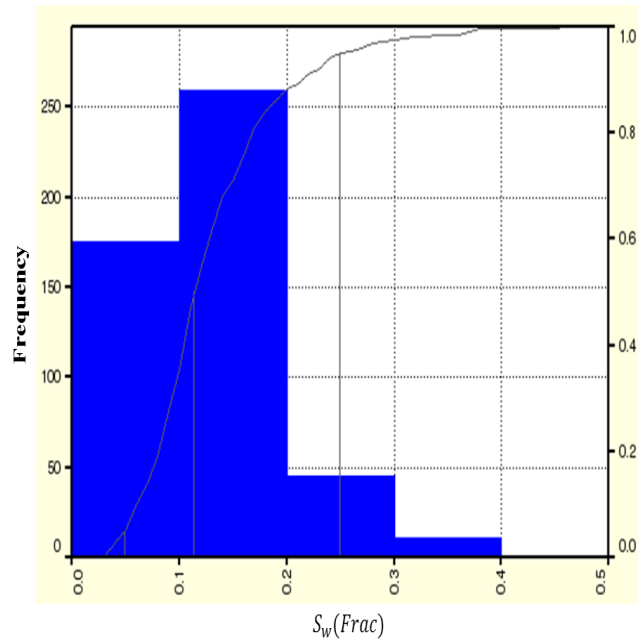


Figure 5.11: Lithofacies-16 water saturation histogram with water saturation mean of
12.9%

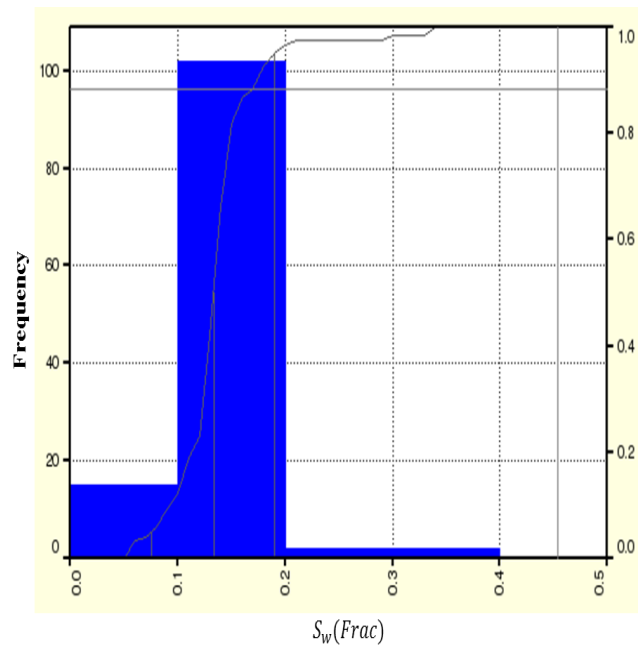


Figure 5.12: Lithofacies-17 water saturation histogram with water saturation mean of
13.9%

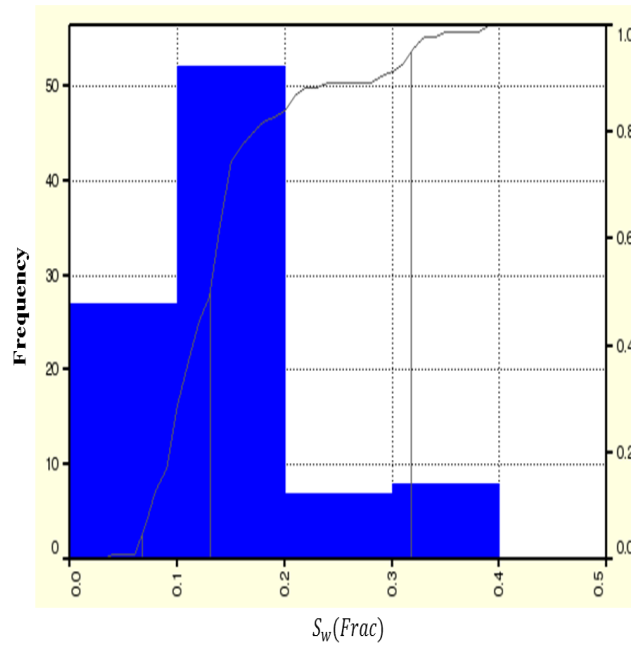


Figure 5.14: Lithofacies-18 water saturation histogram with water saturation mean of 15.4%

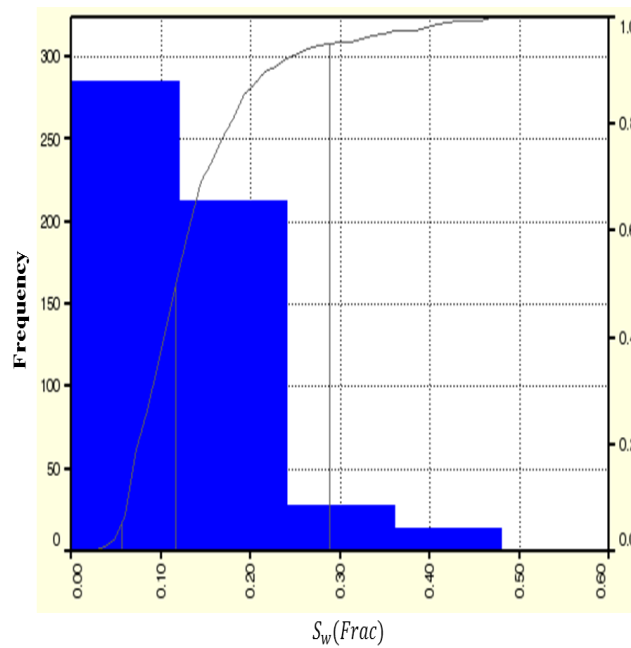


Figure 5.15: Lithofacies-19 water saturation histogram with water saturation mean of 14.4%

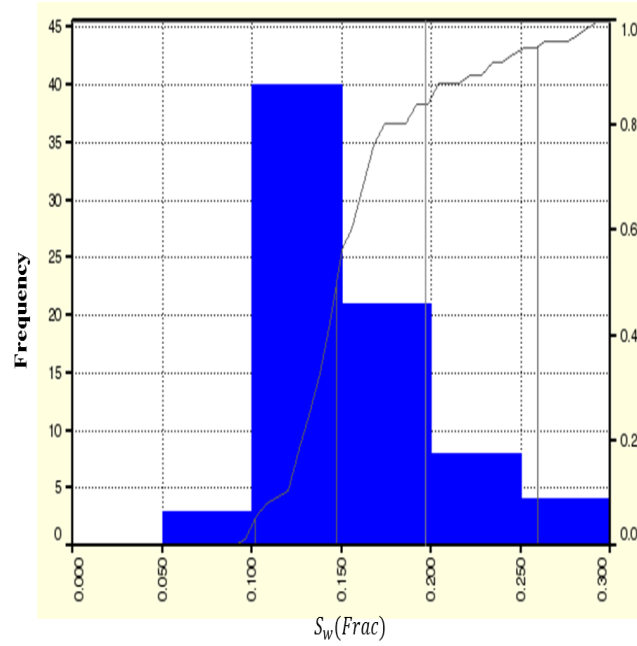


Figure 5.16: Lithofacies-21 water saturation histogram with water saturation mean of
15.8%

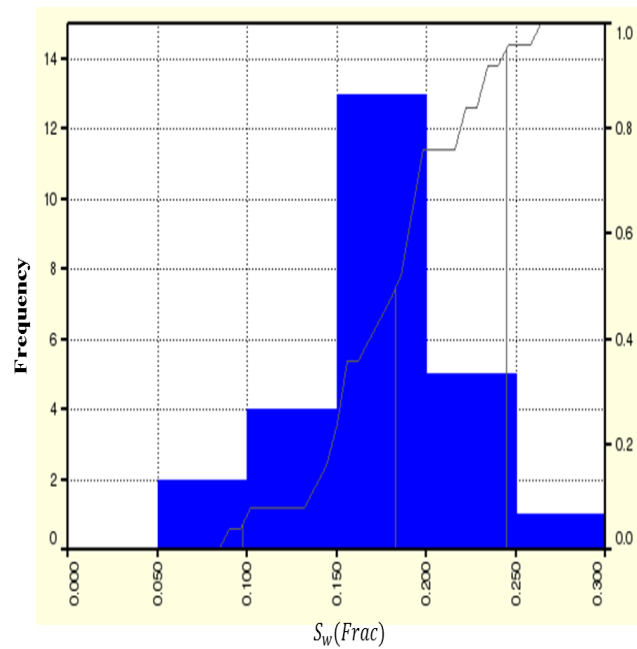


Figure 5.17: Lithofacies-22 water saturation histogram with water saturation mean of
18.0%

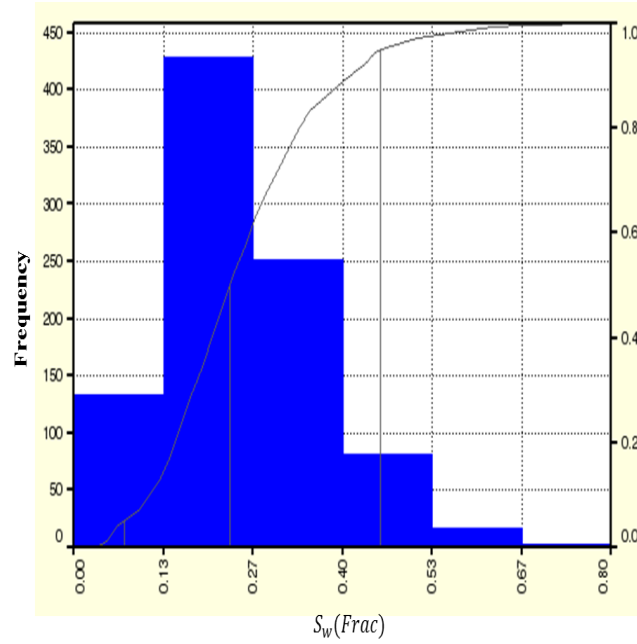


Figure 5.17: Lithofacies-22 water saturation histogram with water saturation mean of 24.7%

Table 5.2: Summary of water saturation mean per lithofacies

Lithofacies	Mean of Water Saturation (%)
1	10.7
4	12.3
8	15.3
9	18.9
15	10.4
16	12.9
17	13.9
18	15.4
19	14.4
21	15.8
22	18
23	24.7

We believe that introducing this factor - geological lithofacies -, we are able to capture the heterogeneity of different types of lithofacies which is illustrated in figures 5.18 to 5.21. It is clearly noticed that when reservoir quality degraded in lithofacies 4 when compared with the same family of depositional environment without diagenesis effect lithofacies 1, the water saturation starts to increase in this interval which honor the reservoir quality in the water saturation calculations. These results are compared to Archie equation based calculations of water saturation in lithofacies 4, which is derived from resistivity measurements, which show big inconsistency at this interval of water saturation difference that exceeds 7.5%. In most cases and especially in giant reservoirs, this 7.5% could lead to difficulty in history matching in reservoir simulation initialization runs.

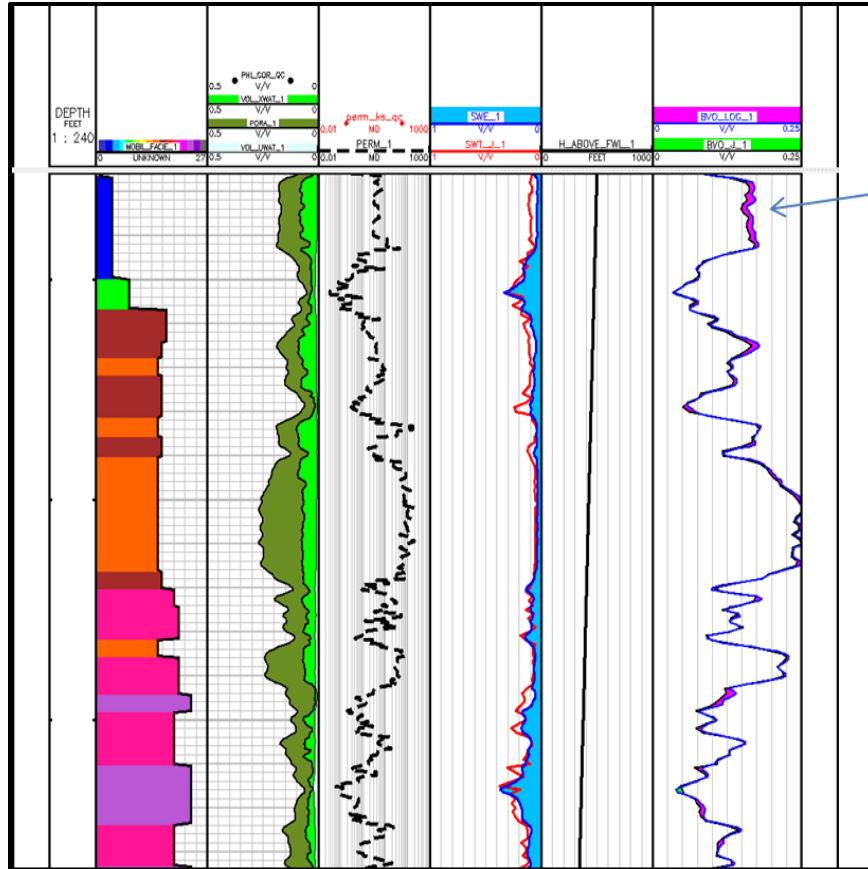


Figure 5.18: well-103 water saturation predicted (red curve -4th track-) compared to Archie water saturation (blue curve -4th track-), 6th track shows the difference between product of predicted water saturation and porosity for our method and Archie in the shaded pinkish area.

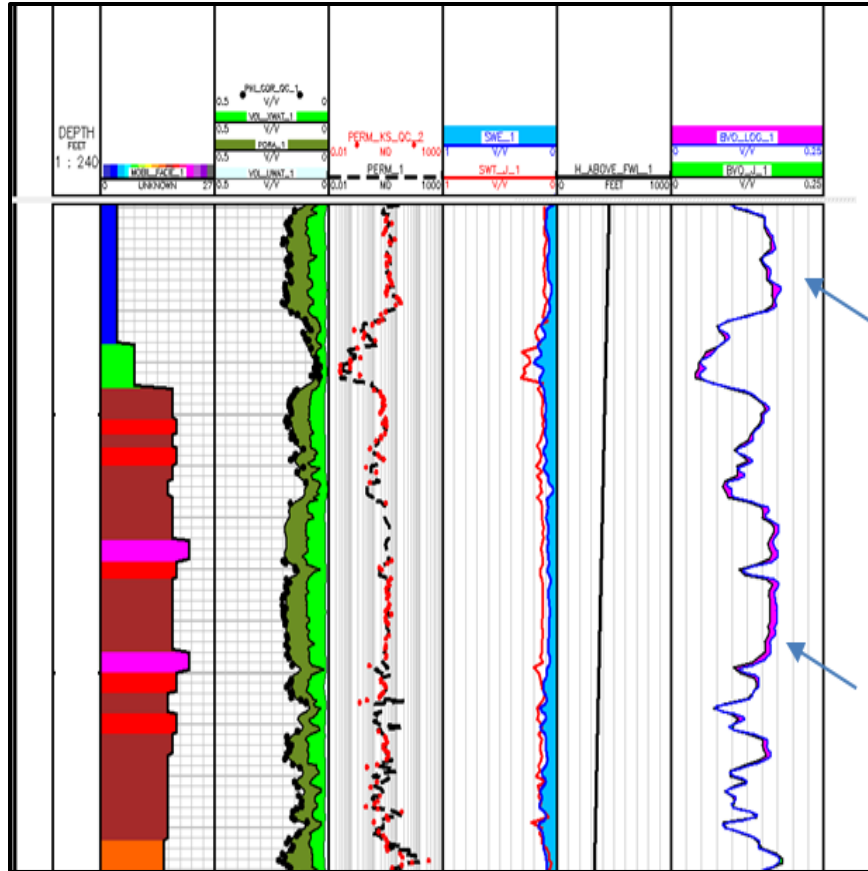


Figure 5.19: well-143 water saturation predicted (red curve -4th track-) compared to Archie water saturation (blue curve -4th track-), 6th track shows the difference between product of predicted water saturation and porosity for our method and Archie in the shaded pinkish area.

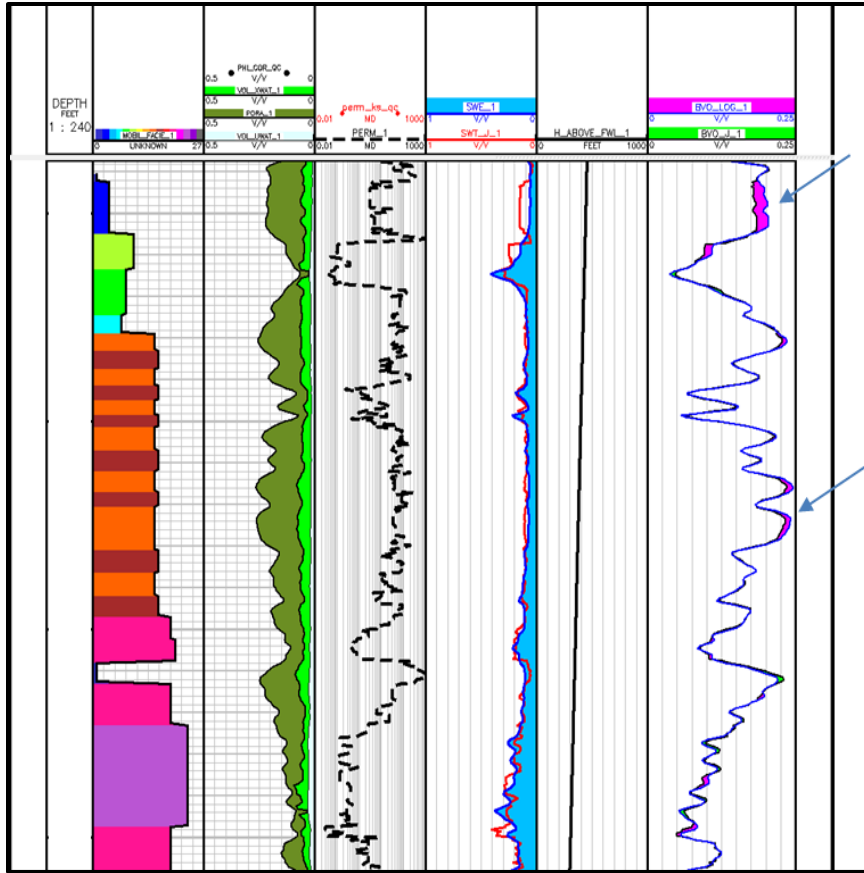


Figure 5.20: well-29 water saturation predicted (red curve -4th track-) compared to Archie water saturation (blue curve -4th track-), 6th track shows the difference between product of predicted water saturation and porosity for our method and Archie in the shaded pinkish area.

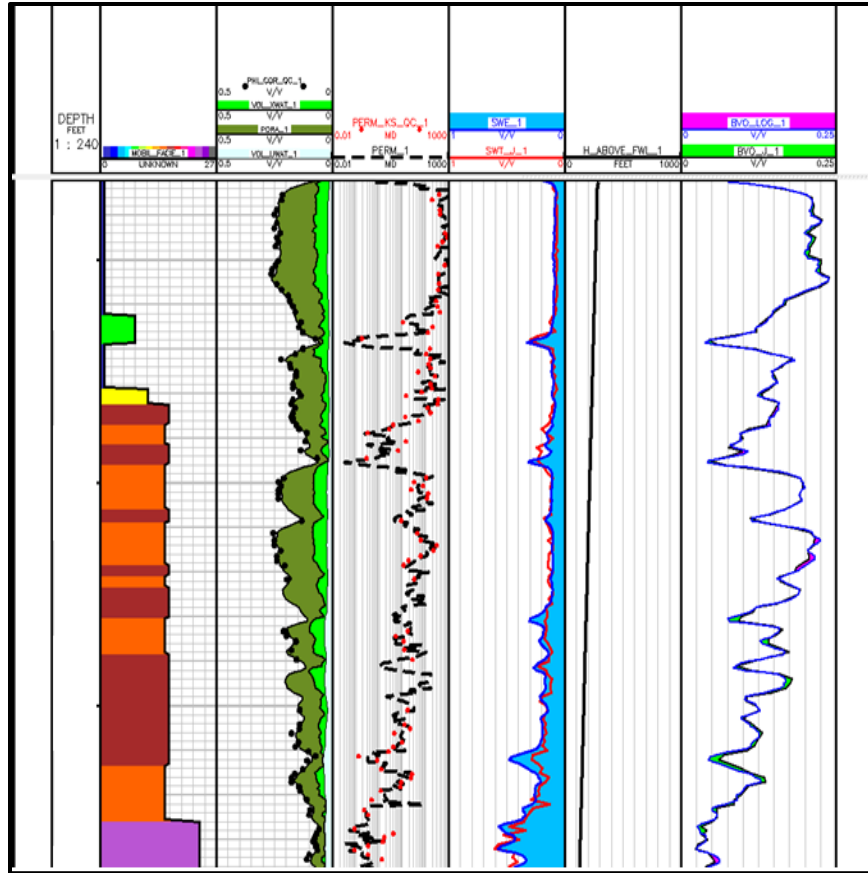


Figure 5.21: well-39 water saturation predicted (red curve -4th track-) compared to Archie water saturation (blue curve -4th track-), 6th track shows the difference between product of predicted water saturation and porosity for our method and Archie in the shaded pinkish area.

When models applied to all lithofacies, it is observed that the maximum P_c and J values are representatives at which we made the assumption to cap the capillary pressure curves to maximum values at reservoir conditions. Figure 5.22 and 5.23 show the histogram of capillary pressure values as well as the J-function calculated value based on the developed Leverette J-function coefficients.

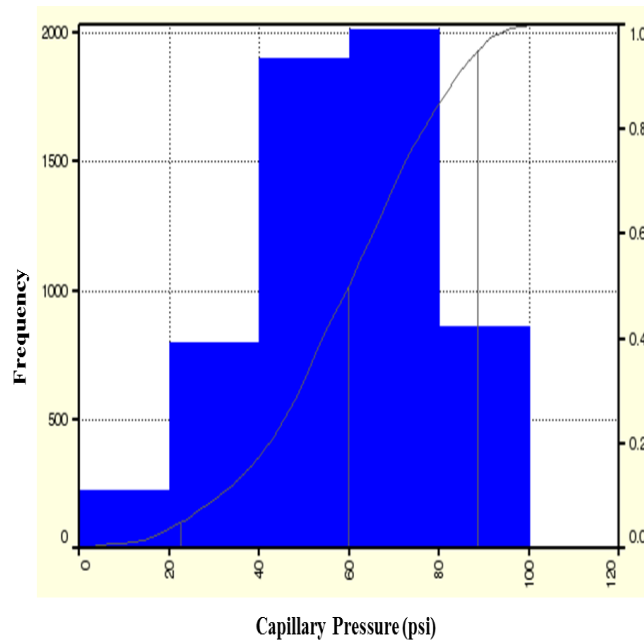


Figure 5.22: Histogram of capillary pressure at reservoir conditions for all lithofacies

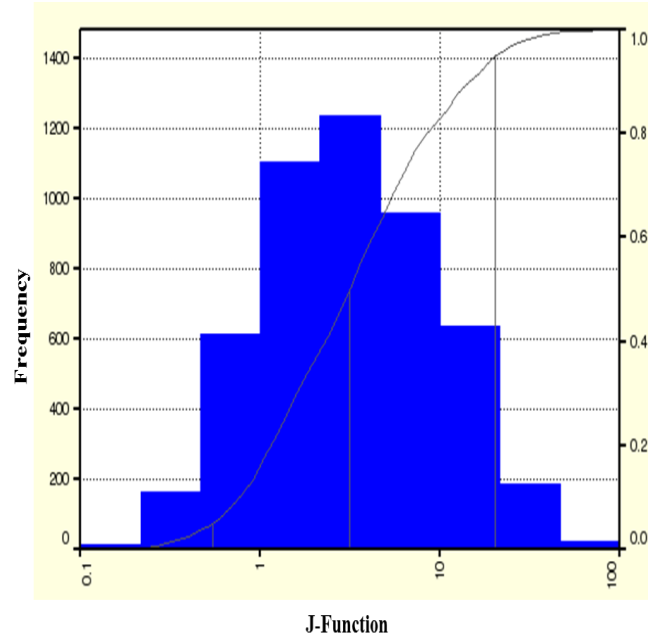


Figure 5.23: Histogram of J-function values calculated at reservoir conditions for all lithofacies

In this chapter, we have developed a robust saturation modeling which will assist in the deployment on geological model where history matching and future field development will be subjective to the accuracy of these models. To sum-up our observation, we have come-up with the following conclusions:

- Optimistic saturation models are built that work well with lithofacies independent J-function although no enough capillary pressure data per lithofacies is available to characterize the different lithofacies and provide reasonable and representative model for saturation.
- In high quality rock, J-function matches the saturation from Archie while in low quality rock the calculated saturation from J-function shows higher irreducible water saturation and thus more optimistic oil volume.
- Uncertainties in lithofacies and permeability are carried out water saturation calculated by J-function; when this is observed it requires further refinement.
- MICP data is used to bench mark and assure that accurate saturation models are captured for higher confidence level in reserves and hydrocarbon in place estimates.

CHAPTER 6

CONCLUSIONS AND RECOMMENDATIONS

In this study, a new workflow is introduced to incorporate lithofacies geological information into petrophysical modeling. Lithofacies inputs helped in achieving an excellent match between core permeability and model predicted permeability which necessitate the integration of geology with reservoir static and dynamic parameters. Geological integration requires a comprehensive knowledge on the geological events sequence that resulted in different carbonates depositional environments which alters rock petrophysical properties specially diagenesis effects. We concluded that the use of MRGC method has provided improved correlation coefficient as this method doesn't require priori knowledge of the training data. Five main parameters were tested against the core permeability to examine their relationships and generate a quality model that would represent the reality which are; density log, neutron log, sonic log, difference between sonic and density/neutron logs, and lithofacies. The prediction is carried out using the permeability value and then compared with a model developed to predict logarithmic values of permeability. These two approaches were compared with KNN=2 and produced comparable statistical assessments, however, it seems that the direct permeability prediction is more robust as it shows better error standard deviation of 1.76 against 1.93 from logarithmic prediction. In addition, error correlation coefficient (R) is also calculated to compare the two approaches which gives 0.75 when compared to 0.59 from direct permeability prediction and logarithmic permeability prediction, respectively.

This was also supported by the root mean squares (RMS) which shows better values in the direct permeability prediction of 201.6 against 241.6 from logarithmic prediction. Therefore, we decided to use the the direct permeability prediction for this study. The model is then validated using kh from transient well testing and production logging data, the model relatively matches with good accuracy the prediction model. This method will assist petrophysicists and reservoir engineers perform simulation runs (static and dynamic) with high confidence to examine reservoir layering and heterogeneities which is an essential part of any field development. In addition, 60 MICP samples are used to generate capillary pressures in the reservoir for each lithofacies. These P_c curves are analyzed and converted to J-function to estimate original irreducible water saturation in the pre-production stage of the reservoir. J-function is plotted versus water saturation to obtain slope and intercept of each lithofacies to be utilized for the prediction in well levels. Saturation height model using J-function shows a good agreement with Archie saturations in good quality lithofacies whereas J-function show higher saturation in low quality lithofacies and thus accurate oil column calculations. In this study, a comprehensive approach was followed to systematically model permeability and then utilize it in the saturation prediction. We urge the future investigator to carefully implement the following recommendations:

- Examine the accuracy of other regression techniques to predict permeability with the same input data.
- Run formation tester to validate permeability model on new wells.
- Revisit physical core description in areas with high uncertainty from modeling.

- Quality check (QC) all well transient testing data when there is huge discrepancy with static flow capacity.
- Run more capillary pressure measurements on samples (MICP) for each lithofacies.
- Examine the capillary pressure data using other techniques and compare water saturation prediction using three different methods: MICP, porous plate, and centrifuge.
- Conduct laboratory experiments to come-up with distinct m & n values of Archie equation for all lithofacies and study the impact on the IOIP calculations.

REFERENCES

1. Ahmed, T. Reservoir Engineering Handbook, third edition. p. 203. 2006
2. Ahmed, Usman, Crary, S.F., and Coates, G.R., “Permeability Estimation: The Various Sources and Their Interrelationships,” JPT. Journal of Petroleum Technology, 1991.
3. Alameri, Mohamed B., Shebl, Hesham, “Reservoir Rock Typing of a Giant Carbonate Field”, SPE 148073, SPE Reservoir Characterization and Simulation Conference and Exhibition, Abu Dhabi, UAE, 9-11 October, 2011.
4. Anouk Creusen et. al., “Property Modeling Small Scale Heterogeneity of Carbonate Facies”, SPE 11145, 2007 SPE/EAGE reservoir Characterization and Simulation Conference, Abu-Dhabi UAE, 28-31 October, 2007.
5. Archie, G.E., “Classification of Carbonate Reservoir Rocks and Petrophysical Considerations”: AAPG Bulletin, v.36, p.278, 1952.
6. Choquette, P.W. and Pray, L.C., Geologic nomenclature and classification of porosity in sedimentary carbonates: AAPG Bulletin, v.54, p.207, 1970.
7. E.M. El-M. Shokir, “A Novel Model for Permeability Prediction in Uncored Wells”, JPT. Journal of Petroleum Technology, 2006.
8. Fleury, Marc. “Resistivity in Carbonates: New Insights”, SPE 77719, SPE Annual Technical Conference and Exhibition, 29 September-2 October, San Antonio, Texas, 2002

9. Gunter et. al., "Early Determination of Reservoir Flow Units Using an Integrated Petrophysical Method", SPE 38679, SPE Annual Technical Conference and Exhibition, San Antonio, Texas, 5-8 October, 1997.
10. H. N. Greder G. V. , P. Cordelier D. Laran, V. Munez, and O. d'Abrigeon. Forty Comparisons of Mercury Injection Data with Oil/Water Capillary Pressure Measurements By the Porous Plate Technique, SCA Annual Technical Conf. - SCA1997-10 (1997).
11. Lacentre, Pablo E., Repsol-YPF, Carrica, Pablo M., "A Method To Estimate Permeability on Uncored Wells Based on Well Logs and Core Data", SPE 81058, SPE Latin American and Caribbean Petroleum Engineering Conference, Port-of-Spain, Trinidad West Indies, 27-30 April, 2003.
12. Leverett. M.C.: "Capillary Behavior in Porous Solids" Petroleum Transactions of AIME 142 (1941) pp 152-169.
13. Lucia, F. J., "Petrophysical parameters estimated from visual descriptions of carbonate rocks; a field classification of carbonate pore space": JPT. Journal of Petroleum Technology, v.35, p.629-637, 1983.
14. L. Tomutsa, S. M. Mahmood, A. Binkmeyer and M. M. Honarpour. Application of Integrated Pore-to-Core Image Analysis to Study Fluid Distribution in Reservoir Rocks, SPE Annual Tech. Conference - SPE 20478 (1990) New Orleans, LA, pp. 137 - 148.
15. Ye, S. J., Rabiller, Philippe. A new Tool for Electrofacies Analysis: Multi-Resolution Graph-Based Clustering. SPWLA 41st Annual Logging Symposium – Paper PP. 2000.

16. Maghsood Abbaszadeh, Hikari Fujii, Fujio Fojimoto, "Permeability Prediction by Hydraulic Flow Units-Theory and Applications", SPE Formation Evaluation Journal, 1996.
17. Paul F. Worthington, "The Application of Cutoffs in Integrated Reservoir Studies", JPT. Journal of Petroleum Technology, 2008.
18. Jennings, J. W. Jr. and Lucia, F. J., "Predicting Permeability from Well Logs in Carbonate with a Link to Geology for Interwell Permeability Mapping", SPE Reservoir Evaluation & Engineering Journal, 2003.
19. Sutadiwiry, Yarra, Abrar, Budi, Henardi, Doni. "Using MRGC (Multi Resolution Graph-Based Clustering) Method to Integrate Log Data Analysis and Core Facies to Define Electrofacies, in the Benua Field, Central Sumatera Basin, Indonesia", International Gas Union Research Conference, Paris, France, 2008.
20. R. W. Wunderlich. Imaging of Wetting and Nonwetting Phase Distributions: Application to Centrifuge Capillary Pressure Measurements, SPE Annual Tech. Conference (1985), Las Vegas, Nevada.
21. J. D. Smith, I. Chatzis and M. A. Ioannidis. A New Technique for Measuring the Breakthrough Capillary Pressure, SCA Annual Technical Conf. - SCA2002-40 (2002), Monterey, California.
22. S. Seth and N. R. Morrow. Efficiency of Conversion of Work of Drainage to Surface Energy for Sandstone and Carbonate, SPE Annual Tech. Conf. and Exhibition - SPE 102490 (2006), San Antonio, Texas.

APPENDIX A

The statistical formulas of error measurements that used in this thesis are defined below including error average ($E_{\bar{x}}$), error standard deviation ($E_{St.D}$), maximum absolute percent relative error (E_{MAX}), Average absolute percent relative error (AARE) and Correlation Coefficient (R).

$$E_{\bar{x}} = \frac{\sum_{i=1}^n E_i}{n} \quad (A-1)$$

Where $E_i = (k_c)_i - (k_p)_i$

$$E_{St.D} = \left(\frac{1}{n-1} \sum_{i=1}^n (E_i - \bar{E})^2 \right)^{1/2} \quad (A-2)$$

Where $E_i = (k_c)_i - (k_p)_i$ and $\bar{E} = \frac{1}{n} \sum_{i=1}^n E_i$

$$AARE = \frac{1}{n} \sum_{i=1}^n \left| \frac{(k_c)_i - (k_p)_i}{(k_c)_i} * 100 \right| \quad (A-3)$$

$$R = \frac{\sum_{i=1}^n ((k_c)_i - \bar{k}_c)((k_p)_i - \bar{k}_p)}{\sqrt{\sum_{i=1}^n ((k_c)_i - \bar{k}_c)^2 \sum_{i=1}^n ((k_p)_i - \bar{k}_p)^2}} \quad (A-4)$$

Where $\bar{k}_c = \frac{1}{n} \sum_{i=1}^n (k_c)_i$ and $\bar{k}_p = \frac{1}{n} \sum_{i=1}^n (k_p)_i$.

$$RMS = \sqrt{\frac{1}{n-2} \sum_{i=1}^n E_i^2} \quad (A-5)$$

APPENDIX B

The initial idea of R Eyvazzadeh is to apply multipliers to matrix permeabilities so as to match the PLT data obtained from the field. The equation to be solved is defined after Dennis Schmitt, Saudi Aramco, Reservoir Description Division which then converted to a soft code used in GEOLOG:

$$(1 - Q_i) kh = \sum_{j=1}^i \alpha_j k_j h_j, \quad i = 1, 2, \dots, N \quad (C-1)$$

Where Q_i is the “percentage flow” obtained from PLT data, kh is the permeability thickness over the interval of the interest. In other words, kh can be expressed as flow capacity for a given interval which its unit is mD-ft. the k_j is the permeability obtained or deduced from cores and α_j is the multiplier that needs to be determined. h_j is the thickness of the layer/interval within which k_j is defined.

When using equation (C-1), h_j is in fact the depth sampling rate and is thus constant. Also, the Q_m is initially defined only at a few points, irregularly spaced. The regularly sampled values Q_i is obtained by linear interpolation in between the actual Q_m . Keeping this in mind, equation (C-1) can be re-written as:

$$\sum_{j=1}^i \alpha_j k_j = G_i, \quad i = 1, 2, \dots, N \quad (C-2)$$

Where $G_i = \frac{(1-Q_i) kh}{h}$. Note that $Q_1 = 100$. In order to avoid $G_i = 0$, Q_1 is set to 0.99998.

To solve this system, let M be the number of different multipliers α_m with $M < N$. M is given by the original data points of the Q_i between which linear interpolation has been performed. It is assumed that α_m belongs to the interval $[N_{m-1}, N_m]$ where the N_j is the index with respect to the analyzed interval. With such assumptions, equation (C-2) leads to an over determined system of the form:

$$\underline{\underline{B}} \cdot \underline{\alpha} = \underline{G} \quad (C-3)$$

Where $\underline{\underline{B}}$ is an $N \times N$ matrix ($M < N$), $\underline{\alpha}$ is an M vector and \underline{G} is an N vector. For m within the interval $[N_{m-1}, N_m]$ (assuming $N_0 = 1$), the elements B_{im} of the $\underline{\underline{B}}$ matrix are given by:

$$\begin{cases} B_{im} = 0 & \forall i < N_{m-1} \\ B_{im} = \sum_{j=N_{m-1}+1}^i k_j & \forall i < [N_{m-1}, N_m] \\ B_{im} = \sum_{j=N_{m-1}+1}^{N_m} k_j & \forall i < N_m \end{cases} \quad (C-4)$$

Only the last two equations apply to the first column of $\underline{\underline{B}}$.

There are many ways, more or less sophisticated to solve such a system and may were tried. At the end, the most simple straightforward solution works perfectly well, i.e.,

$$\underline{\underline{\alpha}} = (\underline{\underline{B}}^T \cdot \underline{\underline{B}})^{-1} \cdot \underline{\underline{B}}^T \cdot \underline{\underline{G}} \quad (\text{C-5})$$

Where the superscripts ^T and ⁻¹ indicate the transpose and the inverse, respectively. Of course, the solution is not unique but no significant variation was observed between the results coming from different algorithms.

VITAE

Name : MESHAL ALI ALAMRI

Nationality : Saudi

Date of Birth : July 9, 1988

Email : alamry.meshal@hotmail.com

Address : Dammam

Academic Background : Petroleum Engineering

Telephone Number : +966569392316